CHARITÉ

Master's Program in Molecular Medicine
at the Charité - Universitätsmedizin Berlin

Master's Thesis

to earn the

Master of Science in Molecular Medicine

ROLE OF BMPs ON NEURO-MESODERMAL AXIAL PROGENIOTORS AND MESODERMAL SUBLINEAGE DIFFERENTIATION

Presented by

Aparna Sekar

Born on *November 26th, 1996*

First Evaluator: Dr. Frederic Koch
Second Evaluator: Professor Dr. Sigmar Stricker

Completed at the *Department of Developmental Genetics, Max Planck Institute for Molecular Genetics on 1st October 2020*

Table of contents

1 ABSTRACT

Development of an embryo is a complex process during which pluripotent cells differentiate in a controlled manner giving rise to multiple cells/tissue types. This process is driven by several pathways that regulate each other. Mesoderm, which initially forms during gastrulation further differentiates to give rise to paraxial, intermediate and lateral mesoderm. Bipotent neuro-mesodermal progenitors (NMPs) at the caudal end of the embryo is an important long-term source for mesodermal and neuroectodermal cells during axial development in embryos. Several markers that play a role in the commitment of NMPs to mesoderm and paraxial mesoderm sublineages have been identified, like *T*,*Tbx6* and *Msgn1*. On the contrary, no such commitment marker exists for LPM. For a thorough investigation of potential LPM commitment markers, large amounts of LPM-like cells are required. We were able to establish a protocol for the differentiation of mESC to LPM through the NMP-like cells. This is also a reliable recapitulation of the events that occur in an embryo. BMPs play an essential role in directing LPM differentiation as well as in the relocation of NMPs during trunk to tail transition.

Several studies have investigated the role of BMPs *in*-vivo with the help of Knock-outs and hyperactivation models. In order to be able to understand these mechanisms at deeper level, beyond the phenotypes of mutants that is observed *in-vivo*, we aim to generate a conditional Bmp4 KO cell line with which *in-vitro* as well as i*n-vivo* experiments could be performed. The conditional KO study would help to elucidate the role of Bmp4 in mesoderm sublineage specification during mid-late trunk stages of embryonic development. This conditional KO is necessary as Bmp4 is required for mesoderm formation during gastrulation and complete KO cells fail to develop into an embryo. Furthermore, BMP11 (GDF11) has been previously shown to facilitate the trunk to tail transition *in-vivo,* but these studies fail to understand the underlying molecular mechanism. Hence, we differentiated GDF11 mutant mESCs to PSM and LPM and with the help of FACS and real time PCR, we were able to show that GDF11 has no effects on ability of NMPs to differentiate into nascent LPM, whereas GDF11 mutants exhibit an accumulation of double positive cells (NMPs) along with an inability to generate paraxial mesodermal cells. This accumulated NMP population seems to be biased towards forming neural tissue even in the presence of Wnt signals. Additional experiments looking deeper at histone modifications of candidate genes and RNA sequencing would be necessary in order to clearly understand the mechanism by which Gdf11 regulated trunk to tail transition.

2. INTRODUCTION

2.1 MOUSE EMBRYOLOGY

The mouse has long been used as a convenient model system to investigate mammalian development. It has many advantages such as easy genetic manipulations, large litter size and comparability of tissues to humans.

Furthermore, the crucial steps during development of mouse embryos are similar to those in humans. Fertilisation, the first step of developmental process occurs in the upper oviduct of the mice. 24h after fertilisation the first cleavage occurs resulting in a 2 cell embryo (Fig 2.1). The preimplantation embryo continues to rapidly divide and give rise to a morula, which is approximately a 16 cell stage with a missing cavity. Embryo of the morula stage undergo compaction, where blastomere lose their individual boundaries, flatten against each other and give rise to a layer of epithelial cells. Compaction is the first visible morphogenetic event of the pre-implantation embryo (Fierro-González, White, Silva, & Plachta, 2013). Compaction is followed by cavitation observed at the 16-32 cell stage of embryo (Motosugi, Bauer, Polanski, Solter, & Hiiragi, 2005). Formation of the fluid filled cavity results in the blastocyst (E3.5) (Fig 2.1) which moves along oviduct, enters and gets implanted in the uterus. The growth of the fluid filled cavity in the early blastocyst results in an accumulation of cells that form the inner cell mass (Eaton & Green, 1963). The late blastocyst consists of three cells types: Trophectoderm, Primitive endoderm and Epiblast. Post implantation, the embryo proceeds to develop pro-amniotic cavity at E5.5. At E6.5 (early gastrulation) the middle germ layer - Mesoderm is formed (Fig 2.1). Mesodermal cells arise at the posterior end from the primitive streak (PS). The PS is the strip of ectoderm that extends from the junction between the embryonic and extraembryonic ectoderm (P. P. Tam & Behringer, 1997) and lies in the posterior end of the embryo, helping in establishment of anterior-posterior axis. The mesodermal cells from the PS rapidly multiply and form a layer between endoderm and ectoderm. The formation of PS marks the beginning of gastrulation (P. P. Tam & Behringer, 1997) and is dependent on Nodal signaling (Arnold & Robertson, 2009) and BMP4 from extraembryonic tissue (Catala, 2005; P. P. Tam & Behringer, 1997). The head process is formed on E7 at the Henson's node (a mass of mesodermal cells forming at the cranial end of PS). The formation of node and left-right patterning of embryo marks the end of gastrulation. Part of the head process gives rise to the notochord. Somitogensis commences at E7.5 and pairs of somites arise from the paraxial

mesoderm slightly anterior to the primitive streak. Simultaneously, the lateral plate mesoderm (LPM) splits into two layers, the somatic and splanchnic LPM. At E8 when the 7-somite stage is reached, the foregut and hindgut are formed, and the embryo exists as a S shaped structure. The heart begins to form anterior to the foregut and the embryo now has blood vessels. Shortly after the 7-somite stage the embryo turns to invert, becomes C-shaped and continues to develop and extend its axis to form trunk to tail.

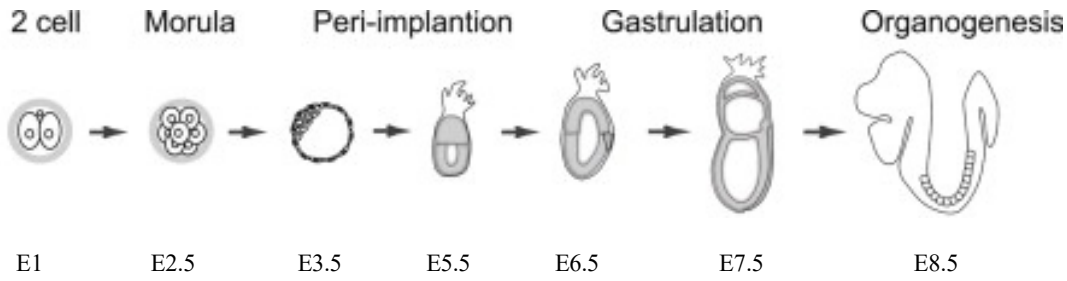

Figure 2.1:
Stages and their timeline in the development of a mouse embryo. Figure adapted from (Kojima, Tam, & Tam, 2014).

2.2 AXIAL PROGENITORS OF THE EMBRYO

Throughout the development of the embryo, a complex system of transcription factors and morphogens play a role in creating specific environments that confer identity to pluripotent and multipotent progenitor cells. The first step of differentiation in an embryo results in the trophectoderm, epiblast and primitive endoderm. Gastrulation is the second major differentiation step where fate of most cells is decided. Additionally, specification of anterior structures of the embryo occurs during gastrulation. Development of rest of the body occurs in a head to tail manner, with cells in the caudal end of the embryo contributing to the tissues of the growing axis. These cells are multipotent and give rise to late germ layers during development (Davis & Kirschner, 2000). Axial progenitors which exist in a niche at the posterior end of the embryo, contribute to the trunk and tail tissue. Some of the axial progenitors are self-renewing and some are bipotent in nature. Fate mapping studies of cells residing in the late primitive streak and tail bud region of the caudal end of chick and mouse embryo have helped to identify the location of axial progenitors in embryo. Labelling cells adjacent to the node (caudal lateral epiblast cells) revealed that these cells contribute to neural as well as somatic tissue (Brown & Storey, 2000) . It has also been shown that cells of the Caudal neural hinge

(CNH) contribute to neural tissue, mesodermal progenitors, somites and PSM by labeling cells of the CNH. This indicates that the cells of the CNH contribute to both neural and mesodermal tissue (Olivera-Martinez, Harada, Halley, & Storey, 2012). Additionally, in mouse embryo, fragments of Node streak borders (NSB) of GFP transgenic embryos were grafted into host embryos which further confirmed that the Caudal lateral epiblast (CLE) and region around the tailbud primitive streak differentiate into both neural and mesodermal sublineages (Cambray & Wilson, 2007). This area of the embryo also displays high Fibroblast growth factor (FGF) and Wnt signalling (Wilson, Olivera-Martinez, & Storey, 2009). It has been shown that the FGF signals decline in the tail bud before axial elongation begins and FGF is required to maintain the pool of axial progenitors that contribute to the development of embryonic axis (Olivera-Martinez et al., 2012) .

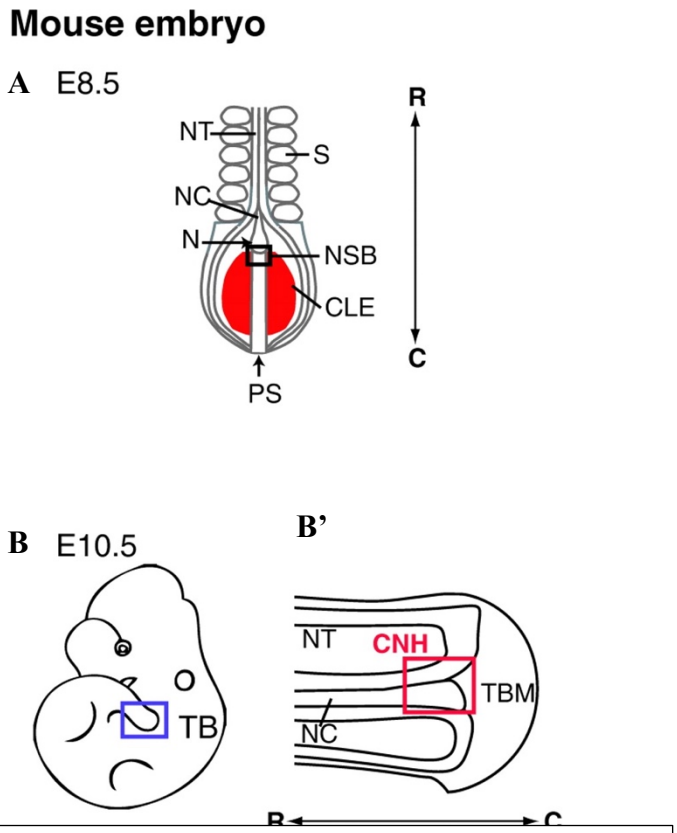

Figure 2.2:
Caudal end of **a.** E8.5 and **b.** E10.5 mouse embryo with the boundaries of NSB, CLE and CNH. Abbreviations: TB-tailbud, R-rostral, C-Caudal, NC- notochord, NT- neural tube, N- node, S-somites.

Neuro- mesodermal progenitors (NMPs) have been identified by their expression of *T* and *Sox2* (Anderson et al., 2013; Chalamalasetty et al., 2014; Garriock et al., 2015; Perantoni et al., 2005;

Wymeersch et al., 2016) . *T* is an early mesodermal marker (Murry & Keller, 2008; Papaioannou, 2014; Showell, Binder, & Conlon, 2004) whereas, *Sox2* is a neural progenitor, as well as pluripotency marker (Mugele et al., 2018; Sheng, dos Reis, & Stern, 2003). Cells identified as NMPs at the CLE/NSB in E8.5 (Fig 2.2) by fate mapping experiments using fragment grafted from GFP transgenic mice to WT embryos (Cambray & Wilson, 2007; Tsakiridis et al., 2014) express both *T* and *Sox2*, adding to existing evidence of using co-expression as a possible NMP marker. In addition, a population of cells that express both *T* and *Sox2* have been identified in the tailbud region of chick embryo which give rise to neural tissue and paraxial mesoderm (Fig 2.3). This has been demonstrated by dye labelling cells of the late tail bud in chick embryo (Olivera-Martinez et al., 2012).

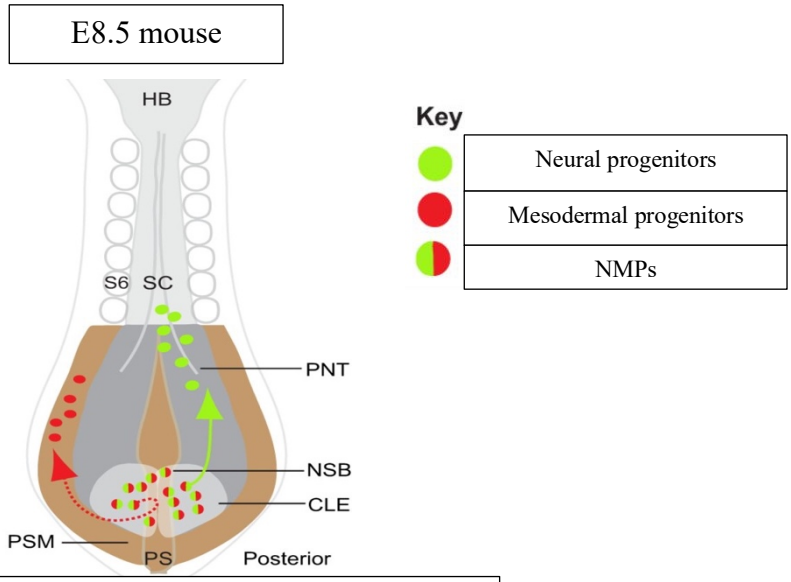

Figure 2.3:
Contribution of NMPs at the CLE/NSB to neural and mesodermal sublineages. (Henrique et al., 2015)

Furthermore, transcriptional regulation of NMPs is controlled by the FGF, Wnt and bone morphogenic protein (BMP) signaling pathways (Goto, Kimmey, Row, Matus, & Martin, 2017; Row et al., 2018; Turner et al., 2014). Expression of *T* and *Sox2* in these cells is induced by FGF and Wnt signals which arise from the CLE and PS. *T* in turn has a positive effect on Wnt signaling thereby creating a positive feedback effect (B. L. Martin & Kimelman, 2008). BMP signals that originate from epiblast cells that are lateral and posterior to CLE, suppress *Sox2* expression, and thereby also define the positional identity of the NMPs. It is possible that even though *Sox2* and *T* are co-expressed in the NMPs, they might mutually downregulate each other (Gouti et al., 2017; Javali et al., 2017; Koch et al., 2017; Takemoto et al., 2011).

NMPs in Wnt activated mutants of *T* have a high *Sox2* expression (Gouti et al., 2014). In mouse, the PSM marker *Tbx6*, which is also a T-box gene, represses *Sox2* (Li & Storey, 2011; Takemoto et al., 2011) . On the other hand, there are also several lines of evidence showing *T* repression by *Sox2*. Homozygous deletion of the Sox2 N1 enhancer in mouse resulted in a higher amounts of presomatic mesodermal precursors and larger somites (Yoshida et al., 2014) and conversely an overexpression of *Sox2* resulted in more neuroectoderm and less mesoderm to be formed through *T* repression (Thomson et al., 2011; Zhao, Nichols, Smith, & Li, 2004).

In order to understand the mechanisms and regulation of NMPs several laboratories have performed differentiation of ESC (embryonic stem cells) to NMPs and their sublineages. All of these experiments used activation of Wnt signaling as a strategy to generate NMP-like cells. The appearance of a small population that is double positive when mEpi cells were cultured with FGF, activin A and CHIRON for 48h was observed in initial attempts to generate NMP like cells (Tsakiridis et al., 2014). CHIRON activates Wnt signaling through degradation of Gsk3β thereby stabilising βcatenin. A more efficient method of generating NMPs was shown in the absence of activin A, where mouse and human ESC were differentiated with FGF2 and CHIRON. This experiment resulted in 80% of T+/Sox2+ cells in the culture (Gouti et al., 2014). Continuous activation of Wnt (with CHIRON) in NMPs further generate mesodermal sublineages, *in vitro*. The bipotent nature of NMPs has also been confirmed by their ability to generate neural tissue in the absence of CHIRON, upon exposure to Retinoic acid (RA) (Gouti et al., 2014; Turner et al., 2014). Furthermore, the functionality of these *in-vitro* generated NMP-like cells have been tested by transplantation into chicken embryo. Grafted NMPs contributed to neural and somatic tissue in chick embryo providing additional evidence of their bipotent nature (Gouti et al., 2014).

2.3 MESODERMAL SUBLINEAGES

The mesoderm is first formed in the PS during gastrulation and is later generated in the tailbud region. The mesodermal cells that flanks the notochord gives rise to paraxial, intermediate and lateral plate mesoderm (James & Schultheiss, 2003). Expression of BMP inhibitors along the axis creates a BMP gradient which then specifies mesoderm subtypes along the mediolateral axis (Pourquié et al., 1996; Tonegawa & Takahashi, 1998). The bipotent axial progenitors that suppress *Sox2* expression and retain *T* expression give rise to presomatic paraxial mesoderm (PSM) (Takada et al., 1994). Additionally, a population of mesodermal progenitors exists, (Fig 2.4) which are at the caudal end of the primitive streak, committed to the mesodermal

sublineage and do not form neural tissue even upon forced expression of Sox2 (Wymeersch et al., 2016). These Lateral/paraxial mesodermal progenitors (LPMP) (Fig 2.4) do not require Wnt signals but are dependent on Bmp4 signals for maintenance of T expression. Depending on the position of cells in LPMP population and their exposure to BMP inhibitors that arise from the node (Pourquié et al., 1996; Tonegawa & Takahashi, 1998), they could either give rise to paraxial or lateral mesoderm.

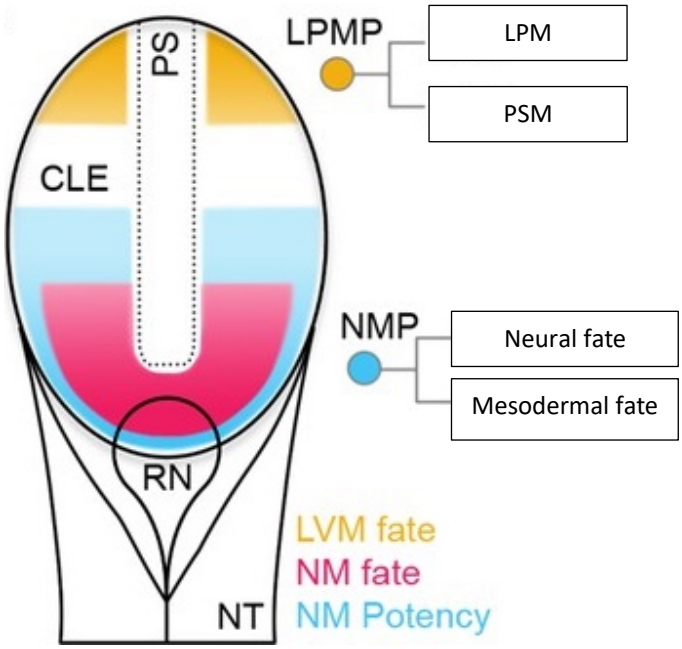

Figure 2.4:
Caudal progenitor zone in embryo consists of two progenitor populations – NMPs and LPMPs. (Wymeersch et al., 2016)

The paraxial mesoderm gives rise to PSM which in turn differentiates into somites of the cervical, lumbar and thoracic regions. This is followed by the specification of somites (Christ, Huang, & Scaal, 2004). The somites form the cartilage of vertebrae and ribs, rib cage muscles, back muscles body wall and limbs (Fig 2.6) (Ben-Yair & Kalcheim, 2005; Christ et al., 2004; Nguyen et al., 2014). Commitment of somites to these axial tissues occurs after the formation of somites. Cells of the paraxial mesoderm are exposed to Noggin produced by the notochord, which confers a protective effect against the BMPs. Protection from BMPs is thus essential to avoid lateralization of the mesodermal cells (Pourquié et al., 1996; Tonegawa & Takahashi, 1998). Transplantation experiments, where Noggin expressing cells were grafted into the LPM region resulted in the formation of PSM (Tonegawa & Takahashi, 1998). This shows that both these mesoderm sublineages arise from common precursors and the importance of BMPs in cell fate

outcome. In addition to the inhibition of BMP signals, the formation of PSM requires Wnt signaling. Lack of Wnt signaling results in the absence of PSM progenitors and somites in mouse embryo (Takada et al., 1994). Wnt further regulates Brachyury (T), *Tbx6* and *Msgn1* which are important transcriptional factors for PSM specification (Fig 2.5) (Takemoto et al., 2011; Wittler et al., 2007) . *T* and *Tbx6* are T box transcription factors both of which are expressed in the primitive streak, and tailbud. Additionally *T* is expressed in the early mesoderm, notochord plate (Wilkinson, Bhatt, & Herrmann, 1990) and notochord and *Tbx6* in the PSM (Chapman, Agulnik, Hancock, Silver, & Papaioannou, 1996). Mutants of T have no or insufficient mesoderm, elucidating the importance of T in mesoderm formation (Gruneberg, 1958; Wilkinson et al., 1990). *Tbx6* which also regulated positively by *T*, is expressed in early PSM and is downregulated in the somites (Chapman et al., 1996).

Tbx6 represses *Sox2* thereby leading to PSM commitment (Fig 2.5). Supporting this, loss of function Tbx6 mice developed ectopic neural tubes at the expense of PSM (Takemoto et al., 2011).

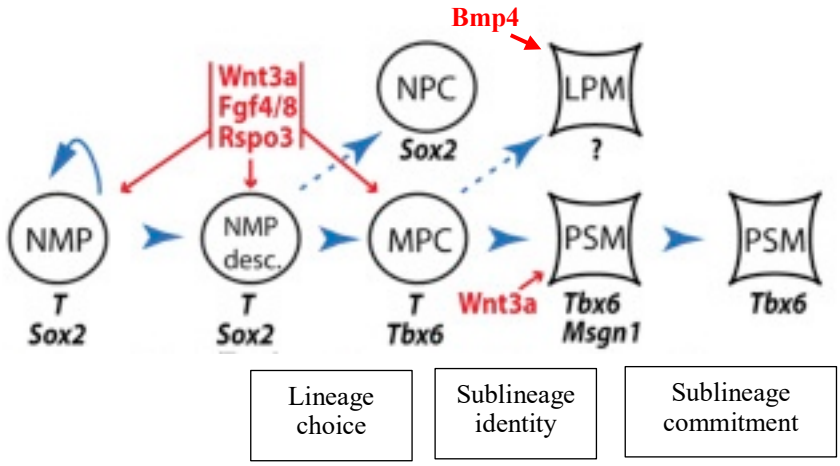

Figure 2.5:
Commitment factors and external signals that drive lineage choices and sublineage commitment. (Koch et al., 2017)

Msgn1 on the other hand is continuously expressed from gastrulation to somite formation (Jeong Kyo Yoon & Wold, 2000). Overexpression of *Msgn1* leads to an expansion in the cells expressing *Tbx6* in the trunk and thereby an expansion of PSM. This result indicates that *Msgn1* positively regulates *Tbx6*. The loss of *Msgn1* results in reduced expression of *Tbx6* in PSM and lack of somites in mice (Chalamalasetty et al., 2014) .

The lateral plate mesoderm further differentiates into the splanchnic and somatic mesoderm (Funayama, Sato, Matsumoto, Ogura, & Takahashi, 1999). The heart , blood vessels and blood cells arise from the splanchnic mesoderm and somatic mesoderm contributes to the mesodermal

tissue of the limbs (Fig 2.6) (Linask, 1992). Similar to the axial and paraxial mesoderm the LPM also originates during gastrulation between ectoderm and endoderm (Davidson & Zon, 2004; Lawson, Meneses, & Pedersen, 1991; Rosenquist, 1970; P. P. Tam & Beddington, 1987) .

The signaling cascades of BMP and Nodal, play an important role in the anterior-posterior and dorso-ventral patterning in the embryo and in the early LPM formation (Arnold & Robertson, 2009; Hill, 2018; Martinez Arias & Steventon, 2018). The ventral side of the embryo is exposed to high levels of BMP signal which confers the boundaries for LPM development in all vertebrates (Ferretti & Hadjantonakis, 2019; Nishimatsu & Thomsen, 1998). Although both BMP and Nodal are required for LPM formation (Xu, Houssin, Ferri-Lagneau, Thisse, & Thisse, 2014), they are not the only factors required. A more complex signaling system which involves Wnt, FGF, RA (Fürthauer, Van Celst, Thisse, & Thisse, 2004; Holley & Ferguson, 1997; Rossant & Tam, 2009; Schier & Talbot, 2005) also influence the establishment of LPM domains in the embryo.

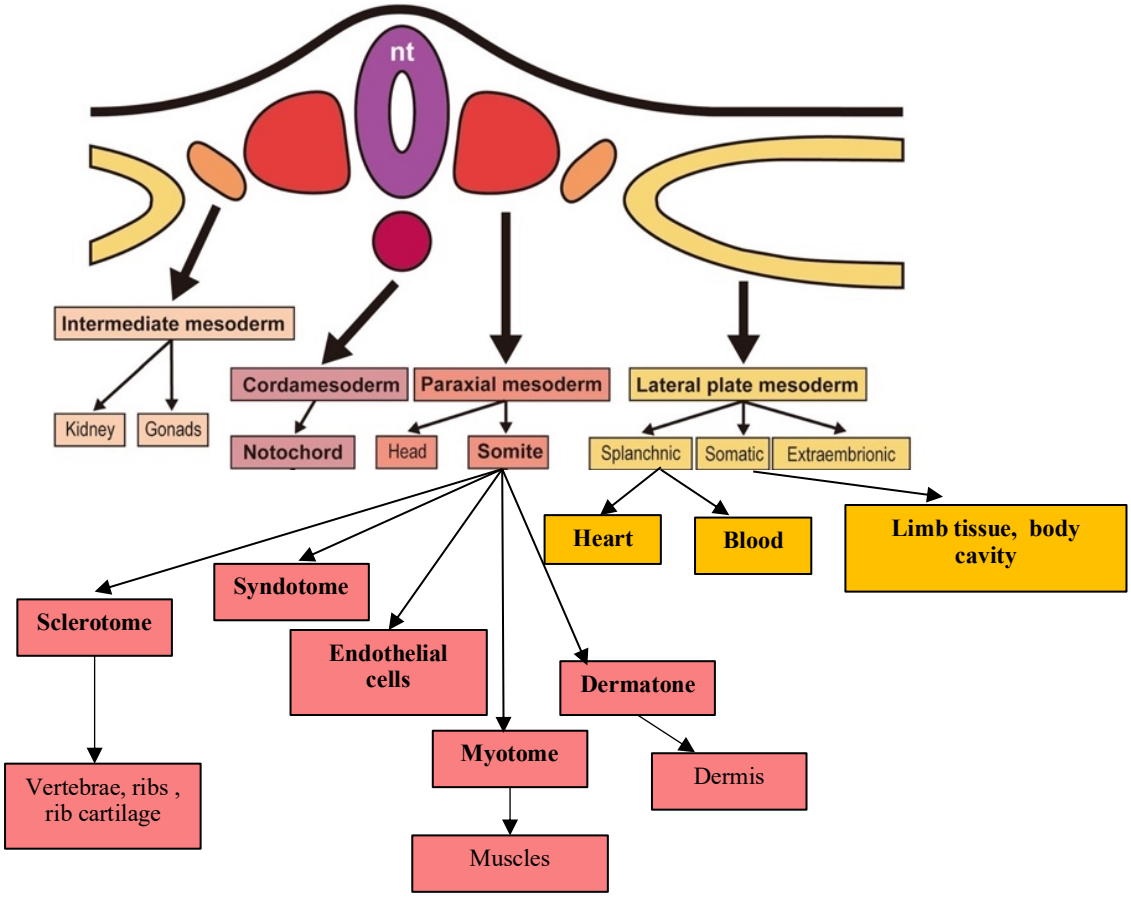

Figure 2.6:
Illustration of the fate of mesoderm sublineages formed in the embryo. Image adapted from (Gilbert & Barresi, 2017)

Even though, the LPM is not molecularly defined because of the complexity of signals involved in their formation, the post gastrulation expression of several transcription factors has helped to understand the LPM patterning. The transcription factors – *Foxf1*, *Hand1*, *Hand2*, *Gata4*, *Bmp4*, *Prrx1* have been used in mouse and chick to identify LPM (Becker, Eid, & Schughart, 1996; Firulli, McFadden, Lin, Srivastava, & Olson, 1998; J. F. Martin & Olson, 2000; Rojas et al., 2005). *Foxf1* along with *Irx3* and *Tbx3* plays an important role in determining whether LPM develop into splanchnic or somatic mesoderm (Mahlapuu, Ormestad, Enerbäck, & Carlsson, 2001; Rallis, Del Buono, & Logan, 2005). Expression of *Foxf1* is maintained as early LPM differentiates into splanchnic mesoderm. Maintenance of *Foxf1* causes a downregulation of *Irx3,* which is required for somatic mesoderm development (Mahlapuu et al., 2001). Gata6 is expressed in nascent LPM, but is also an important transcription factor for heart development and hence a marker for the splanchnic mesoderm (Olson, 2006; Watanabe & Buckingham, 2010). *Foxf1* is expressed universally in the LPM before the subdivision. When somatic mesoderm is generated, they express *Irx3* and only the splanchnic mesoderm continues to express *Foxf1* (Funayama et al., 1999).

2.4 BONE MORPHOGENIC PROTEINS

Bone morphogenic proteins (BMP) belong to the TGFβ superfamily of proteins and was initially thought to induce bone and limb formation. Later it has been shown to play an important role in embryogenesis (Bragdon et al., 2011). Type1 and type2 transmembrane serine/threonine kinases are activated when BMP ligands bind to them. Activated receptors phosphorylate Smad – 1,5,8 which then forms a complex with Smad4 to bind BMP response element in the nucleus and transcribe target genes (Bragdon et al., 2011). BMPs are generated as an inactive pro-protein that needs to be cleaved by proprotein convertase to yield the active ligand. The pro-domain, also cleaved by the enzyme, helps in the folding and secretion of active protein (Hammonds Jr. et al., 1991).

BMP expression during gastrulation is required for mesoderm formation (Beppu et al., 2000; Mishina, Suzuki, Ueno, & Behringer, 1995; Winnier, Blessing, Labosky, & Hogan, 1995) as well as patterning after gastrulation. This has been demonstrated in mice deficient for BMP4 ligand as well as mice deficient with the receptor. In addition, BMP4 is also required at later stages for mesoderm lineage specification (Czyz & Wobus, 2001; Loebel, Watson, De Young, & Tam, 2003; Nakayama, Lee, & Chiu, 2000; Ng et al., 2005; Suzuki et al., 2006) . Further, BMP4 has been identified to play a role in tailbud growth by maintaining mesodermal progenitors in the mouse

tailbud and somite differentiation at later stages of development in both the chick and frog embryo (Row & Kimelman, 2009; Sharma et al., 2017) .

As mentioned earlier, BMP4 is a key morphogen which is required to drive LPM formation in embryo. Exploiting this role of BMP4 in LPM generation, several *in-vitro* studies have been conducted to differentiate HPSC to LPM using BMP4 along with FGF2 (Cheung, Bernardo, Trotter, Pedersen, & Sinha, 2012). These LPM cells have further been differentiated into epicardial cells (Iyer et al., 2015) (splanchnic mesoderm) to additionally validate the identity of the differentiated cells.

In addition to BMP4 another protein belonging to the same family, BMP11 (GDF11), also plays a role during development, belongs to the TGFβ superfamily of proteins, binding to type 1 TGF superfamily receptors, mainly Activin receptor like kinases 4 and 5 (ALK4, ALK5) (Andersson, Reissmann, & Ibáñez, 2006) . This protein plays a role in the anterior posterior (A-P) patterning of the growing embryo (Wellik, 2007; Wilson et al., 2009; Wymeersch et al., 2016). GDF11 is initially expressed around E8 in the primitive streak and later strongly expressed in the tailbud region of mouse embryo around E9.5 (McPherron, Lawler, & Lee, 1999; Nakashima, Toyono, Akamine, & Joyner, 1999; P. P. L. Tam & Tan, 1992). The growth of the trunk is facilitated by the contribution of cells of the axial progenitors to the PSM. The positional identity of the somites which then form the thoracic and lumbar regions is predetermined in the PSM by morphogens that are secreted from the primitive streak (Carapuço, Nóvoa, Bobola, & Mallo, 2005; Kieny, Mauger, & Sengel, 1972; Nowicki & Burke, 2000; Saga & Takeda, 2001). These morphogens control the expression of Hox genes and thereby ensure precise body patterning of the embryo (Tickle, Summerbell, & Wolpert, 1975; L. Zhang, Lander, & Nie, 2012) . GDF11 has been identified as a morphogen that contributes to the axial identity of cells by modifying Hox gene expression in the vertebral axis (Jurberg, Aires, Varela-Lasheras, Nóvoa, & Mallo, 2013; Matsubara et al., 2017; McPherron et al., 1999). The role of GDF11 in A-P patterning has been shown in several experiments where GDF11 was knocked out or hyperactivated in mice. Hyperactivation of GDF11 results in posteriorly directed vertebral transformations (Lee & Lee, 2013) and GDF11 null mice show alterations in the vertebral axis as a result of expansion of anterior Hox genes and shifting of the posterior Hox genes more posteriorly (Jurberg et al., 2013; Liu, 2006; McPherron et al., 1999). Ectopic expression of *Gdf11* in chick embryos resulted in an anterior displacement of posterior Hox genes (Liu, 2006) which support the evidence that *Gdf11* repress anterior Hox genes and stimulate posterior Hox genes (Aires, Dias, & Mallo, 2018). Although the exact mechanism of action of GDF11 is not yet clearly known, recent studies have indicated

that GDF11 does not act as a global morphogen that is secreted in the tailbud, but rather acts locally to provide tissue identity along the axis (Suh et al., 2019). GDF11 also plays a central role in trunk to tail transition by reallocating bipotent NMPs from the anterior PS to the tailbud region (McPherron et al., 1999). Expansion of tailbud progenitors that is observed in the mutant embryo as well as *in-vitro* by culturing cells of the tailbud progenitor population from Gdf11$^{-/-}$ embryo (Aires et al., 2019) combined with the observation of mutants having longer trunks and shorter tails indicated the role of GDF11 in the timely regulation of trunk to tail transition (Jurberg et al., 2013). On the other hand, continuous expression of *Oct4* results in extension of trunk length (Aires et al., 2016). This has been shown via transgenic expression of *Oct4* in mice, resulting in an extended trunk. Additionally, snake embryos maintain *Oct4* expression for longer periods thereby delaying the expression of posterior Hox genes resulting in an extended trunk (Aires et al., 2016). These findings support that maintenance of OCT4 is required for trunk extension (Aires et al., 2016; DeVeale et al., 2013). Since Oct4 and Gdf11 seem to have opposite functional effects on trunk growth, it is possible that *Gdf11* facilitates the trunk to tail transition via downregulation of *Oct4,* although the expansion of tailbud NMPs is *Oct4* independent (Aires et al., 2019).

2.5 HOX CLUSTER OF GENES

The Hox gene cluster plays an important role in conferring positional identity of cells in an embryo during development. During development, these genes are expressed co-linearly, thus playing an important role in the segmentation of vertebrate body plan.

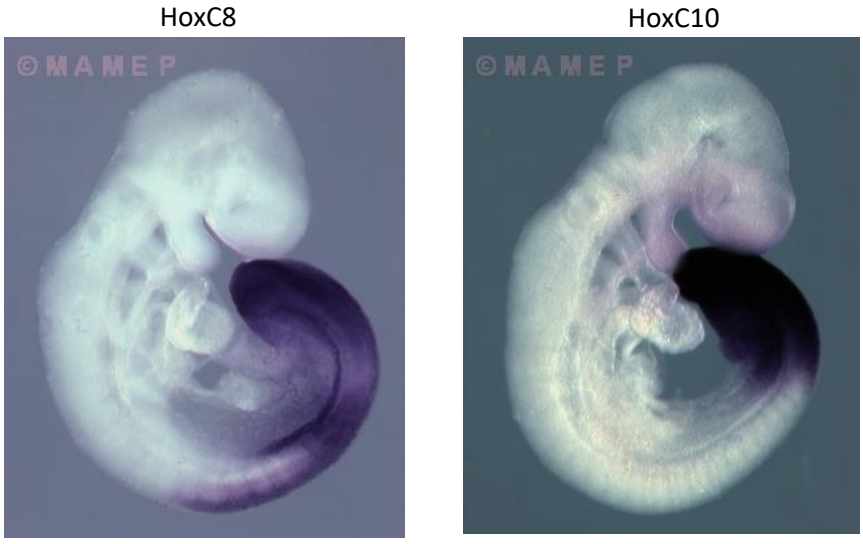

Figure 2.7:
Whole mount in-situ hybridisation of embryo showing localized expression of HoxC8 and HoxC10 in the trunk region. E9.5

Hox genes are first expressed during early gastrulation, the time point where the body axis begins to develop (Duboule, 1994). Two of these genes, HoxC8 and HoxC10 are expressed during the growth of the embryonic trunk (Fig 2.7). HoxC8 is essential for mouse forelimb and skeletal development (Shashikant & Ruddle, 1996) and this has been shown in HoxC8 null mice, which show neuromuscular defects in forelimbs and defects in ribs and vertebrae of the thorax (Le Mouellic, Lallemand, & Brûlet, 1992). Furthermore HoxC8 regulates Wnt, BMP and FGF indirectly (Lei, Juan, Kim, & Ruddle, 2006). HoxC10 is strongly expressed in the hindlimb region of mice embryo (Peterson, Jacobs, & Awgulewitsch, 1992) and is expressed in the late trunk stages.

3. OBJECTIVE

In this project we have attempted to 1. Elucidate the role of BMP11(GDF11) and BMP4 during differentiation of NMP-like cells into paraxial mesoderm and lateral plate mesoderm with the help of knock-out and rescue experiments. 2. Establish a differentiation protocol for generating LPM from NMPs with use of BMP4. This protocol would be similar to the events that occur *in-vivo*. Furthermore, generation of sufficient LPM-like cells would provide material for additional analysis like ChIP-seq experiments to identify LPM lineage commitment genes and markers. 3. To establish a conditional Bmp4 knockout cell line with CRE driven by HoxC8 and HoxC10 genes. Bmp4 null ESCs exhibit incomplete gastrulation resulting in death of the embryo. Future prospects of understanding the role of Bmp4 through *in-vivo* experiments require Bmp4 at early timepoints for successful gastrulation. Hence a conditional KO cell line is necessary.

4. MATERIALS AND METHODS

4.1 CELL CULTURE AND DIFFERENTIATION PROTOCOL

4.1.1 CELL CULTURE

Mouse embryonic stem cell (mESC) lines modified from F1G4 mice cell line (George et al., 2007) were maintained in embryonic stem (ES) medium containing 1:10,000 LIF (Murine Leukemia Inhibitory Factor ESGRO) (ES+LIF) in plates coated with mitotically inactive NMRI primary embryonic fibroblast at 37°C and 7.5% CO_2. Fibroblast cells were plated at a density of 3-4 x 10^4cells/cm^2 on 0.1% gelatinised (Sigma #G-1393) plates. All cell lines used

for the differentiation experiments and CRISPR experiments were modified from F1G4 mESC. The F1G4 hybrid parent ES cell line was generated by crossing 129 and C57BL/6 mice.

Table 1 : Contents of ES medium

Components of ES medium	**Working concentration**
Knockout Dulbecco´s Modified Eagle´s Medium (DMEM), 4500mg/ml glucose with sodium pyruvate (Gibco)	400ml
ES cell tested fetal calf serum (FCS)	15%
100X glutamine, 200mM (Lonza)	2mM
100X penicillin (5000U/ml) / streptomycin (5000U/ml) (Lonza)	1X
100X non-essential amino acids (Gibco)	1X
500X 2-mercaptoethanol (2-ME) (55mM Invitrogen)	1X
100X nucleosides (Chemicon)	1X

4.1.2 FREEZING AND SPLITTING OF CELLS

mESC colonies were split and/or frozen when 80% confluence was reached. Plates were first washed twice with PBS (in the case of cells cultured in 2i+LIF cells were collected in a falcon to avoid any loss of mESC colonies after PBS wash). Colonies were then disaggregated with either 1 ml of accutase in the case of 2i+LIF or 1 ml 1X Trypsin (0.5g/l)-EDTA (0.2g/l) solution (Gibco) (T/E) for cells grown on Corning Synthemax II-SC Substrate (SIIC) or feeder coated plates respectively and incubated at 37ºC for 5-10min. The enzyme was then neutralised with 2ml of PBS or ES medium and the plates were washed twice with PBS. Harvested cells were then pelleted at 1000rpm for 5min. mESC were then resuspended in 1ml of appropriate medium and counted using the Luna automated cell counter, haemocytometer (Biosystems). Required number of cells were then re-plated in 6cm plates or cells were frozen. In order to freeze mESC, cells were first resuspended in 0.5 freezing volume of 2X resuspension medium (ES cell medium containing 20% FCS), following which same volume of 2X freezing medium (ES cell medium with 20 % FCS and 20% DMSO (Dimethyl sulfoxide)) was added. 1ml

aliquots was transferred to each freezing vial and frozen in -70°C O/N (Overnight) before being transferred to liquid nitrogen.

4.1.3 CULTURING mESC FOR DIFFERENTIATION EXPERIMENTS

mESC colonies on NMRI feeder plates were passaged by washing with PBS and incubated with 1ml T/E in order to obtain single cells, which were then plated on 6cm CellBIND surface dishes (Corning) coated with SIIC in 2i+LIF medium (Koch et al., 2017; Sim et al., 2017) for at least 2 passages. The 2i+LIF medium comprised of Advanced Dulbecco's Modified Eagle Medium F12 (DMEM/F12) (Gibco) and Neurobasal medium (Gibco) (1:1), supplemented with 1X Pen/Strep (Lonza), 1X Glutamax (Gibco), 1X NEAA (Gibco), 1X Na-Pyruvate (Gibco), 0.11mM 2-ME (Gibco), 1X N2 supplement (Gibco), 1X B27 supplement without vitamin A (Gibco), 1µM PD 0325901 (Stemgent), 3µM Chiron 99021 (Stemgent) and 1X LIF. These mESC with ground state pluripotency were then used for differentiation. Differentiation experiments were performed in N2B27 medium (Gouti et al., 2014; Turner et al., 2014) with the following components: Advanced Dulbecco's Modified Eagle Medium F12 (DMEM/F12) (Gibco) and Neurobasal medium (Gibco) (1:1), 1X N2 supplement (Gibco), 1X B27 supplement without vitamin A (Gibco), 40µg/mL BSA Fraction V 7.5% (Gibco), 0.11mM 2-ME (Gibco), 2mM L-Glutamine (Lonza) and 1X Pen/Strep (Lonza).

4.1.4 GENERATION OF BMP4 CONDITIONAL KNOCK-OUT CELL LINE

4.1.4.1 ELECTROPORATION OF CRISPR PLASMID INTO BAC-BMP4

Bmp4 KO mES cell line were cultured on feeder plates in ES+LIF medium for 3 passages following which 1 million cells were plated on 10cm dish with NMRI feeder cells. 3 million cells in PBS were taken for electroporation with 5µg PX459 (CRISPR plasmid), 10µg bacterial artificial chromosome (BAC) and the 5µg CRIPR template. As a control, 5µg of BAC was electroporated into the KO mESC line. Plasmid and BAC DNA were electroporated into BMP4 KO cells with Gene Pulser Cuvette (Bio-Rad) using Gene Pulser (BioRAd). Electroporation was carried out with a voltage of 240V and 500µF. Following electroporation, cells of the cuvette were added to 10ml ES medium and centrifuged.

Cells electroporated with the BAC are here on called as Bmp4-ΔloxP-Neo and the cells electroporated with BAC and CRISPR plasmid are called floxed-ΔloxP-Bmp4-ΔloxP-Neo. Both cell lines were resuspended in ES medium and plated on three 6 m dishes with appropriate feeder cells. Bmp4-ΔloxP-Neo cells were plated on EF1N feeder plates (feeder with NEO resistance) and floxed-ΔloxP-Bmp4-ΔloxP-Neo cells were plated on DR4 feeders (feeders with

NEO and PURO resistance) and cultures for 36h in ES+LIF medium. Bmp4-ΔloxP-Neo cells were then selected with 350µg/ml of Neomycin (NEO) for 7 days and floxed-ΔloxP-Bmp4-ΔloxP-Neo were selected with 250µg/ml of NEO + 1µg/ml of puromycin (PURO) for 3 days followed by 250µg/ml NEO for 4 more days. Colonies were picked depending on enough amount and size of colonies grown in the plate.

4.1.4.2 PICKING OF ES CELL COLONIES

Firstly, plates were washed twice with PBS. Individual colonies in PBS were picked into 30µl of T/E in wells of a 96 well U-bottomed plate. Colonies in trypsin were then incubated at 37°C for 10min. Activity of trypsin was neutralised with the addition of 60µl of ES+LIF medium and cells were mixed well to obtain a single cell suspension. Single cell suspension of each clone was then added to 500µl of ES+LIF medium in 48 well plates coated with NMRI feeder cells.

4.1.4.3 GENOTYPING AND FREEZING

When the cells reached their confluence on the 48 well plate, colonies were washed with PBS and trypsinised with 100µl of T/E followed by incubation at 37°C for 10min. Trypsin was neutralised with 400µl of resuspension buffer and mixed thoroughly with a multichannel pipette. Cells were then added to cryopreservation tubes containing 400µl of freezing medium and frozen at -70°C O/N.

An additional 500µl of ES medium was added to the 100µl of cells in 48 well plate and transferred to another 48 well plate coated with 0.1% gelatin. These cells were allowed to grow for 2 days and later lysed using 500µl of Lairds buffer containing 1:100 proteinase K. Cells were incubated for 30min with the lysis buffer and then transferred to 1.5ml tubes to be incubated at 56°C shaker O/N. DNA was then precipitated using 500µl of Isopropanol (IPA) followed by gently inverting the tubes and centrifuged for 30min at 15000rpm. DNA pellets were then washed with 1ml of 70% EtOH and centrifuged again for 20min. Pellet was resuspended in 30µl of TE after EtOH was completely removed.

This DNA of all clones were used as a template for genotyping to verify the BAC integration. Takara Hot Start PCR protocol and GoTaq was used for the purpose of genotyping and the presence of correct BAC integration was verified on a 1% agarose gel. Clones were also sequenced around the 5´loxP site with the Primer Pair 4 (Table 2).

Primers used for genotyping are as follows :

Table 2 : List of primers used for genotyping of cells after electroporation

Primer Pair	Forward primer	Reverse Primer	Size of PCR product
1-Bmp4-ΔloxP-Neo	C711	S22	403 bp
2- Bmp4-ΔloxP-Neo , ΔloxP-Bmp4-ΔloxP	S85	S62	898 bp
3- Bmp4-ΔloxP-Neo , ΔloxP-Bmp4-ΔloxP	C577	S61	985 bp
4-ΔloxP-Bmp4-ΔloxP	C710	S86	1,219 bp
5-ΔloxP-Bmp4-ΔloxP-Neo	C710	Lox P forward	1,300 bp and 300 bp
6-Bmp4-ΔloxP-Neo	C710	Lox P forward	1,300 bp

4.1.4.4 EXPANSION OF ES CELLS FROZEN FROM 48 WELL PLATES

Subclones of Bmp4-ΔloxP-Neo and floxed-ΔloxP-Bmp4-ΔloxP-Neo that were frozen from the 48 well plate was thawed and plated on 1 well of a 6 well plate with NMRI feeder cells and cultured in ES+LIF medium for two days. Based on the density of colonies observed after two days, cells were split and plated on 6 cm plates coated with feeders at a density of ½ 6 well or 1/3rd 6 well in ES+LIF and further cultured for two days. 0.5 million cells of each clones were then plated again on 6cm plates with feeder and allowed to grow in ES+LIF for two more days.

4.1.5 DIFFERENTATION OF mESC TO NEURAL MESODERMAL PROGENITORS (NMPs)

Mouse embryonic stem cells with T::H2B-mCherry and Sox2::H2B-Venus reporter BACs cultured in 2i+LIF media (Koch et al., 2017) was digested with 1ml accutase and plated as single cells in 6 well plates coated with SIIC at a density of 5000cells/cm^2. These cells were plated in N2B27 medium supplemented with 10ng/ml FGF2 for two days (D1-D2) and consecutively one day of exposure to 10ng/ml FGF2 + 5μM CHIR99021 (D3) (Gouti et al., 2014).

4.1.6 DIFFERENTIATION INTO PARAXIAL MESODERM

mESC line with of T::H2B-mCherry and Sox2::H2B-Venus reporter BACs was used in order to establish the mesoderm differentiation protocol. Further specification of above mentioned NMP-like cells into pre-somatic mesoderm (PSM)/mesoderm progenitor was obtained by culturing the NMP like differentiated mESC for an additional 72h in N2B27 + 5µM CHIR99021 (D4-D6) (Gouti et al., 2014) (Fig4.1) .

4.1.7 DIFFERENTIATION INTO LATERAL PLATE MESODERM

mESC line with Tbx6::H2B-mCherry and Foxf1::H2B-Venus reporter BACs was used to establish the differentiation of NMPs to LPM. Upon obtaining mESC differentiated into NMPs (D1-D3), cells were cultured under two different conditions. mESC was cultured in the presence of 20ng/ml BMP4 (B20) in N2B27 media or in the presence of 20ng/ml FGF2 + 20ng/ml BMP4 (FB20) in N2B27 for 36 hours (D4-D6) (Fig4.1).

Cells from each time point were washed twice with PBS following which colonies were disaggregated using 1ml accutase and incubated for 5-10min. Neutralisation of the enzyme was done by adding 2ml of PBS, with which the wells were also washed to obtain all cells. Cell pellets obtained by centrifugation for 5min at 1000rpm were resuspend in 250µl of PBS. 100µl from the sample was taken for Real-Time PCR (qPCR) profile of total cells and the rest was used for FACS. qPCR was performed to assess the gene expression profiles of early as well as late LPM markers.

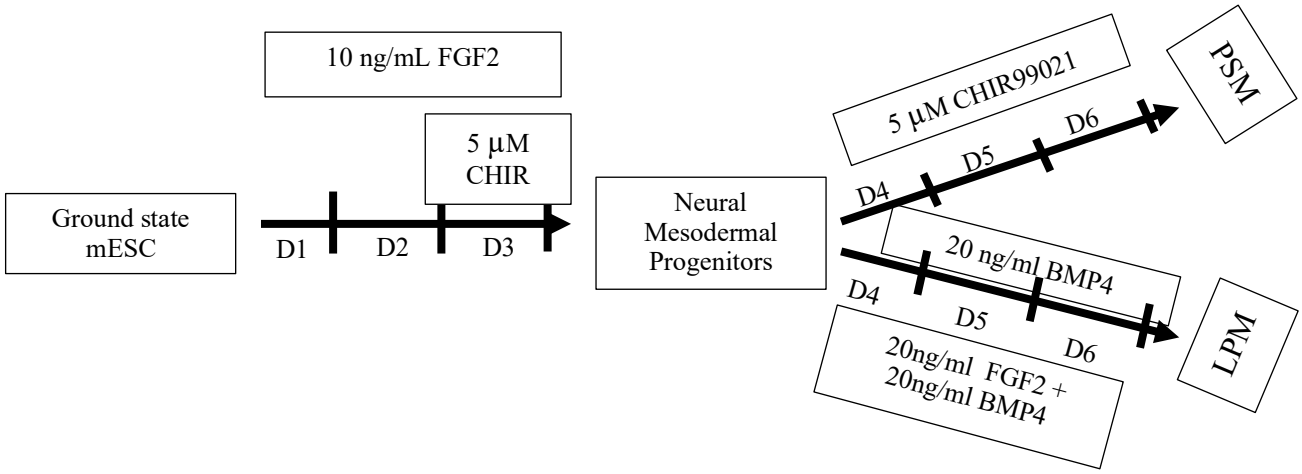

Figure 4.1:
A schematic representation of differentiation of mESC to NMPs and further differentiation into PSM or LPM.

4.2 DIFFERENTIATION OF GDF11 MUTANTS INTO PARAXIAL MESODERM

An mESC line in which the 3rd exon of Gdf11 is knocked-out containing T::H2B-mCherry and Sox2::H2B-Venus reporter BACs was differentiated into NMPs and further into mesoderm progenitor / paraxial plate mesoderm as per the above mentioned differentiation protocol.

Colonies of each day were then digested with accutase to obtain a single cell suspension and later analysed and sorted by Fluorescence activated cell sorting (FACS) (BD FACS Aria II). Cells were sorted based on mCherry (T^{mC}), Venus ($Sox2^{V}$) or mCherry + Venus (T^{mC} / $Sox2^{V}$) reporter expression. In addition to FACS, gene expression profiles of differentiated cells for mesodermal progenitor and NMP markers were analysed by qPCR.

4.3 DIFFERNTIATION OF GDF11 MUTANTS INTO LATERAL PLATE MESODERM

An mESC line in which the 3rd exon of Gdf11 is knocked-out containing T::H2B-mCherry and Sox2::H2B-Venus reporter BACs was differentiated into NMPs and further into lateral plate mesoderm as per lateral plate differentiation protocol. For this experiment the cells were treated with FB20 condition after the initial three days of differentiation into NMPs.

Colonies of each day were then incubated with 1ml accutase to obtain a single cell suspension and analysed for expression of early and late lateral plate mesoderm markers by qPCR.

4.4 RESCUING THE EFFECTS OF GDF11 IN KNOCK-OUT CELLS

GDF11 KO mESC line with of T::H2B-mCherry and Sox2::H2B-Venus reporter BACs was differentiated for 3 days into NMP like cells. After the initial three days, some cells were induced with 20ng/ml of recombinant GDF11 along with 5µM CHIR99021. Cells induced at D3 were analysed by FACS and qPCR at the following timepoints – 0.5 days, 1.5 days, 2.5 days after GDF11 addition. Cells of the same cell line were also induced at D3.5 of differentiation and analysed after 1 day, 2 day, 3 days of GDF11 addition. As a control in both points of rescue, 4mM concentration of HCl was added along with 5µM CHIR99021.

4.5 RNA PURIFICATION AND REVERSE TRANSCRIPTION

Total RNA was isolated using the RNeasy Micro Kit (Qiagen) (RNA clean up and concentration protocol) as per the manufacturer's instructions. Cells sorted by FACS were sorted into tubes containing 350µl RLT buffer and 3.5µl 2-ME. The volume of RLT buffer,

100% EtOH and 2-ME were adjusted according to the number of cells that were sorted. After the addition of RW1 buffer, DNase 1 digestion step was performed with 70µl of RDD buffer, 10µl of DNase 1 (RNase free DNase1 set – Qiagen) and 1µl of DNase 1 Recombinant, RNase free (Roche) to remove genomic DNA.

First strand of cDNA synthesis was performed using the QuantiTect Reverse Transcription Kit (Qiagen) with template RNA concentration of 200ng in 12µl of nuclease free H_2O. Genomic DNA elimination step was included and incubated at 42°C for 2 minutes after addition of 2µl gDNA wipeout buffer, 7X (supplied with the kit), followed by cDNA synthesis at 42°C for 30 min on adding Reverse Transcription master mix. Heat inactivation of the reverse transcriptase was done by incubating the reactions at 95°C for 3min. Synthesised cDNA was then diluted with 80µl of nuclease free water and stored at -20°C until it was used for qPCR.

Table 3 :

T	Fw - AACTGGTCTAGCCTCGGAGT Rv - CTCACAGACCAGAGACTGGG
Sox2	Fw - AGCGCATGGACAGCTACG Rv - CATCGGTTGCATCTGTGC
Oct4	Fw - TCAGCTTGGGCTAGAGAAGG Rv - TGGGAAAGGTGTCCCTGTAG
Tbx6	Fw -GGCCAGTGACTGATACTCGG Rv - CCTGAGCTTGGAGAACCAGG
Msgn1	Fw - GCCTGGACTCTTCTGACACC Rv - TAGGACTCCAGAGAAGGAGCTG
Pax3	Fw - GCGTCTCTAAGATCCTGTGCAG Rv - GATTTCCCAGCTAAACATGCCCG
Gdf11	Fw - TTTCGCCAGCCACAGAGCAACT Rv - CTCTAGGACTCGAAGCTCCATG
Foxf1	Fw - CCTGTCTGGCAGCATCTCCAC Rv - GACTGTGAGTGATACCGAGGGA
Hand1	Fw - CAAAAAGACGGATGGTGGTCGC Rv - TGCGCCCTTTAATCCTCTTCTCG
Tbx3	Fw - GGTTTTCGAGACACTGGCAATGG Rv - TGGGCAAAGCAGTTGAAGGCTG
Gata6	Fw-ATGCGGTCTCTACAGCAAGATGA Rv - CGCCATAAGGTAGTGGTTGTGG
Irx3	Fw - TGTAGTGCCTTGGAAGTGGAG Rv - GCGTCCAGATGGTTCTGTG
Pmm2	Fw - AGGGAAAGGCCTCACGTTCT Rv - AATACCGCTTATCCCATCCTTCA
Nc2	Fw - CCCCTTTCTGAAGCACTCTG Rv - TAAGGCGTCATTTCCCAAAG

4.6 QUANTITATIVE PCR (qPCR)

Primers (oligos) for qPCR were designed using Primer3 software and all samples for each time point, were run as biological triplicates.

qPCR was performed using the StepOne plus RT PCR system (Applied Biosystems) with GoTaq qPCR master mix containing SYBR and 20µl of the CXR reference dye (Promega).

Pmm2 was used as the endogenous reference control and each plate had an internal reference control which was used to compare expression levels between the timepoints of differentiation.

Primer sequences used for the qPCR are mentioned in Table 3.

4.7 GENERATION OF BMP4 CONDITIONAL KOCKOUT IN EMBRYONIC STEM CELLS

4.7.1 CLONING OF FLOXED BMP4 EXON INTO PLASMID

4.7.1.1 PCR FOR THE INTRODUCTION OF LOXP SITES

PCR was performed using primers designed to introduce EcoRI restriction site and loxP sequence in the 3' UTR of the third exon and before the beginning of the third exon. 1µl of BAC DNA with BMP4 gene (RP23-77M3) in DH10β cells, prepared from 2mL overnight (O/N) (using the DNA prep protocol) culture containing Chloramphenicol (CHL), was taken in a reaction containing 0.5µl PrimeSTAR Hot start DNA Polymerase (Takara), dNTP mixture, 5X primeSTAR buffer (Mg 2+) and 1µl of each forward and reverse primer. The amplified DNA fragment along with the EcoRI and loxP sequence was verified on an agarose gel (1kb band) and purified from the gel using the QIAquick Gel extraction Kit (Qiagen).

The cycling protocol for the Prime star PCR (Takara) reaction is as follows:

Table 4 :

	98°C	5 min
	98°C	10 sec
Annealing temperature	60°C	10 sec
Elongation temperature	72°C	1min/kb
	72°C	7 min
	4°C	infinite

Table 5 : Primer pair used for loxP and EcoRI sequence insertion

	Primer name	Primer sequence
C583	Bmp4-flox-rv	3 **TTTTTTGAATTC*ATAACTTCGTATAGCATACATTATACGAAGTTAT***TGGTATGTGTAGGTGGTTGA 5
C584	Bmp4-flox-fw_new	3 **TTTTTTGAATTC*ATAACTTCGTATAATGTATGCTATACGAAGTTAT***CTCAGAAAAGCTCATGGGCC 5

Nucleotides highlighted in blue represent the sequence on BAC where the primers bind. Nucleotides in bold are the EcoRI recognition sequence. LoxP sequence is represented in bold and italics.

4.7.1.2 RESTRICTION DIGESTION AND PURIFICATION

Amplified PCR product and pR6K plasmid (vector purified from O/N LB with Ampicillin-AMP) was digested with EcoRI in 10x buffer B. 2µl of thermosensitive alkaline phosphatase was added to the digested vector plasmid to dephosphorylate the ends. 0.2µl of BSA was added to the digested PCR product to avoid unwanted cleavage. Vector and fragment digests were purified from agarose gel using the QIAquick Gel extraction Kit (Qiagen) and the concentration of DNA was measured using a nanophotometer (Implen).

4.7.1.3 LIGATION AND TRANSFORMATION

Ligation of vector and fragment was performed using the Rapid DNA ligation system (Promega). An insert to vector ratio of 2:1 was taken in a reaction along with 2X rapid ligation buffer, T4 DNA ligase and incubated at room temperature for 15-20min. As a control, ligation reaction containing only the pR6K plasmid was set up. Ligated plasmid was transformed into bacteria (Pir+ve) with Pir gene by heat shock method. Cells were then plated on agar with AMP and incubated at 37°C O/N. Colonies were inoculated in 5mL LB with AMP and kanamycin (KAN). Cells were incubated overnight at 37°C, 800 rpm.

4.7.1.4 PLASMID DNA PREPARATION AND SEQUENCING

Transformed plasmid DNA obtained from O/N cultures were then digested with XmnI in 10X buffer B (Promega) and size separated on 1% agarose gel to verify the correct orientation of

PCR fragment ligated into the vector. Plasmids containing the fragment in the right orientation were selected for sequencing with M13 Rv primer and PGK Rv primer.

Table 6 : Primer for sequencing the template plasmid

Primer name	Primer sequence
M13 reverse	CAGGAAACAGCTATGACC
PGK reverse	GAGGCGCTTTTCCCAAGG

4.7.2 HOMOLOGOUS RECOMBINATION OF FLOXED BMP4 EXON INTO BAC

4.7.2.1 TRANSFORMATION OF PSC101 PLASMID INTO BAC (WT.BMP4)

500µl of overnight culture of cells containing BAC was resuspended in 1mL LB with CHL and incubated at 37°C and 800rpm for 2h. Cells were then pelleted at 13,000rpm for 30sec and washed twice with 1.5mL cold cell culture grade water. E.coli cells containing BAC was then electroporated with 2µl of pSC101 plasmid , containing arabinose inducible Redα, Redβ, Redg and RecA proteins, under a voltage of 1.8kV.

Transformed cells were incubated in 1mL of fresh LB at 30°C shaker for 45min and then plated on agar plates with AMP and CHL. Single colonies were then inoculated in liquid LB containing appropriate antibiotic and DNA was purified from this culture. Transformation was verified by restriction digest with HindIII and size separated in agarose gel to confirm the presence of both BAC and the pSC101 plasmid.

4.7.2.2 PCR TO GENERATE TEMPLATE FOR RECOMBINEERING

Primers designed with sequence homologous to the BAC followed by sequence of the pR6K plasmid containing floxed BMP4 exon was designed and used to generate a PCR product with which homologous recombination was performed. Two sets of primers were used for this purpose in order to increase the probability of successful recombination. A pR6K plasmid clone whose sequence was verified to contain the floxed BMP4 by genotyping was used as the template.

Table 7 : Primers used for amplification of fragment for homologous recombination

	Primer name	Primer sequence
C708	Bmp4-flox-recombin_fw1	GTTTCTTGTTTTTGTTTTGTTTGTTTGTTTGTTTTTTTTTTTTTTTTTGT **ATAACTTCGTATAATGTATGCTATACGAAGTTATCTCAGAAAAGCTCATGGGCC**
C 712	bmp4-flox-recombi-fw 2	TCCTCCCCTTAGGTTTCTACTATATAAGCAGAATTCAACCAATTCTGCTA **ATAACTTCGTATAATGTATGCTATACGAAGTTATCTCAGAAAAGCTCATGGGCC**
C709	Bmp4-flox-recombin_rv1	TTTTTTTTTTTTTTTAAGATAAAAGTCCAGCTATAGGGAAGCAGTTTGTG **AAATTATGTACCTGACTGAT**

Highlighted nucleotides are homologous to the BAC sequence and nucleotides in bold represent the sequence of plasmid where the primers bind and amplify.

4.7.2.3 RED -ET RECOMBINEERING

120µl of O/N BAC (30°C) culture (WT Bmp4 + pSC101) was added to 1.4ml of LB with tetracycline (TET) and CHL and incubated at 30°C and 1000rpm for 2 hours in a heating block. Cells from one of the tubes was induced with 30µl of 10% L-arabinose. No L-arabinose induction was done with the control tube. Post induction tubes were incubated at 37°C on the heating block for 1h. Cells were then centrifuged for 30sec at 10,000rpm, 4°C and washed twice with 1ml cold cell culture grade water. Cells were finally resuspended in 20-40µl of cell culture grade water, following which 13µl of PCR product (for recombineering) was added and transferred to a cool 1mm electroporation cuvette. PCR product was electroporated into DH5α cells containing BAC and pSC101 plasmid at 1.8kV with BioRad gene pulser. Immediately after electroporation, 1ml LB was added and samples were incubated at 37°C for 1h. These cells were then plated on minimal agar plates with KAN and incubated O/N at 37°C. On the following day, single colonies were inoculated in 5ml LB with CHL and KAN. DNA from these cultures were prepared the next day. Verification of recombination was done by amplification of the region where the PCR product (modified Bmp4) would have integrated in the BAC followed by size separation on a 1% agarose gel. Successful recombination should result in 3kb amplified fragment whereas WT clones would result in a 1.5kb amplified fragment. This PCR was done using the genotyping primers and recombineered BAC as template.

Clones containing the 3kb bands were selected and further verified by sequencing.

Table8: Genotyping primers and primers used for sequencing

	Primer name	Primer sequence
C710	BMP_geno_fw	GGAGTCCAAGGGTGGTGGAG
C711	BMP_geno_frv	CTACCCACAGCCCCATCTCG
S 85	Bmp4-seq-fw	GTCCCCACTGAACTGAGTGCC
S 61	Neo_fw	CTCCTGTCATCTCACCTTGC
C 577	bmp4_geno_fw	GGTCAAGGTGAGTTGTTTAGGG
S86	BMP4 lastex-Rv	TCAGCGGCATCCACACCCCT
S 62	em7_rv	CTATGCCGATATACTATGCC

4.7.3 INSERTION OF SECOND LOXP SEQUENCE WITH CRISPR - CAS 9 SYSTEM

4.7.3.1 gRNA synthesis

Oligos for guide RNA (gRNA) were generated in silico and ordered from Sigma. The two oligonucleotides were annealed at 95°C for 5min followed by reducing temperature at a rate of -5 °C/min until a temperature of 25°C was reached.

4.7.3.2 LIGATION

PX459 plasmid containing puromycin (PURO) resistance was digested with Fast digest BbsI enzyme (NEB) and buffer for 30min at 37°C. Restriction digested plasmid was made up to a volume of 100µl using clean H_2O and purified using QIAquick PCR purification kit (Qiagen) as per the manufacturer's instructions.

50ng of BbsI digested PX459 plasmid was ligated along with 1µl of 1:250 diluted mixture of annealed oligos. The ligation reaction was set up in 10X ligation buffer (NEB) with 1µl of T4 ligase (NEB) and incubated at RT for 30min. Ligated CRISPR plasmid was then transformed into DH5α cells by heat shock method and plated on agar plates with AMP. Ligated plasmids were again digested with BbsI to as a control. Restriction site will be absent in the ligated plasmid and hence resemble the undigested plasmid. Single colonies were then inoculated in

5ml LB O/N following which plasmid was purified and prepared for sequencing with U6 promoter primer.

4.7.3.3 LARGE SCALE CRISPR PLASMID PREPARATION

Plasmid clone (#5) verified for the presence of gRNA sequence was picked for the large scale plasmid purification using Qiagen Plasmid Maxi Kit (P1,P2,P3 buffers) and Qiagen Tip 500 column. 100ml of LB with AMP was inoculated with glycerol stock of cells containing the plasmid and incubated at 37°C O/N. Cells were then spun down at 4°C, 4000rpm for 30min and the recommended procedure was followed (as per manufacturer's instructions). An additional precipitation step was performed following the wash with IPA and centrifugation. the pellet was resuspended in 270µl of nuclease free H_2O and added to a clean 1.5ml Eppendorf, to which 30µl of 3M Na/Acetate was added. 1ml of 100% ethanol was carefully added to the sides of the tube and inverted a few times. The tube was centrifuged for 20min at 4000rpm after which the pellet was washed again with 70% ethanol and resuspend in TE after all the ethanol has evaporated.

4.7.3.4 LARGE SCALE PURIFICATION OF BAC

The BAC clone containing th Bmp4 with loxP sequence on the 3' end was selected to be used for the CRISPR knock in. This BAC containing one loxP site is a product of the homologous recombination. 200ml of O/N culture of cells containing the mBAC (Bmp4-loxP-Neo) was purified using NucleoBond BAC 100 kit (Machery-Nagel) according to manufacturer's instructions. Cells were pelleted in falcon at 4000rpm, 4°C for 30min and then resuspend in S1, following which S2 buffer was added. Tubes were then incubated at RT for 3min. Pre cooled S3 buffer was added and tubes were inverted 2-4 times. Samples were then incubated for 5min on ice. Meanwhile the NucleoBond Folded filter was equilibrated with N2 buffer and lysate was passed through the filter. The filtrate was collected in a fresh tube. The NucleoBond BAC100 column was also equilibrated with the N2 buffer, after which the collected filtrate was passed through the column for binding. After the column was washed twice with buffer N3, DNA was eluted with pre-warmed N5 buffer (elution buffer). DNA was precipitated the same way as for the plasmids above, using Na/Acetate and later washed with 70% EtOH. Completely dry pellets were resuspended in 100µl of Tris-EDTA.

4.8 IN-SILICO GENERATION OF SEQUENCES

All steps and sequences for cloning strategies was performed in-silico with the CLC workbench 20. This software was also used to generate images of bands on agarose gels and vector/construct maps.

5. RESULTS

5.1 BMP4 CONDITIONAL KNOCKOUT CELL LINE

Electroporation of the BAC (floxed Bmp4) into Bmp4 KO ESCs which contain BACs for CRE expression driven by either HoxC8 or HoxC10 drivers, would result in conditional inactivation of Bmp4 gene. This inactivation of Bmp4 corresponds to the timepoints of development where expression of Hox genes that drive CRE expression is active**.** HoxC8 is expressed during the mid-trunk stage and HoxC10 is expressed around the late trunk stage of embryonic axial growth. Due to the role of BMP4 during gastrulation, a complete Bmp4 KO would be fatal at earlier stages to the developing embryo (Winnier et al., 1995). Hence, establishment of a conditional KO cell line would circumvent this issue and help to understand the timepoint of Bmp4 expression in mesoderm sublineage differentiation.

5.1.1 GENERATING FLOXED BMP4 GENE RECOMBINATION TEMPLATE

The third exon of the Bmp4 gene in the BAC was flanked with EcoRI restriction sequence and loxP sequence with the help of primers (Table 6) (Fig 5.1).

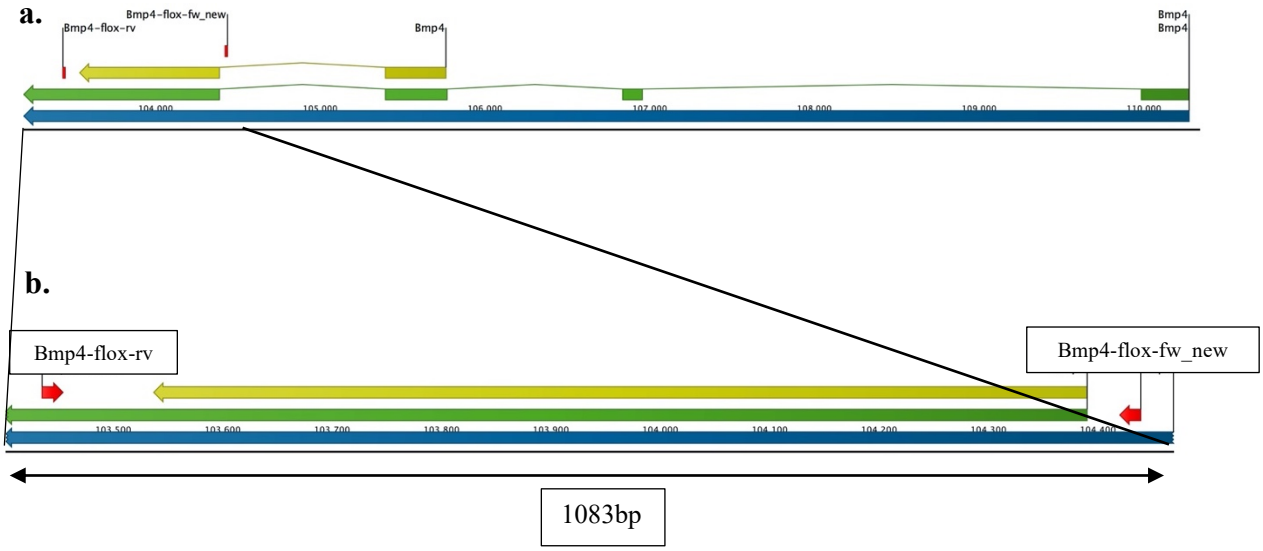

Figure 5.1 :
a. Map of BAC fragment containing the Bmp4 gene. **b.** Fragment amplified by PCR with primer binding sites indicated by arrows.

The resulting PCR product is a 1083bp fragment (Fig 5.1, 5.2-a) and its size confirmed by running the amplified product on an agarose gel (Fig 5.2-b).

The fragment in figure 5.2-b was purified from the gel and further digested with EcoRI enzyme. The digested PCR fragment was ligated into EcoRI digested pR6K vector (Fig 5.3). The ligated plasmid was transformed by heat shock into Pir+ve bacteria and selected on AMP and KAN agar plates. pR6K/Pir+ve cells are used in order to reduce the background due to co-electroporation of template and vector. Since both ends of the plasmid and PCR product were digested with EcoRI, ligation can occur in two different orientations. In order to identify plasmid clones with the gene in the right orientation, ligated plasmid was digested with XmnI. Clones which contain plasmids with floxed Bmp4 in the right orientation yield two fragment of size 1376bp and 4713bp (Fig 5.4-a). On the other hand, clones with floxed Bmp4 in the wrong orientation yield fragments of size 4204bp and 1885bp (Fig 5.4-a).

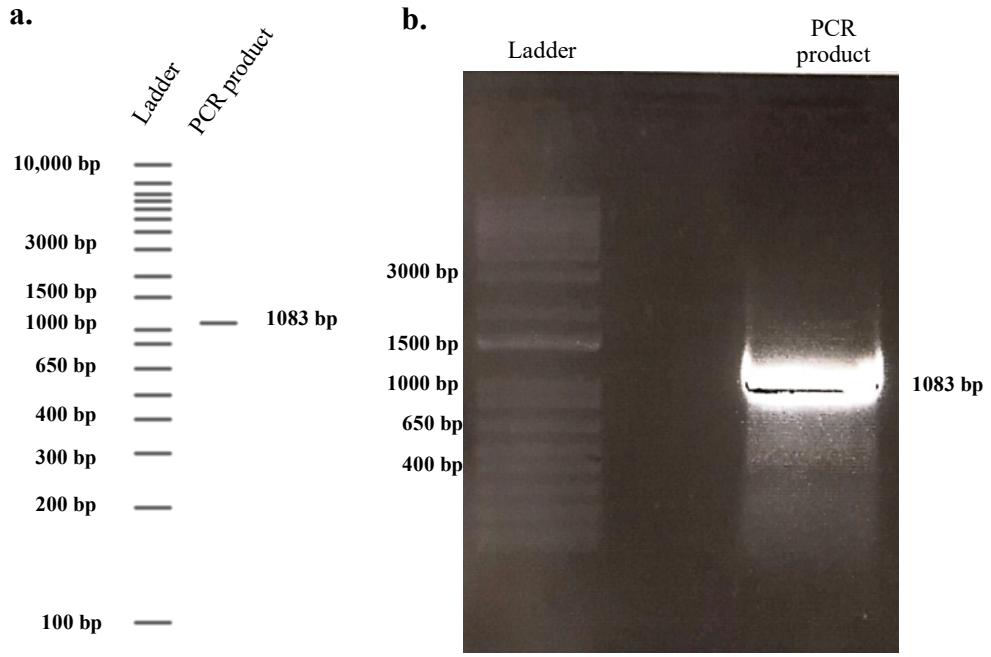

Figure 5.2 :
a. In silico image of the amplified PCR product. **b.** Image of 1% agarose gel with the 1083bp amplified PCR product.

Clones 2,3,4,5,6 and 8 contain the plasmid with the gene in the correct orientation (Fig 5.4-b). Two of these clones with correct orientation (#2, #3) were selected for sequence verification with M13 reverse and PGK reverse primers (Fig 5.5). Sequencing results confirm the presence of floxed Bmp4 ligated into the pR6K plasmid (Fig 5.5).

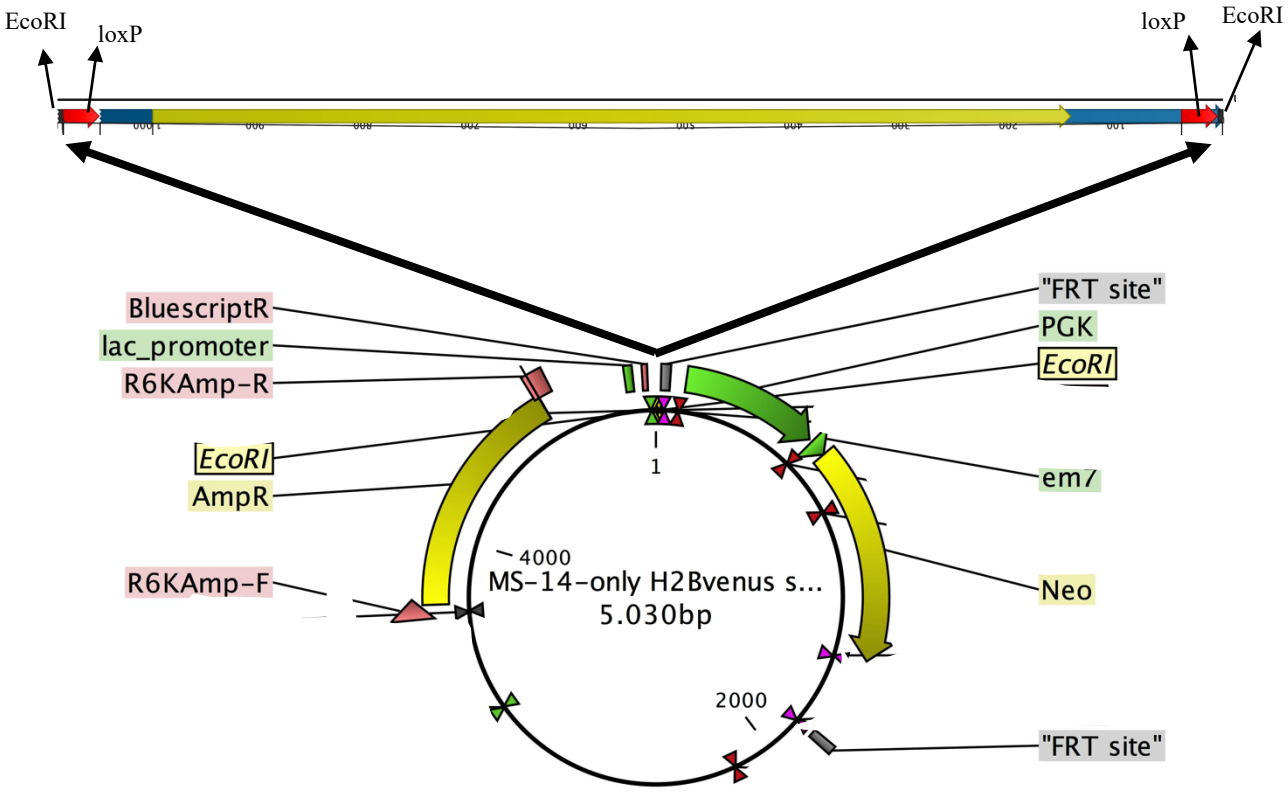

Figure 5.3 :
Map of EcoRI digested pR6K fragment containing AMP resistance and PGK promotor along with floxed Bmp4 gene (PCR product in correct orientation). Image also indicates the location in which the digested PCR product gets ligated into pR6K.

5.1.2 HOMOLOGOUS RECOMBINATION

5.1.2.1 ELECTROPORTATION OF pSC101 PLASMID INTO BAC CONTAINING CELLS

The pSC101 plasmid was electroporated into E.coli cells containing the WT Bmp4 BAC , plated on agar plate containing KAN and incubated at 30°C, since the pSC101 plasmid only replicates at 30°C. Single colonies were picked from agar plates and inoculated into LB containing TET and CHL. DNA was then purified from O/N cultures and successful electroporation was verified by digestion with HINDIII. The digested product was run on an agarose gel and results in multiple low intensity BAC fragments and two prominent bands of size 1.5kb and 5.6kb corresponding to the pSC101 plasmid. (Data not shown)

5.1.2.2 AMPLIFICATION OF FLOXED-BMP4 FOR HOMOLOGOUS RECOMBINATION

The ligated pR6K was used as a template to amplify the region containing floxed-Bmp4 gene along with the Neomycin (NEO) resistance cassette (Fig 5.6-b). Primers (Table 6) were

designed to include sequences homologous to the region in BAC were recombination is desired. PCR amplification results in a 3kb fragment (Fig5.6-a). This fragment was excised and purified from 1% agarose gel (Fig 5.6-a) and used for RED-ET recombineering.

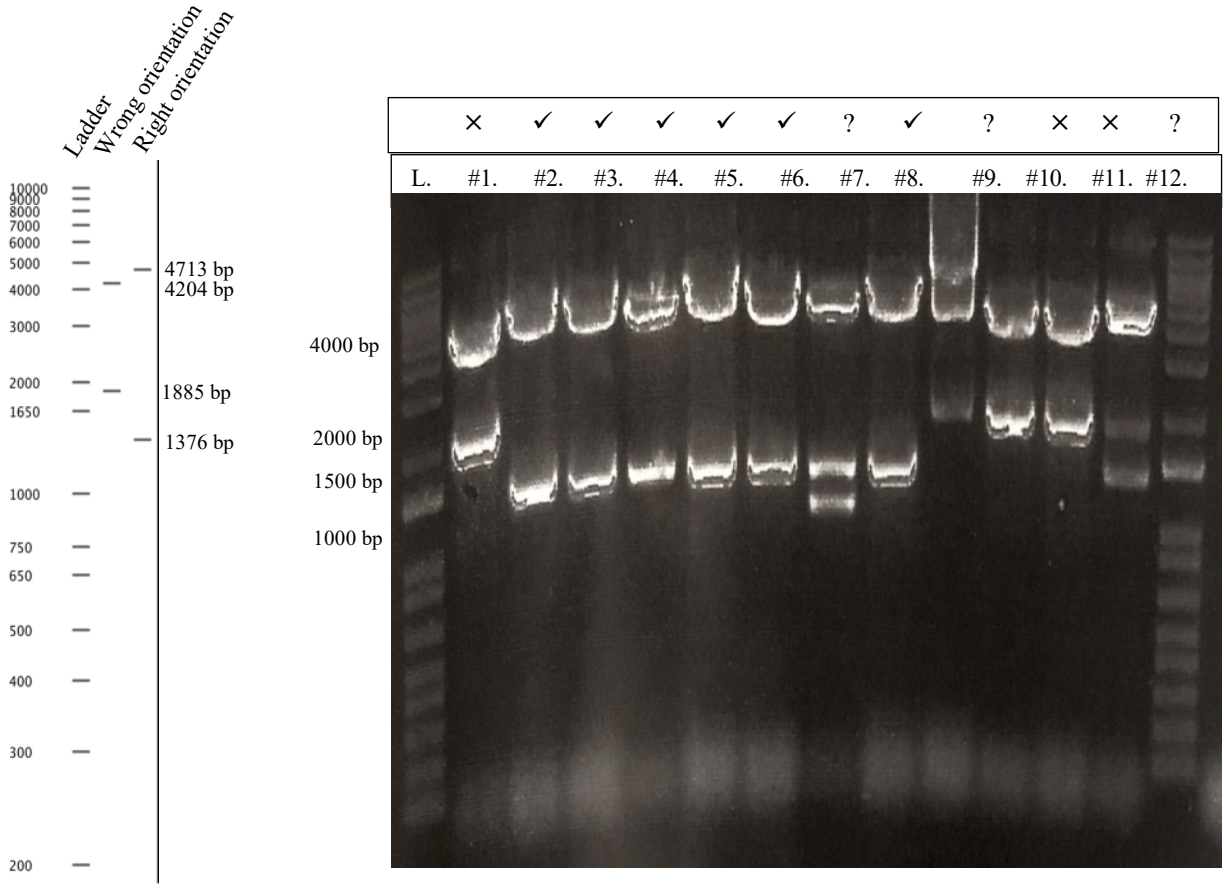

Figure 5.4 **:**
a. XmnI restriction digest of plasmid with floxed Bmp4 insert in the right and wrong orientation. **b.** Image of several clones selected after transformation into Pir+ve bacteria and digested with XmnI. (Lanes marker with "✓" and "x" indicate clones with right and wrong orientation PCR product respectively. Lanes marked "?" could be clones with double insertions).

Figure 5.5 :
Map of ligated plasmid aligned with in-silico generated sequence of plasmid R6K containing the ligated fragment in the right orientation. Primer binding sites are indicated by red arrows and loxP site indicated by blue arrows. The gap is an unsequenced region due to low sequence quality.

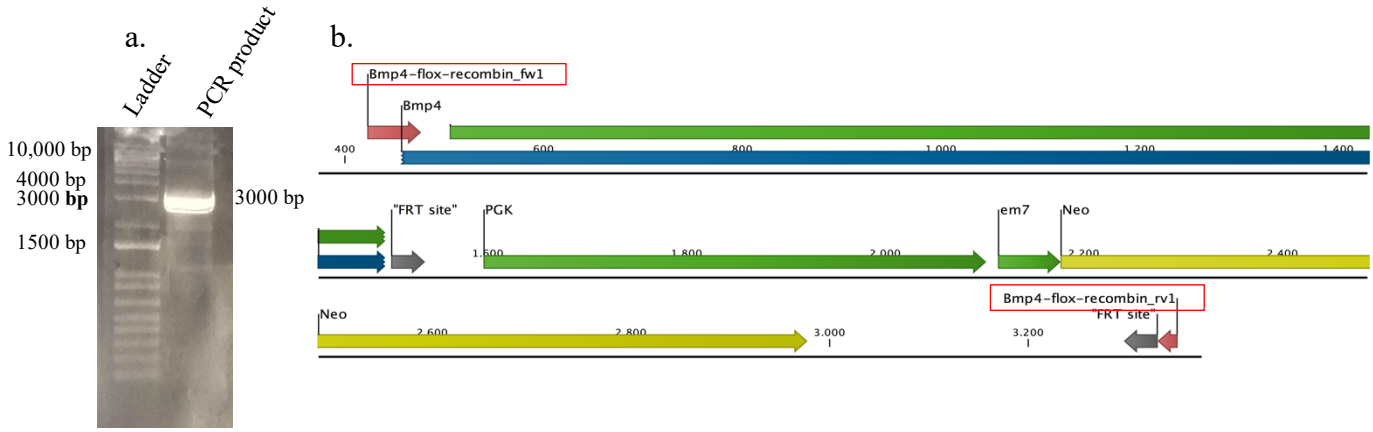

Figure 5.6 :
a. Amplified fragment on pR6K containing floxed Bmp4-NEO for recombination. **a.** 3kb PCR product separated on 1% agarose gel. **b.** Red arrows show the location of primer binding. Image generated with CLC software.

5.1.2.3 RED ET RECOMBINEERING

This method of recombineering uses the bacteria containing both BAC and pSC101. The homologous recombination is mediated by phage protein pairs like reda/redb whose expression is inducible by L-arabinose. Expression of these proteins increase the efficiency of homologous recombination.

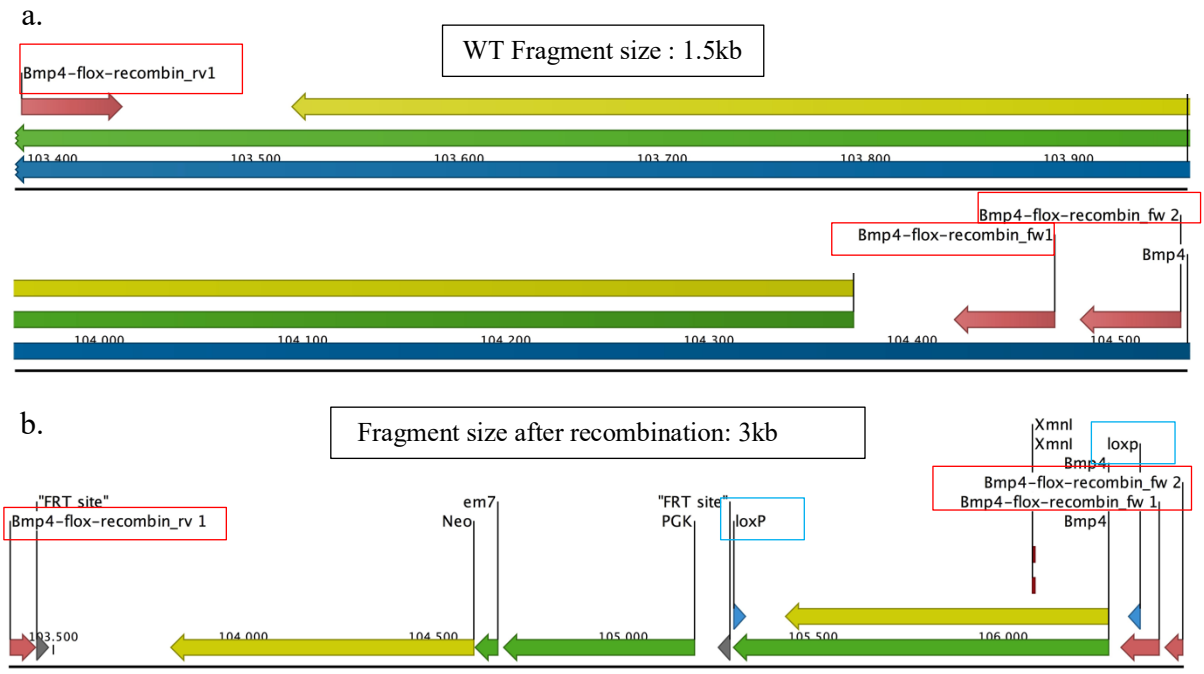

Figure 5.7 :
a. Map of the WT BAC backbone before recombination. Red arrows represent the BAC homolog in primers used for recombination. This is the location of expected recombination on WT BAC. **b.** Image of the expected sequence after recombination. Blue arrows represent loxP sites and red arrows represent recombineering primer binding sites.

Since the plasmid replicates only at 30°C, removal of plasmid is possible by culturing cells at 37°C. This way random recombination events are stopped from occurring later as well as BAC instability. The induction of RED proteins is followed by electroporation of modified gene fragment flanked by homologous BAC sequences (Fig 5.6) into cells containing WT BAC (Fig 5.7-a) and pSC101.

Recombineered clones (Fig 5.7-b) were then selected on agar plates containing KAN followed by inoculation of single colonies in LB with CHL and KAN. The WT fragment is 1.5kb in size, and it becomes a 3kb fragment after recombination (Fig 5.7-b). Further the BAC acquires NEO resistance after recombination, which is then used for antibiotic selection.

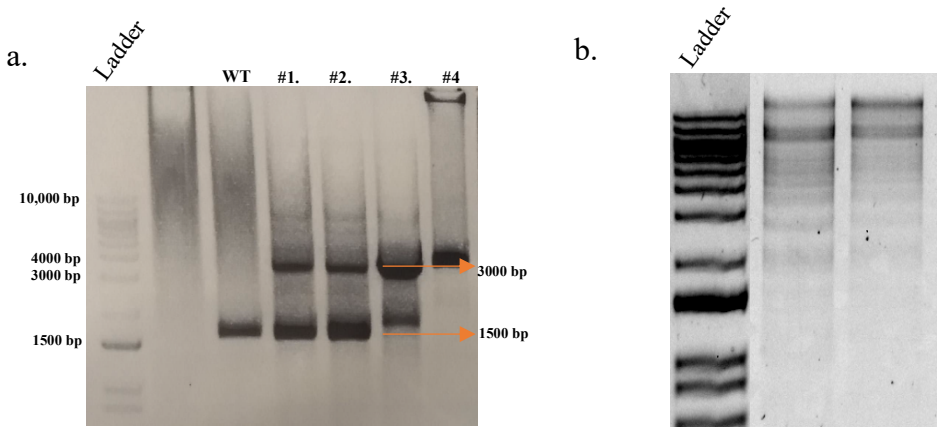

Figure 5.8 :
a. Fragment amplified from the recombineered BAC using genotyping primers. WT BAC show a 1.5kb PCR product. Clones 1,2,3 show 1.5kb (WT) and 3kb (mBAC) fragments. Clone 4 shows only 3kb fragment.
b. HINDIII digest of #3 and #4 to verify the integrity of BAC backbone after recombination.

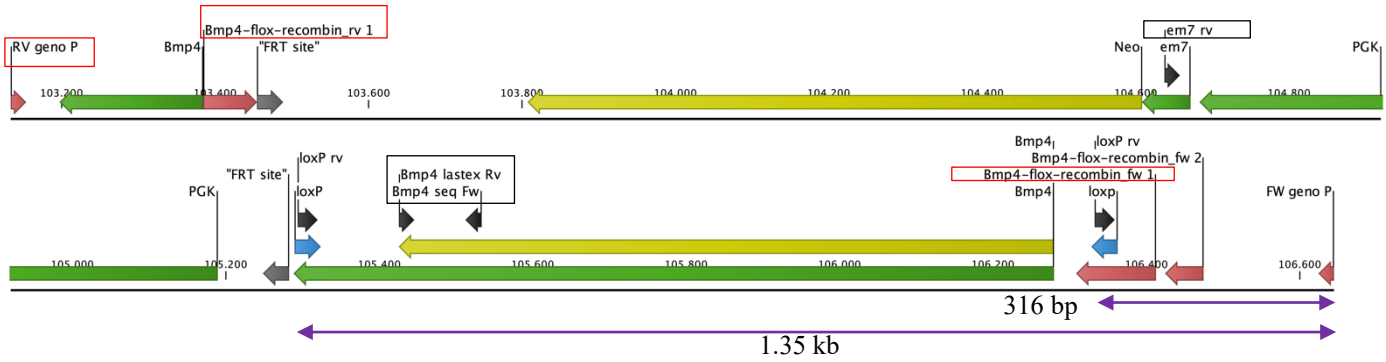

Figure 5.9 :
Map of the expected sequence after recombination with primers used for genotyping. Blue arrows represent loxP sites and red arrows represent recombineering primer binding sites and genotyping primers, black arrows represent primers used for sequencing. Violet arrows in the bottom show the expected PCR products for loxP site verification.

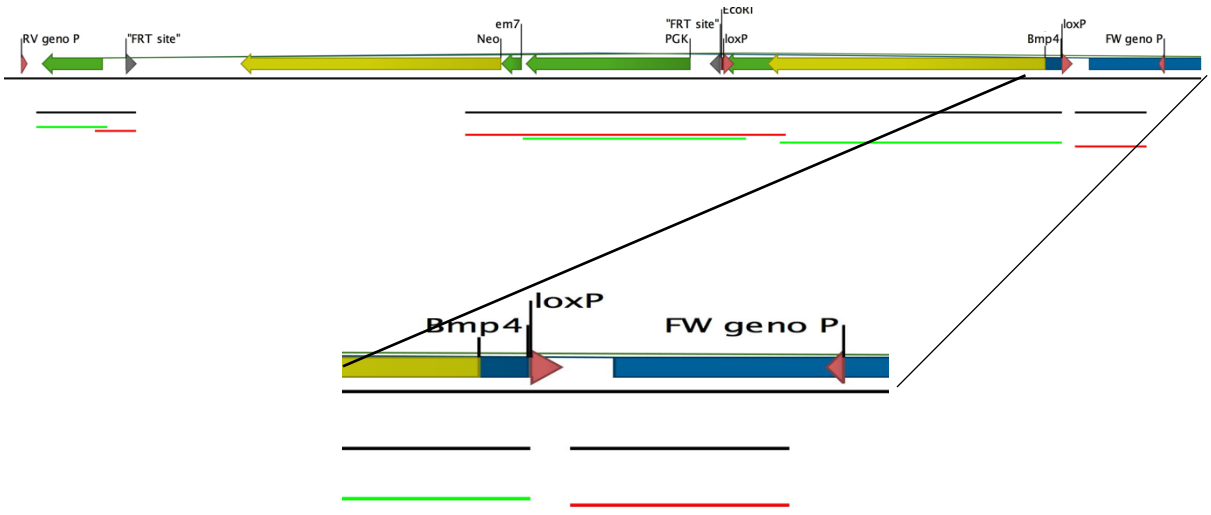

Figure 5.10 **:**
a. Sequenced clone after recombination aligned to the recombineered BAC sequence. Multiple primers were used in order to span the insert sequence. The black line represents the consensus sequence. **b.** A zoom on the sequence alignment including the missing 5' loxP sequence.

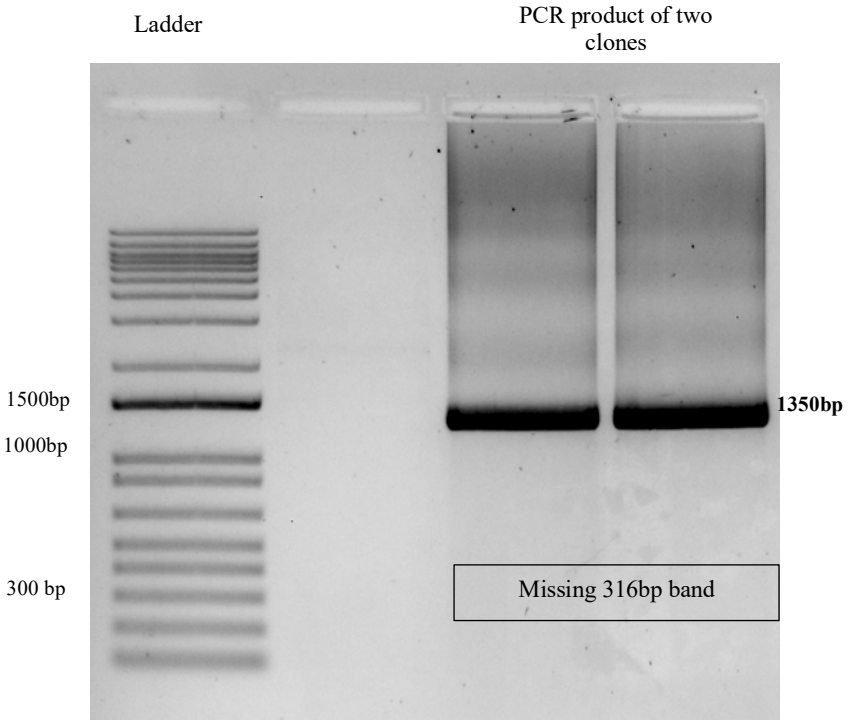

Figure 5.11 :
Image of gel showing the PCR product of reaction with the recombineered BAC primer for loxP site and Fw genotyping primer. Only one fragment around the size of 1.3kb is observed.

The 3kb fragment containing the resistance cassette and floxed-Bmp4 was amplified (Fig 5.8) with primers (genotyping primers) that bind to the respective 5' and 3' regions of the BAC outside of the 50bp homologous sequence used for recombineering (Fig 5.9). Some clones showed both the WT 1.5kb band in addition to the 3kb band (Fig 5.8-a). This can be due to the presence of mixed clones or inefficient amplification.

Additionally, in order to verify BAC integrity, clones were digested with HINDIII (Fig 5.8-b). A clone containing only the 3kb was selected for sequencing with primers (black arrows in Fig 5.9). It was observed that although 3' loxP sequence along with the resistance cassette was present in the selected recombineered clones, the 5' loxP site was missing (Fig 5.10).

In order to verify if the 5' loxP sequence is missing or whether the lack of loxP sequence was simply due to inefficient sequencing, an additional PCR was performed with primer binding to the loxP site and forward genotyping primer (Fig 5.9).

Presence of both loxP site would result in two fragments of size 316bp (product of 5' loxP site and other primer) and 1.35kb (product of 3' loxP site and other primer) (Fig 5.8). PCR products on agarose gel show only the 1.5kb fragment and the lack of smaller fragment confirmed the absence of 5' loxP sequence (Fig 5.11). Therefore, we co-electroporated this BAC along with a template at the same time to perform a CRISPR-mediated knock-in of the missing loxP site.

5.1.3 INSERTION OF 5' LOXP SITE WITH CRISPR-CAS9 SYSTEM

BbsI digested pX459 CRISPR plasmid was verified by size separation on a 1% agarose gel along with undigested plasmid (Fig 5.12-b). The digested plasmid was used for ligation with oligos coding for gRNA. Ligated plasmid containing oligos coding for gRNA sequence was then transformed into competent cells and the sequence was verified by sequencing with primers that bind to the U6 promoter (Fig 5.12-a). Ligated pX459 CRISPR plasmid along with linearised BAC (restriction digested with PI-SceI) and the template designed (with a point mutation in the PAM sequence) for the insertion of loxP site was electroporated into the Bmp4 KO ESCs. The template was an oligo instead of a dsDNA, since use of a template oligo has been shown to be more efficient. As a control, linearised BAC (Bmp4-loxP-Neo) was also electroporated into Bmp4 KO ESCs. This can serve as a control for CRE based inactivation and a WT control, since no KO would occur. These cells were then cultured in appropriate selection media containing NEO and PURO following which single colonies were picked and expanded.

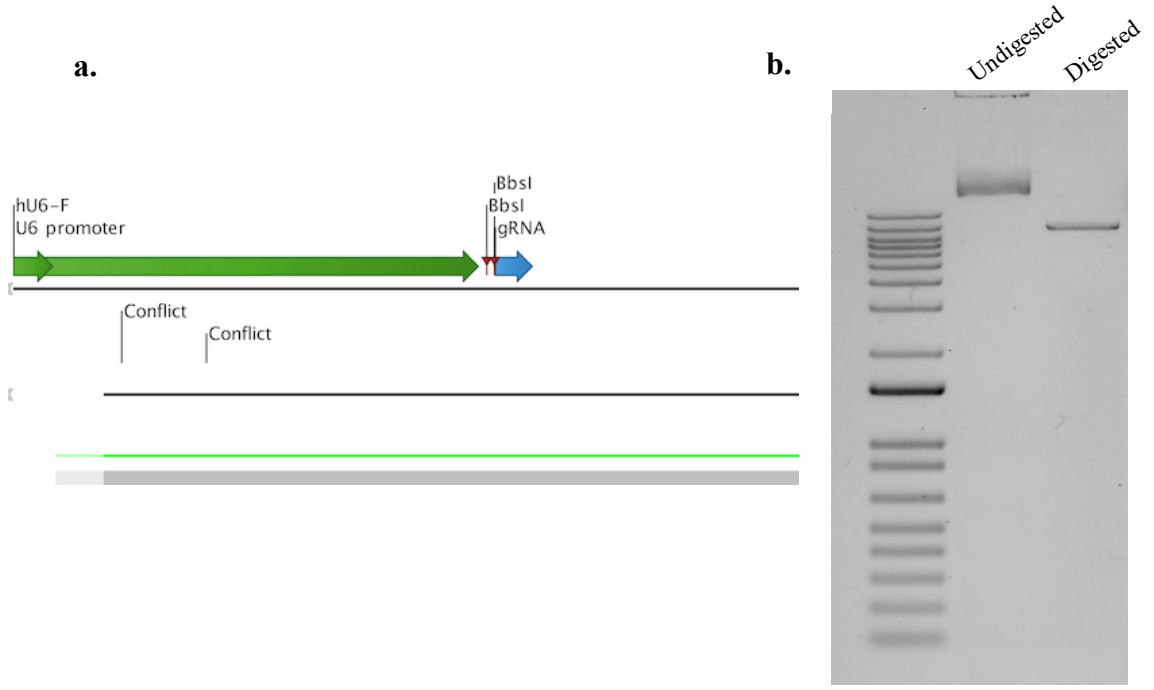

Figure 5.12 :
a. Sequencing result of pX459 after ligation of gRNA. The blue arrow indicated the location and sequence of gRNA. **b**. Digested and undigested pX459 size separated in a 1% agarose gel.

Subclones were then genotyped using primers mentioned in Table 2 to verify the integration of BAC on a 1% agarose (Fig 5.13). Since the insertion of loxP site cannot be verified by size separation gel, the presence of loxP site was verified by sequencing. The region of the Bmp4 gene expected to have the loxP sequence insertion was amplified by PCR (Primers S86 and C710 -Fig 5.14). PCR product of size 1.2kb (Fig 5.14) was excised from gel, purified and sent for sequencing. Sequencing results show that for all the three selected clones the 5´loxP site was still absent (Fig 5.15).

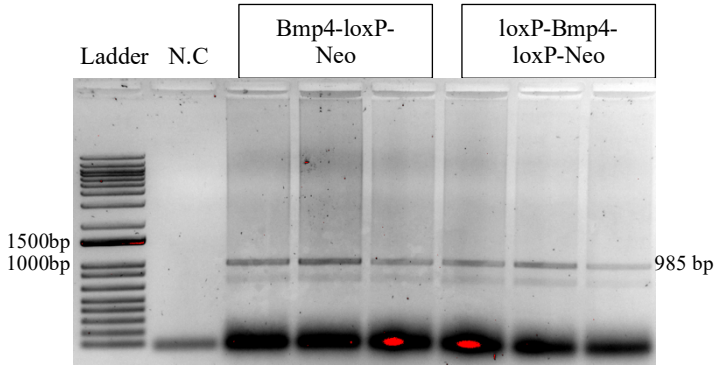

Figure 5.13 :
Genotyping to verify BAC integration. Forward primer binds to Neo cassette (S61) and reverse primer binds on the BAC backbone (C577). DNA from the parental F1G4 mice was used as a negative control (N.C).

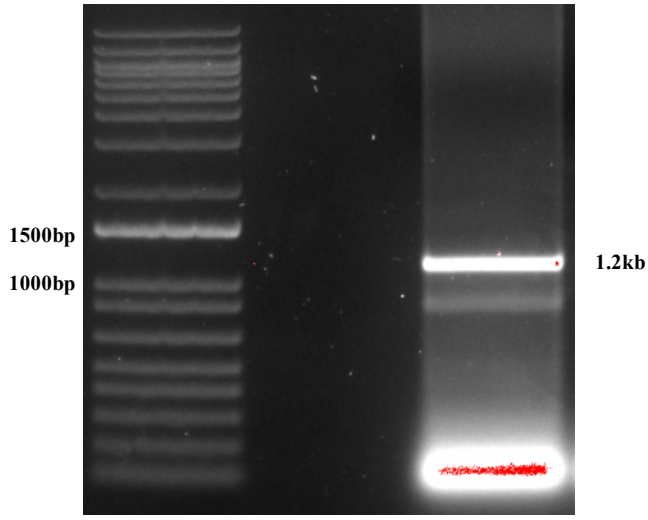

Figure 5.14 :
Amplified fragment of the 5' end of the Bmp4 gene containing the loxP site. Primers used for the amplification were Geno Fw primer and Bmp4 last exon Rv.

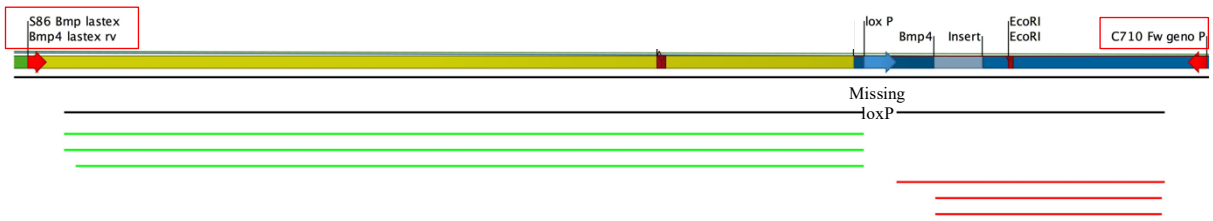

Figure 5.15 :
Sequence of the 1.2kb PCR product sequenced with two primers around the 5´loxP site.

Insertion of the 3' loxP site along with the resistance cassette was possible by recombineering although the 5'loxP sequence was missing. This could be due to the presence of a polyA repeat sequence net to the region of 5' loxP insertion or the point of recombination occurring somewhere in the exon. Hence, we used CRISPR-Cas9 system to introduce the 5' loxP site. Genotyping results of mESC clones where CRISPR system was employed also revealed that the loxP site was still absent. Hence the establishment of a conditional KO mESC line was unsuccessful. It is necessary to use a different strategy in order to successfully flox the Bmp4 exon and establish the conditional KO. Even though differentiation experiments have not been performed with the conditional Bmp4 KO, we wanted to employ recombinant BMP4 on mESC to establish a LPM differentiating protocol.

5.2 BMP4 DIRECTS NMPS TO DIFFERENTIATE INTO LPM

Several experiments where HPSC have been used to generated LPM in the presence of BMP4, activin A and FGF2 have been published. Some of them have also further differentiated LPM to cardiac progenitors by continuous exposure to BMP4 (Iyer et al., 2015; P. Zhang et al., 2008). Adapting from these studies, we tried to generate LPM from the NMP/Mesodermal progenitor population (D3), which is comparable to the events *in-vivo*. (Section-4.1.7).

Two clones selected from mESC line containing Tbx6::H2B-mCherry (henceforth referred to as $Tbx6^{mC}$) and Foxf1::H2B-Venus (henceforth referred to as $Foxf1^{V}$) reporter BACs were used to test the effects of two different treatments on differentiation of ground state pluripotent mESC to lateral plate mesoderm. Cells were initially differentiated into NMPs by culturing in N2B27 + 10ng/ml FGF2 for 48h (D1-D2) followed by exposure to N2B27 + 10ng/ml FGF2 + 5μM CHIR for 24h (D3). Cells from this stage, were further differentiated with either N2B27 + 20ng/ml BMP4 (B20) or N2B27 + 20ng/ml BMP4 + 20ng/ml FGF2 (FB20) for 72h (D4-D6) in order to optimize the differentiation protocol for lateral plate mesoderm (Fig 5.16). Cells at each time point from D4-D6 were then analysed by flow cytometry to quantify the reporter expression and by qPCR to measure relative RNA expression levels of early LPM markers (*Foxf1*, *Hand1*, *Tbx3*) and late LPM markers (*Gata6*-splanchnic LPM, *Irx3*-somatic LPM*). Pmm2* was used as housekeeping control. In addition, the expression of early and late LPM markers would also support the success of the differentiation protocol. The expression level of genes at the different timepoints have been normalized to their respective expression level at D3.

Figure 5.16:
Schematic representation of the LPM differentiation protocol.

After 4 days of differentiation with B20, 85.9% express $Foxf1^{V}$ whereas 14% of the cells are negative for both reporters (mCherry and Venus) (Fig 5.17-a.i). The number of cells that are $Foxf1^{V}$ decreases to 73% after 5 days (D5) and conversely, the number of double negative cells increases to 26.8% (Fig 5.17-a.ii). The same trend, a decreasing number of $Foxf1^{V}$ cells and increase of double negative cells is also observed after 6 days (D6) (Fig 5.17-a.iii).

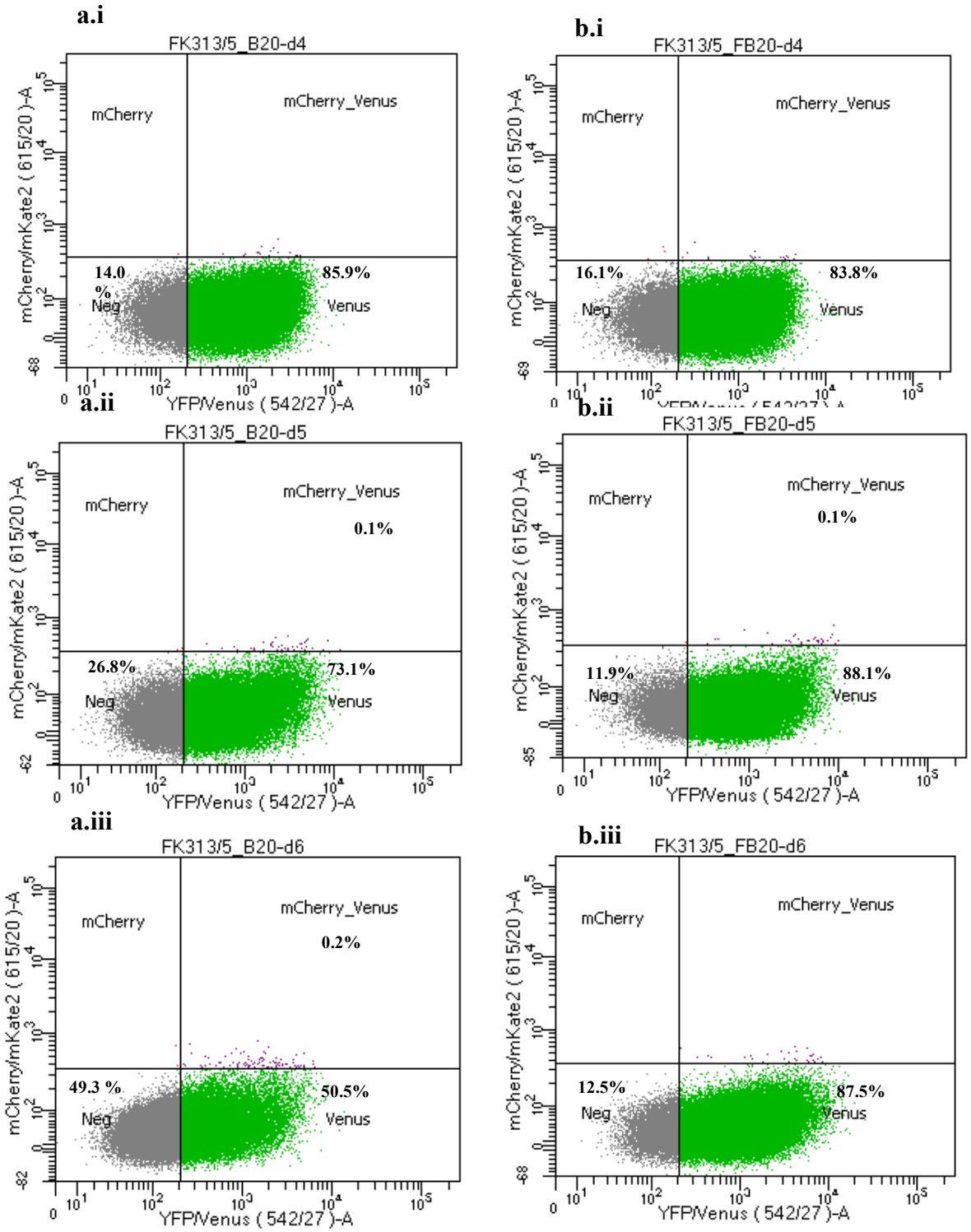

Figure 5.17 :
Fluorescence measured by FACS during the days of differentiation for the clone numbered 313/5.
a. Fluorescence measured for cells treated with 20ng/ml of r.BMP4 after 3 days of initial differentiation.
b. Fluorescence measured for cells treated with 20ng/ml of r.BMP4 and 20ng/ml FGF2 after 3 days of initial differentiation.

Cells (clone1) treated under FB20 condition display similar levels of Venus reporter expression from D4 to D6 (Fig 5.17-b). Although the percentage of Foxf1^{V} cells increases from 83.8% to 88.1% on timepoints D4 and D5 respectively, percentage of Foxf1^{V} cells subsequently decreases to 87.5 % at D6. Flow cytometry profile under this differentiation protocol also reveals that around 0.1-0.2% are double positive cells (Foxf1^{V} / Tbx6^{mC}). Since Tbx6 is a marker for early paraxial mesoderm, it is possible that some mesodermal progenitor cells are also generated during this differentiation protocol. This observation supports that LPMP can differentiate into LPM and PSM cells.

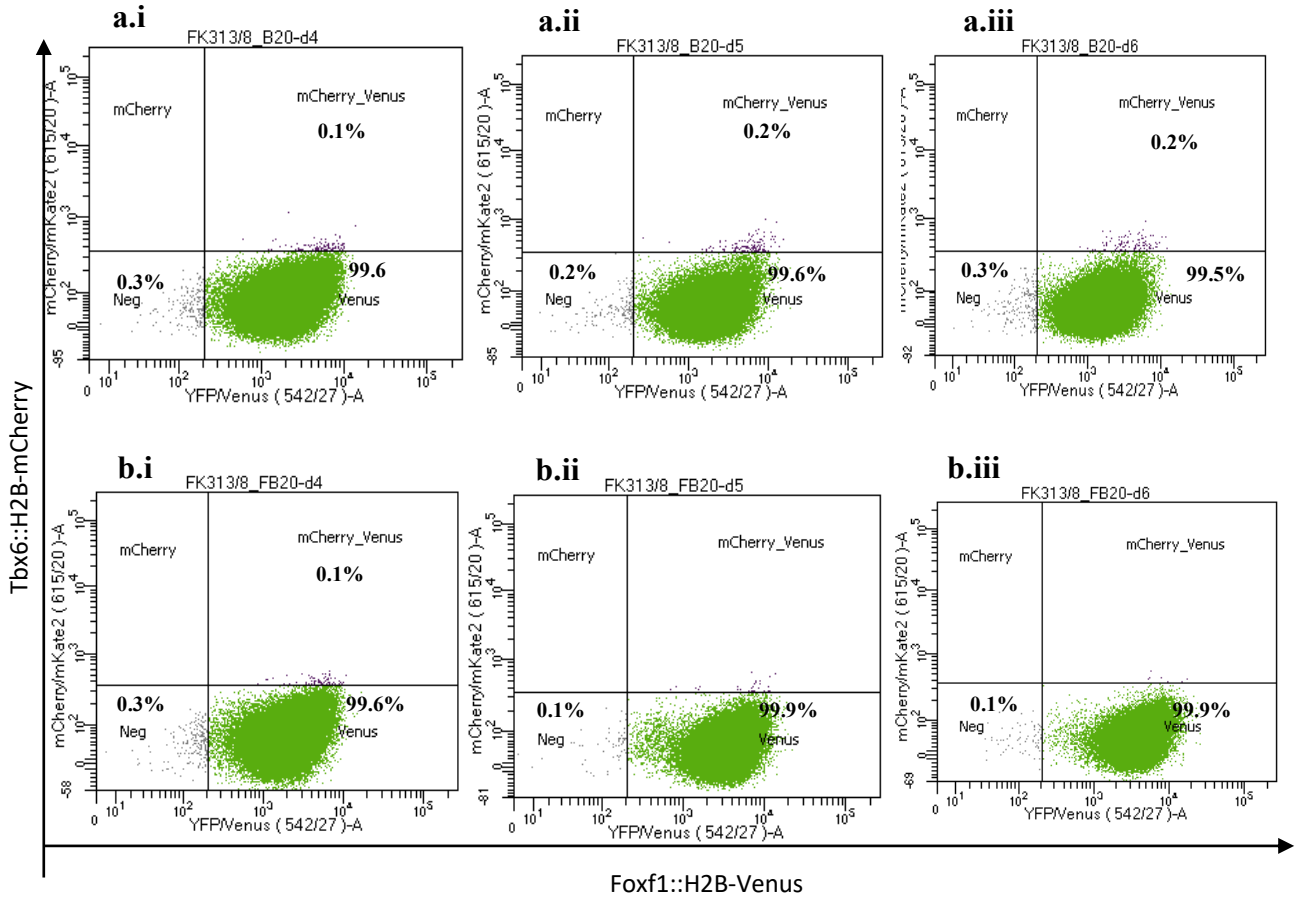

Figure 5.18 :
Fluoresce measured by flow cytometry during the days of differentiation for the clone numbered 313/8**. a**. Fluorescence measured for cells treated with 20ng/ml of r.BMP4 after 3 days of initial differentiation. **b**. Fluorescence measured for cells treated with 20ng/ml of r.BMP4 and 20ng/ml FGF2 after 3 days of initial differentiation.

In order to account for the different rates of differentiation between different clones, another clone (clone2) was also selected for differentiation into LPM. FACS data of clone2 over the timepoints D4-D6 (Fig 5.18-a, 5.18-b) of differentiation revealed a consistent 99% of Foxf1^{V} cells under both B20 and FB20 treatment conditions (Fig 4.18-a, 4.18-b). To confirm whether the 99% Foxf1^{V} cells observed in FACS is a result of highly efficient differentiation protocol

or gene independent reporter expression, FACS was done for the initial timepoints D1-D3 (data not shown). FACS of early days of differentiation for clone2 showed that 99% of the bulk population was already positive for Venus reporter (Foxf1$^{V)}$ at D0, which is cells cultured in 2i+LIF medium and the percentage decreased to 95% and 92% after day 2 and day 3 respectively (data not shown). In case of clone1, 36% of the bulk population was Foxf1^{V}+ve at D0 and this number remained the same after day 1. The percentage decreased to 5% after 2 days of differentiation with FGF2 and after the third day of differentiation, 10% of the bulk population was Foxf1^{V}+ve (data not shown). This indicated that mESCs cultured in 2i+LIF medium express some level of *Foxf1,* which is then downregulated when differentiating with FGF2. Addition of CHIRON again mildly induces *Foxf1* expression. The results observed during the early timepoints in clone2 suggests that reporter integration is nonfunctional and Venus expression is not Foxf1 expression dependent. The flow cytometry data of this clone cannot be analysed due to this unreliable reporter expression. Since we do not expect differences on the transcript level of genes, the qPCR data of this clone was still considered as biological replicate.

To further characterize the expression of early and late LPM genes in mESC during differentiation, qPCR was performed at the bulk RNA level across the D4-D6 timepoints and both conditions.

qPCR data from both clones were used as biological replicates to study their gene regulation profile. Expression of *Foxf1* decreases from D4 to D5 by 3-fold in the B20 treatment and by 2-fold in the FB20 treatment. The expression level of *Foxf1* after 6 days (D6) is maintained in B20 treatment and slightly downregulated in the FB20 treatment (Fig 5.19-a). Thus, Foxf1 is regulated similarly in both treatment conditions.

Hand1 also being an early LPM marker is decreasing from D4 to D6 in both the treatments, B20 and FB20. Under the B20 treatment, *Hand1* is downregulated 4-fold from D4 to D5, whereas a 2-fold downregulation is observed for FB20 treated cells during the same time. These results are reproducible across both biological replicates. From D5 to D6, *Hand1* is further downregulated by approximately 3.2-fold under the B20 treatment and 2.3-fold under FB20 treatment (Fig 5.19-b). Thus, the extent of *Hand1* downregulation is more pronounced when applying the B20 treatment as compared to the FB20 treatment, but generally *Hand1* is downregulated in both conditions as differentiation progresses.

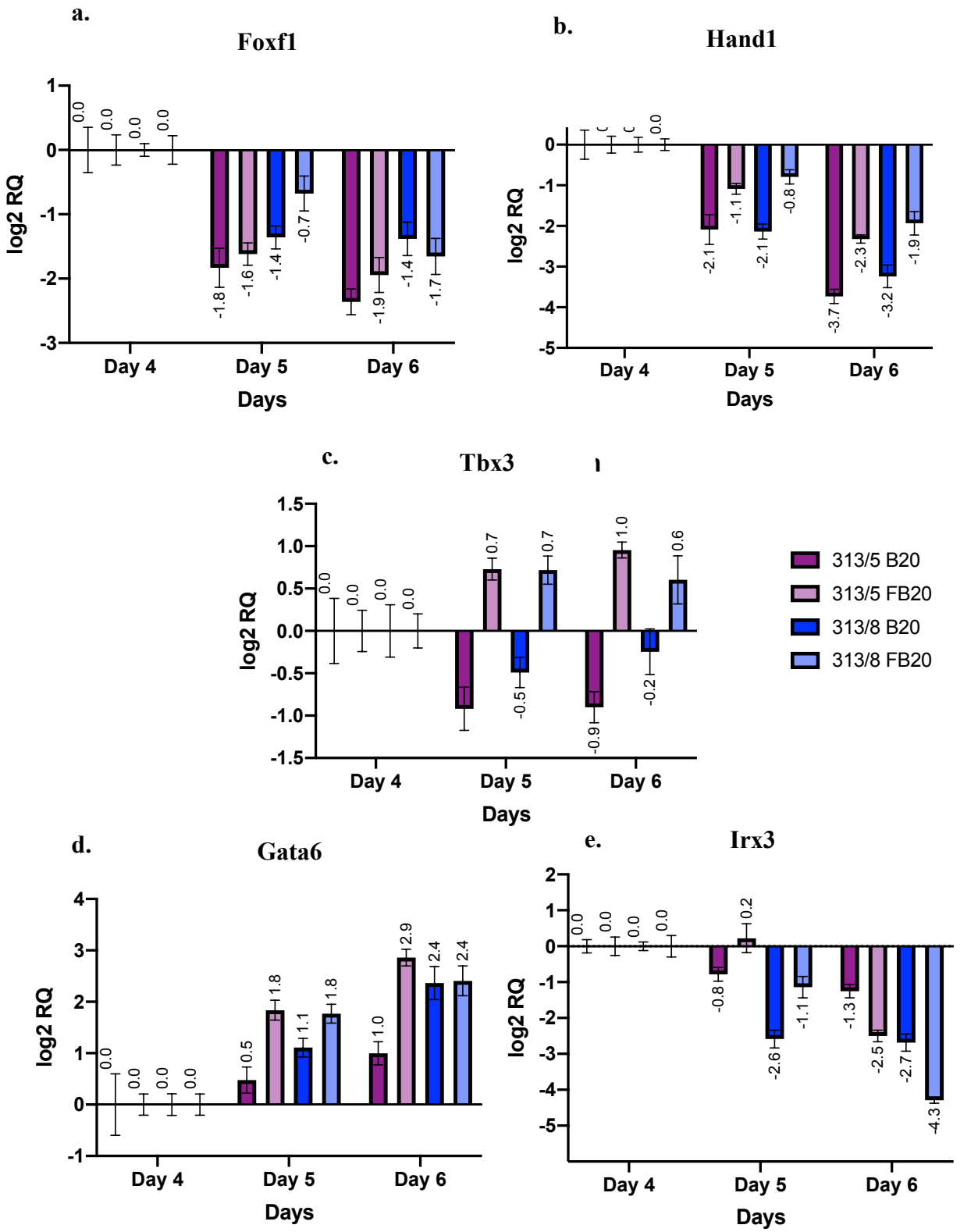

Figure 5.19:
Expression profile of late LPM markers over D4-D6 of LPM differentiation. Expression for genes at each time point is normalized to the respective expression level at D4. Bars represent log2 relative fold change±error. **a.** Relative *Foxf1* expression **b.** Relative *Hand1* expression **c.** Relative *Tbx3* expression. **d.** Relative *Gata6* expression **e.** Relative *Irx3* expression

In addition to the well-known early LPM markers, the expression of *Tbx3* was also analysed by qPCR. It was observed that its expression is mildly reduced at D5 in the case of B20 condition, whereas a slight increase under FB20 treatment was observed at D5. The expression levels are maintained between days 5 and 6 of differentiation (Fig 5.19-c).
To verify whether splanchnic or somatic LPM is generated as a result of the different differentiation conditions, expression of two late LPM markers for splanchnic and somatic LPM were measured. *Gata6* expression is upregulated by 4-fold from D4-D5 in the FB20 condition and by 1-fold in cells treated with B20 during this time. From D5 to D6, both B20 and FB20 treated cells additionally upregulate *Gata6* by 2-fold (Fig 4.19-d).
Expression of *Irx3* is deviating from what is expected to be observed as NMPs differentiate into LPM. Its expression is downregulated as cells differentiate under the LPM differentiation protocol. This trend holds true for both the treatments. The lowest expression is observed at D6 (Fig 5.19-e). Higher extents of *Gata6* upregulation and *Irx3* downregulation in differentiation with FB20, indicates that under this protocol, splanchnic LPM is being generated rather than somatic LPM. The universal downregulation of *Irx3* in both differentiation protocol also suggests that the conditions of differentiation facilitate splanchnic LPM differentiation. Since the detectable differences of gene expression between the B20 and FB20 differentiation protocols were negligable, FB20 was used for additional experiments where LPM differentiation was desired. Differentiation of mESC into LPM *in-vivo* is also dependent on FGF and well as BMP4 in the posterior end of the developing embryo and previous protocols to differentiate HPSC to LPM have also employed FGF2 along with BMP4.

Maintenance of mesodermal progenitors in the tailbud region of the embryo requires BMP signaling (Sharma et al., 2017). In order to understand the role of BMPs in differentiation of mesodermal progenitors into the mesodermal sub-lineages, the above established LPM protocol using BMP4 was used to differentiate Bmp11 (Gdf11) KO mESCs to mesodermal progenitor cells and then subsequently LPM.

5.3 GDF11 HAS NO EFFECT ON LPM DIFFERENTIATION

Gdf11 mutants have shown a displacement of limb position in both chick and mice embryo (Liu, 2006; McPherron et al., 1999). GDF11 acts via *Isl1* to facilitate the proliferation of caudal most LPM progenitors which give rise to the hind limb tissue (Jurberg et al., 2013). This made us

question if GDF11 has any effects on the ability of early mesodermal progenitors to differentiate into nascent LPM.

NMP-like/mesodermal progenitor like cells at D3 of differentiation, upregulate *Foxf1* expression after 24h (D4) of differentiation with FGF2 and BMP4. WT cells upregulate *Foxf1* expression by 256-fold from D3 to D4 and then downregulate expression by 2.8-fold at D5. This expression level is then maintained from days 5 to 6. *Foxf1* is regulated in a similar fashion in the GDF11 KO cell line, where *Foxf1* is upregulated by 128-fold from D3 to D4, downregulated by 2-fold at D5 and then the levels are maintained at D6 (Fig 5.20-a).

Similarly, *Hand1* in WT cells is upregulated by 2000-fold from D3 to D4, downregulated by 3-fold at D5 and its expression is maintained over the days 5 to 6. Expression of *Hand1* in Gdf11 KO cells follows that of the WT cells (Fig 5.20-b).

Tbx3 is also upregulated from D3 to D4 in both WT and Gdf11 KO cells and its expression is maintained at days 5 and 6 of differentiation. (Fig 5.20-c).

Although *Gata6* is also upregulated at D4 in comparison to D3, the extent of upregulation is less than what was observed for the early LPM markers. Between D3 and D4, *Gata6* expression increased 4-fold, a further 2.5-fold at D5 and peaks at an 18-fold increase at D6 as compared to D3 (Fig 5.20-d).

Irx3 expression is upregulated by 3-fold at D4, this level is maintained at D5 following which the expression is downregulated by 8-fold at D6. This applies for both WT and Gdf11 KO cells.(Fig 5.20-e).

Tbx6 being a marker for early mesoderm as well as a PSM marker was measured as a control to observe if any PSM cells are being made under this protocol. As expected, we observed that its expression is strongly downregulated from D3 to D4 and then maintained at these low levels (Fig 5.21).

Differentiating both Gdf11 KO and WT cells into LPM and measuring LPM markers has revealed that the expression level of early and late LPM marker at each timepoint of differentiation between the WT and mutant is similar. Further the regulation in WT cells from D4-D6 is similar to what was previously observed during the establishment of the LPM differentiation protocol. This experiment further helps to understand the regulation of markers from D3 to D4 and behavior of cells after the first 24h exposure to BMP4. At D4, expression of early LPM markers peak in comparison to the levels at D3.

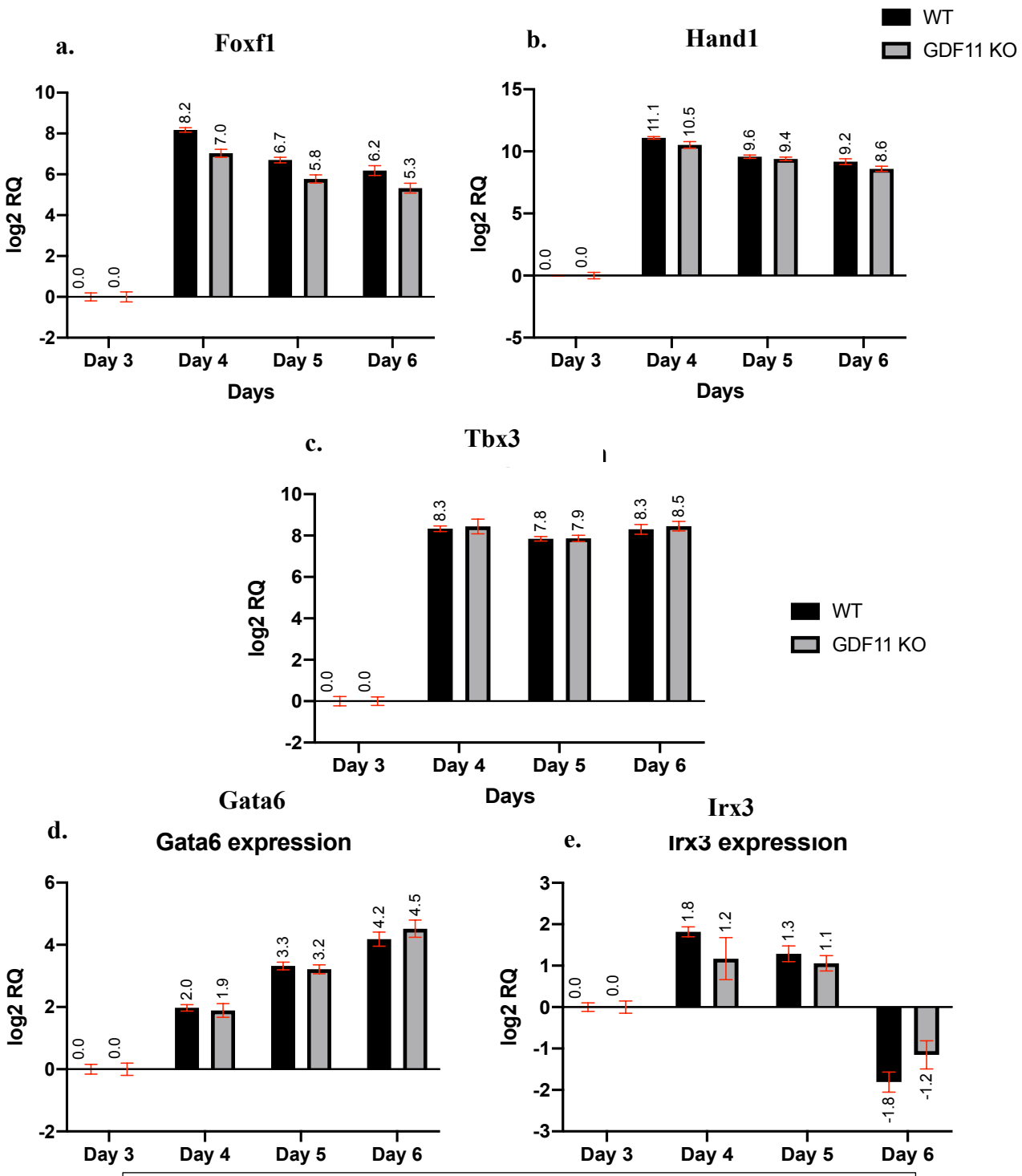

Figure 5.20:
Log2 fold Expression profile of early LPM marker for WT and GDF11 KO cells over 4 timepoints of differentiation. **a.** *Foxf1* regulation. **b.** *Hand1* regulation. **c.***Tbx3* regulation **d.** *Gata6* expression. **e.** *Irx3* expression. All data has been normalized to expression levels at D3. Bars represent Relative expression ± error. Expression normalised to D3.

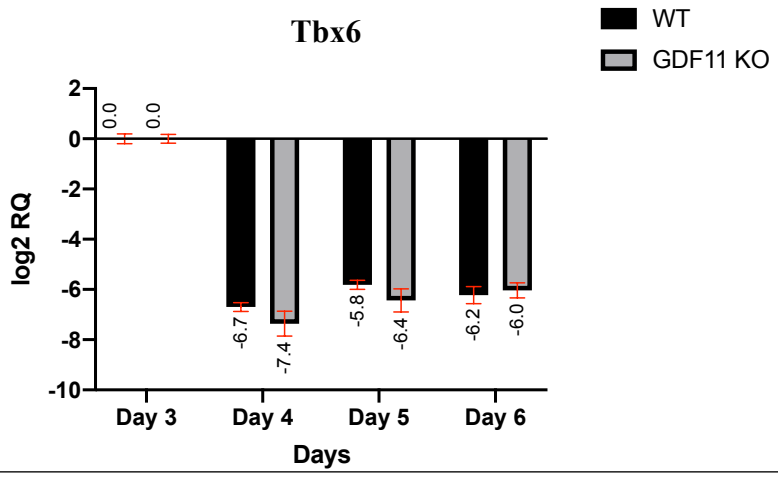

Figure 5.21 :
Log2 fold expression profile of *Tbx6* for WT and Gdf11 KO cells over 4 timepoints of differentiation. Graphs represents relative expression ± error.

Additionally, *Tbx6* is downregulated during this timepoint correlating with the increase in expression of early LPM markers. Hence, NMPs/mesodermal-like progenitors under BMP4 signals upregulate LPM markers and GDF11 does not play a role in the differentiation of NMPs into nascent LPM.

Since PSM also originates from NMPs and contribute to somites and trunk growth in the embryo, we wanted to further study the effects of GDF11 in the development of PSM tissue by differentiating Gdf11 KO cells with the PSM differentiation protocol along with WT cells as control.

5.4 GDF11 MUTANTS ACCUMULATE NMPs

Wild type and Gdf11 KO mutant cells with T::H2B-mCherry and Sox2::H2B-Venus reporter BACs were used for the PSM differentiation. Cells were plated on wells of a 6 well plate and analyzed by FACS and qPCR at 24h timepoints. The two replicates of each differentiation experiment are hereby referred to as DE-1 and DE-2. On days 1 and 2 (D1 and D2), cells of the WT and mutant exhibit comparable FACS profiles with around 99% of cells being $Sox2^{V}$+ve (data not shown). The first difference in FACS profile is observed after 3 days, where some cells begin to differentiate into NMPs and co-express T and Sox2 (T^{mC}+/$Sox2^{V}$+). At D3, WT cells have a majority of double positive cells along with fewer $Sox2^{V}$ single positives as well as T^{mC} single positive cells (Fig5.22-1.a.i, 2.a.i).

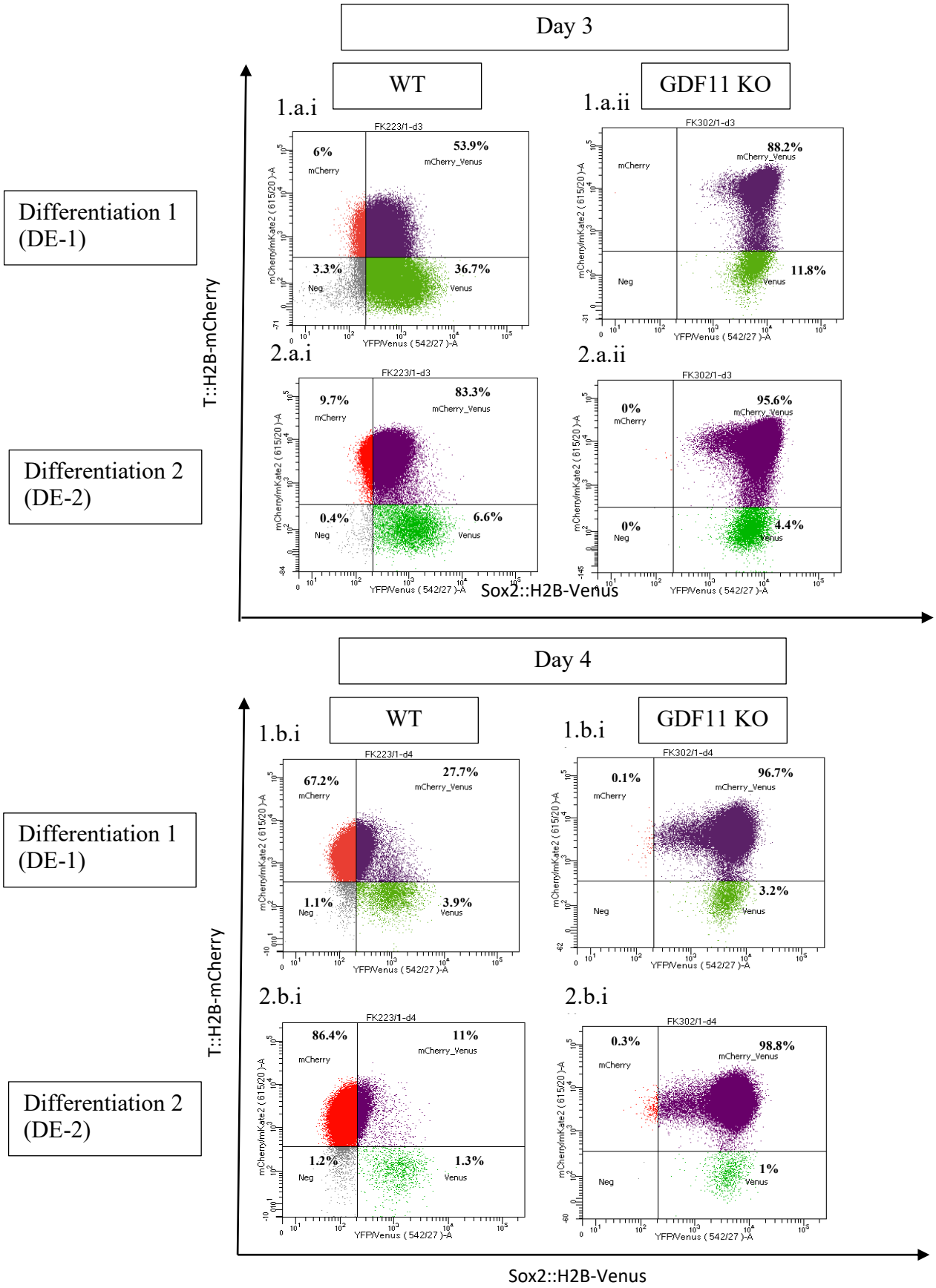

Figure 5.22 :
FACS profile from **1.**DE-1 and **2**.DE-2 of WT (**i**) and mutant cells (**ii**) showing mCherry+/Venus+ cells in violet, single Venus+ve cells in green and single mCherry+ve cells in red**. a.** Profile after 3 days of differentiation. **b.** Profile after 4 days of differentiation.

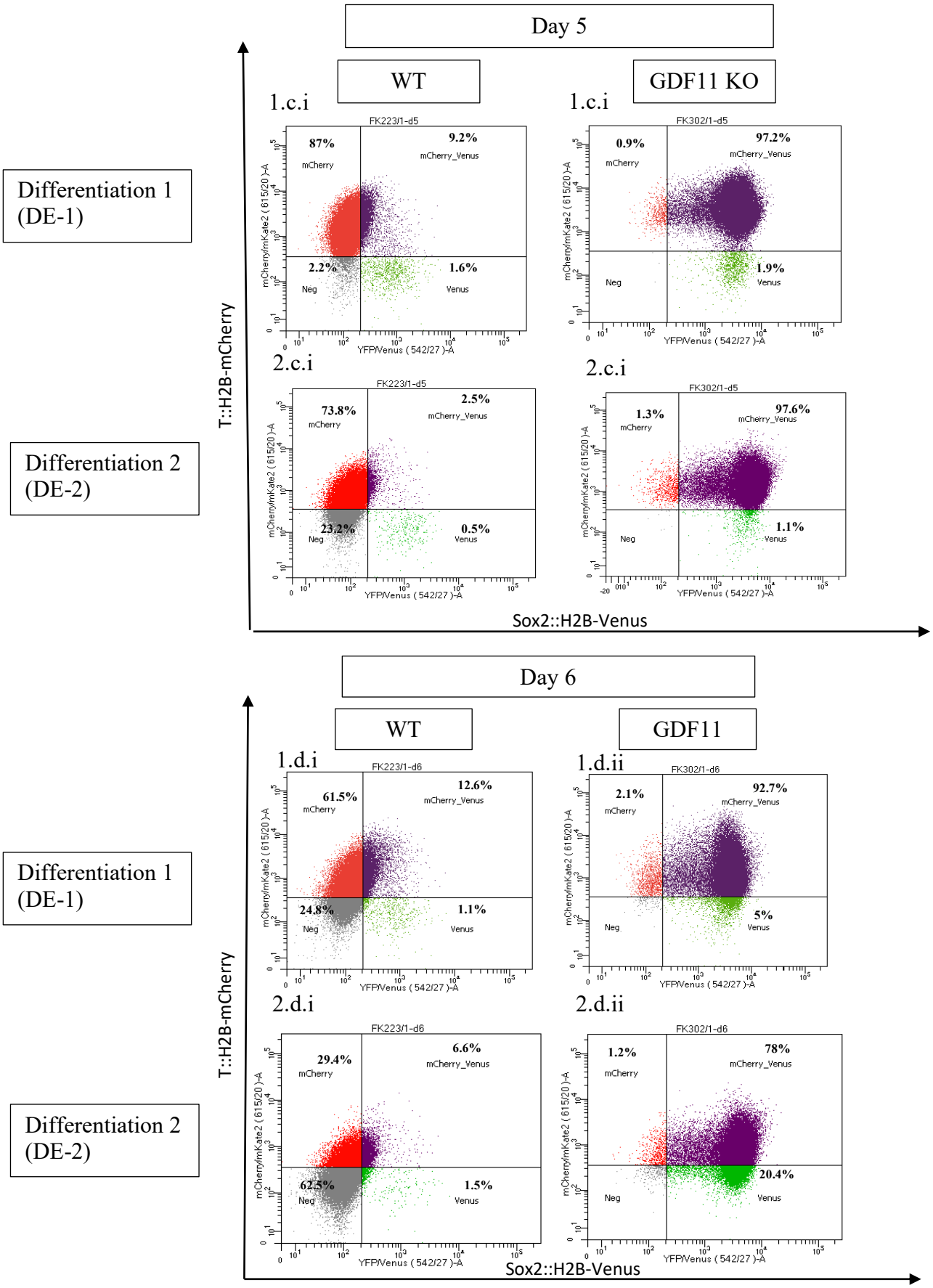

Figure 5.23 :
FACS profile from **1.**DE-1 and **2**.DE-2 of WT (**i**) and mutant cells (**ii**) showing mCherry+/Venus+ cells in violet, single Venus+ve cells in green and single mCherry+ve cells in red**. c.** Profile after 5 days of differentiation. **d.** Profile after 6 days of differentiation.

The mutant cells also display a major population of double positive cells in this timepoint in addition to few $Sox2^{V}$ single positive cells (Fig5.22-1.a.ii, 2.a.ii). In comparison to WT, mutant T^{mC}+/$Sox2^{V}$+ cells display higher levels of both T^{mC} and $Sox2^{V}$. The mutant $Sox2^{V}$ single positive cells also have a higher Sox2 reporter activity (Fig5.22-1.a.ii, 2.a.ii). Although no T^{mC}+ve cells were observed in the mutant cells at D3, some cells of the T^{mC}+/$Sox2^{V}$+ population differentiate towards T^{mC}+ve single cells (mesoderm)(Fig5.22-1.a.ii, 2.a.ii). At D4, the major population in WT is T^{mC}+ and the percentages of $Sox2^{V}$+ and T^{mC}+/$Sox2^{V}$+ population has decreased in comparison to D3 (Fig5.22-1.b.i, 2.b.i). Some cells that were $Sox2^{V}$+ve at D3 have now become double positive. Mutant cells at D4 still consist mostly of T^{mC}+/$Sox2^{V}$+ and percentage of $Sox2^{V}$+ has decreased (Fig5.22-1.b.ii, 2.b.ii). The double positive mutant cells still maintain high Sox2 reporter activity although the overall population displays less T fluorescence activity (on average) in comparison to D3 double positives (Fig5.22-1.b.ii, 2.b.ii). Additionally, some double positive cells become single TmC+ cells (Fig5.22-1.b.ii, 2.b.ii). The same trend continues for both WT and mutant cells at D5 (Fig5.23-1.c, 2.c). More WT cells are now T^{mC}+ve and fewer mutant cells are transitioning to be T^{mC}+ve. The number of T^{mC}+/$Sox2^{V}$+ and $Sox2^{V}$+ cells are fewer than D4 in WT (Fig5.23-1.c.i, 2.c.i) and the population remains reproducible to D4 in mutant cells (Fig5.23-1.c.ii, 2.c.ii). At D6, the percentages of WT T^{mC}+ cells are fewer, as cells now become double negative and a slight increase in T^{mC}+/$Sox2^{V}$+ population is observed (Fig5.23-1.d.i, 2.d.i).

Mutant cells also reduce the percentages of T^{mC}+/$Sox2^{V}$+ population, some double positive cells become $Sox2^{V}$+ve, in addition to double positive cells with reduced T expression becoming T^{mC}+ singles (Fig5.23-1.d.ii, 2.d.ii). As a result the number of $Sox2^{V}$+ve cells is higher than D5 (Fig5.23-1.c.ii,2.c.ii). It appears as though the whole double positive population of GDF11 KO reduces T expression. In general, while WT cells already have T^{mC}+ve cells, mutant cells retain double positive cells with high T and Sox2 levels resulting in an accumulation of T^{mC}+/$Sox2^{V}$+ population. This is observed in both differentiation experiments, even though DE-2 WT cells have differentiated more homogenously and faster in comparison to DE-1.

The populations in FACS were sorted on D3-D6 of differentiation and expression of makers for mesoderm lineage commitment were measured by qPCR

5.4.1 EXPRESSION OF NMP AND MESODERMAL MARKERS DURING DIFFERENTIATION

T is an early mesoderm marker (Murry & Keller, 2008; Papaioannou, 2014; Showell et al., 2004), which is initially expressed along the primitive streak during gastrulation. Furthermore, *T* along with expression of *Sox2* is a marker for axial mesodermal progenitors-NMPs (Cambray & Wilson, 2007; Tsakiridis et al., 2014).

Expression of *T* in the bulk of WT and mutant cells during differentiation is downregulated over the differentiation time points (Fig5.24-a and b). *T* expression in WT cells (T^{wt}) is downregulated from D3-D4 following which the T^{wt} expression is maintained in DE-1 and further downregulated in DE-2 at D5. The oppositive trend is observed at D6, where T^{wt} expression is maintained in DE-2 and downregulated in DE-1. This observation likely corresponds to the speed of differentiation and T^{mC}+ percentages observed in the WT FACS data. Similarly, T expression in mutant cells (T^{m}) of DE-1 is also downregulated, as observed in the FACS profiles and is comparable to T^{wt} expression in DE-1 (Fig5.24-a). WT cells show slightly higher T expression in comparison to mutants at D5 and D6, whereas, in DE-2 at D5 and D6, higher T expression was detected in mutant (Fig5.24-b). This can be accounted by the difference in rates and homogeneity of differentiation observed in WT cells of DE-1 and DE-2, while the mutant cells between the two experiments differentiate at a similar rate.

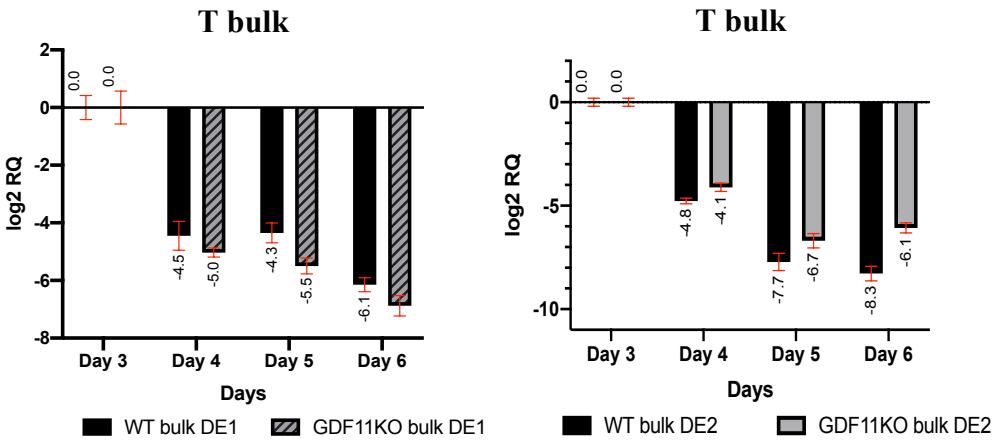

Figure 5.24:
Expression profile of *T*. Graph represents log2 fold Relative expression ± error of T normalised to D3 for both WT and Gdf11 KO. ***a.*** *T* expression in DE-1. **b**. *T* expression in DE-2

Generally, expression of T in bulk of WT and Gdf11 KO cells is downregulated in comparison to D3. In DE-2 T^{m} expression is higher than T^{wt} expression.

The protocol used for differentiation of mESCs, drives NMPs towards the mesodermal sub lineage. *Sox2* along with *T* is a NMP marker and *Sox2* is a marker for neural tissue. To see whether neural cells are generated during differentiation, we measured *Sox2* expression.

DE-1 expression of *Sox2*^{wt} is maintained from D3 to D6. On the other hand, DE-1 *Sox2*^{m} is maintained from D3 to D4 after which it rises to 3-fold at D5 following which *Sox2*^{m} decreases again at D6 (Fig5.25-a). DE-2 *Sox2*^{m} expression at D3 is 8-fold higher to D3 *Sox2*^{wt} expression (data not shown). *Sox2*^{wt} in DE-2 is upregulated by 3-fold at D4 and then the levels are maintained until D6. *Sox2*^{m} does not vary from D3 to D6 (Fig5.25-b). This difference in expression of *Sox2*^{wt} between DE-1 and DE-2 could be because of higher expression of *Sox2*^{wt} resulting in an increase in Sox2^{V}+ cells at D3 in DE-1 than DE-2 (as seen in FACS profile).

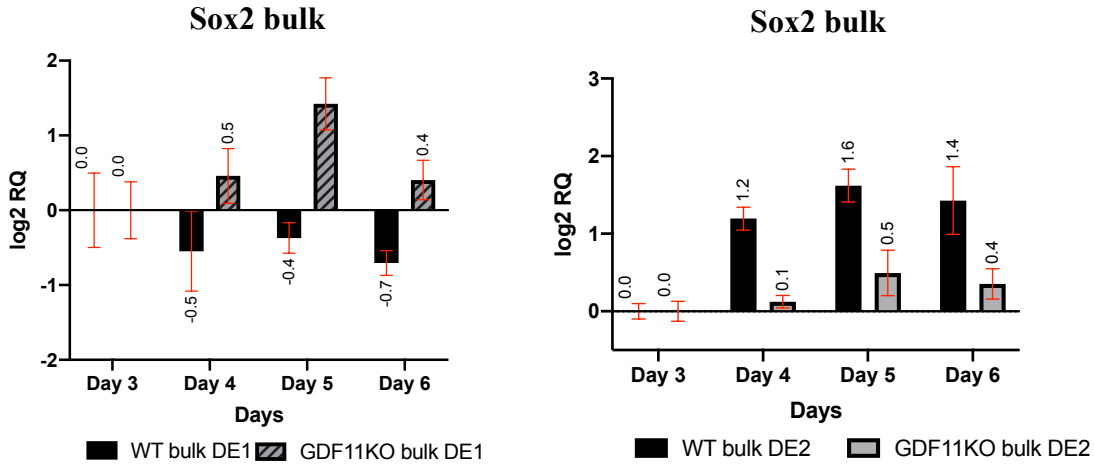

Figure 5.25:
Expression profile of *Sox2*. Graph represents log2 fold Relative expression ± error of *Sox2* normalised to D3 for both WT and Gdf11 KO. ***a.*** *Sox2* expression in DE-1. **b**. *Sox2* expression in DE-2

Sox2 expression between the two experiments is differentially expressed. *Sox2*^{wt} is maintained in one experiment and upregulated in the other whereas, *Sox2*^{m} expression is upregulated in one experiment and maintained in the other. The mechanism of regulation that cause these variations are not clearly understood.

Since there is evidence that Gdf11 could indirectly downregulate Oct4 during its role in trunk to tail transition, we expected to see an upregulation of *Oct4* in Gdf11 KO cells.

The pluripotency marker, *Oct4* is downregulated as cells differentiate. This observed in both WT and mutant of both differentiation experiments. The extents of downregulation between WT and mutant are also similar (Fig 5.26-a, Fig5.26-b). Therefore, we observe the opposite effect of our initial expectation.

In addition to the above-mentioned markers, expression of *Tbx6*, which is an early mesoderm marker was measured. *Tbx6* is required for the commitment of cells to the mesoderm lineage (Koch et al., 2017)(Takemoto et al., 2011).

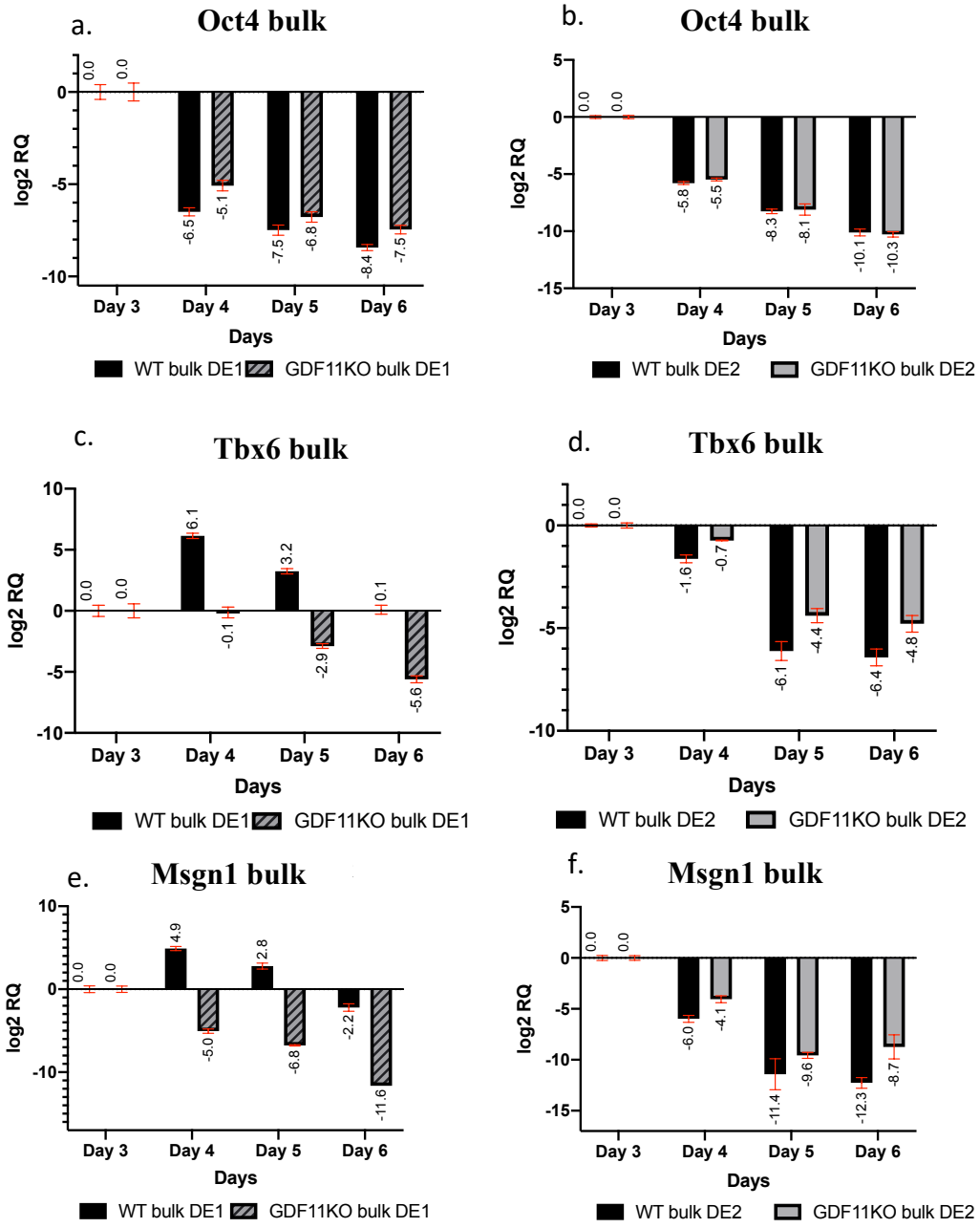

Figure 5.26:
Graph represents log2 fold Relative expression ± error, normalised to D3 for both WT and Gdf11 KO. ***a.*** *Oct4* expression in DE-1. **b**. *Oct4* expression in DE-2 ***c.*** *Tbx6* expression in DE-1. **d**. *Tbx6* expression in DE-2. ***e.*** *Msgn1 expression* in DE-1. **b**. *Msgn1* expression in DE-2

Tbx6^{wt} expression peaks at D4 in DE-1 with an increase of 32-fold, becomes downregulated 8-fold at D5 and further downregulated by 8-fold at D6 to reach similar levels as on D3 (Fig 5.26-c). Mutant cells at D4 of DE-1, maintain similar level of *Tbx6*^{m} as observed at D3.
Cells then downregulate *Tbx6*^{m} expression by 8-fold at D5 and an additional 6-fold at D6. *Tbx6*^{m} expression at D3 is 32-fold higher than D3 *Tbx6*^{wt} DE-1 cells (Fig5.26-c). The WT and mutant cells of DE-2 appear to differentiate comparably, both of them displaying peaking levels *Tbx6* expression at D3 with subsequent downregulation. *Tbx6*^{wt} is downregulated by 3-fold at D4, an additional downregulation of 21-fold at D5 and this low level is maintained at D6 (Fig 5.26-d). Mutant cells downregulate *Tbx6*^{m} by less than 2-fold at D3 followed by a 32-fold downregulation and maintain this low level at D6. As observed the extent of downregulation is comparable between the WT and mutant (Fig 5.26-d). *Tbx6*^{m} expression is reproducibly higher than *Tbx6*^{wt}.
Furthermore, an early PSM marker which is regulated by *Tbx6*, *Msgn1* was measured. *Msgn1* commits progenitor cells to the PSM sub lineage. Supporting this, *Msgn1*^{wt} expression in DE1 follows *Tbx6*^{wt} expression. Expression of *Msgn1*^{wt} is upregulated by 32-fold at D4, further downregulated by 4-fold at D5 and an additional 32-fold on D6. *Msgn1*^{m} expression does not exactly follow *Tbx6*^{m} of DE1(Fig 5.26-e). Rather, *Msgn1*^{m} expression is already downregulated by 32-fold at D4 and further downregulated by 64-fold at D6. At D3 of DE-1 expression of *Msgn1*^{m} is 500 -fold higher than *Msgn1*^{wt} expression at D3 (data not shown).
Both *Msgn1*^{wt} and *Msgn1*^{m} expression of DE-2 follow Tbx6 of DE-2 and are reproducibly downregulated (Fig 5.26-f).
Bulk expression data of these genes only help to understand general dynamics of expression. DE-2 WT and mutant cells express markers more homogenously in comparison to DE-1 experiment. In both experiments, *Msgn1* follows *Tbx6 e*xpression and both these markers are downregulated as differentiation proceeds. As far as bulk gene expression is concerned, WT and Gdf11 KO cells are regulated similarly although the flow cytometry profiles show an accumulation and delayed differentiation into mesoderm sub lineage. In order to look at gene regulation in specific population, cells were sorted according to the expression of reporters and then measured by qPCR for the above-mentioned genes.

Expression of *T*^{wt} in T^{mc}+/Sox2^{V}+ sorted cells is downregulated by approximately 20-fold from D3-D4 (Fig 5.27-a), upregulated by 2-fold at D5 and subsequently downregulated by 6-fold from D5 to D6 . Downregulation of *T*^{m} in T^{mc}+/Sox2^{V}+ population at D4 is comparable to WT *T* expression at D4, following which this low level of expression is maintained until D5 and

further downregulated by 5.6-fold (Fig 5.27-a). Expression of T^{wt} in mCherry cells (single positive) is downregulated by 32-fold from D3-D4 and then expression level is maintained from D4-D5 following which expression level is further downregulated from D5-D6 by 10-fold (Fig 4.27-c). T^{wt} and T^{m} expression at D5 and D6 is comparable in T^{mC}+ cells. Since no mutant cells were present for T-mCherry (single positive) at D3 and D4, real-time expression data is not available for these time points (Fig 5.27-c). Although it would not be expected that cells sorted for $Sox2^{V}$ reporter expression would express *T* mRNA, *T* expression is downregulated in both WT and mutant $Sox2^{V}$+ve cells at D3 in comparison to bulk expression of T at D3.(Fig 4.27-b). Expression of T^{wt} and T^{m} is comparable to the dynamics observed in double positive population.

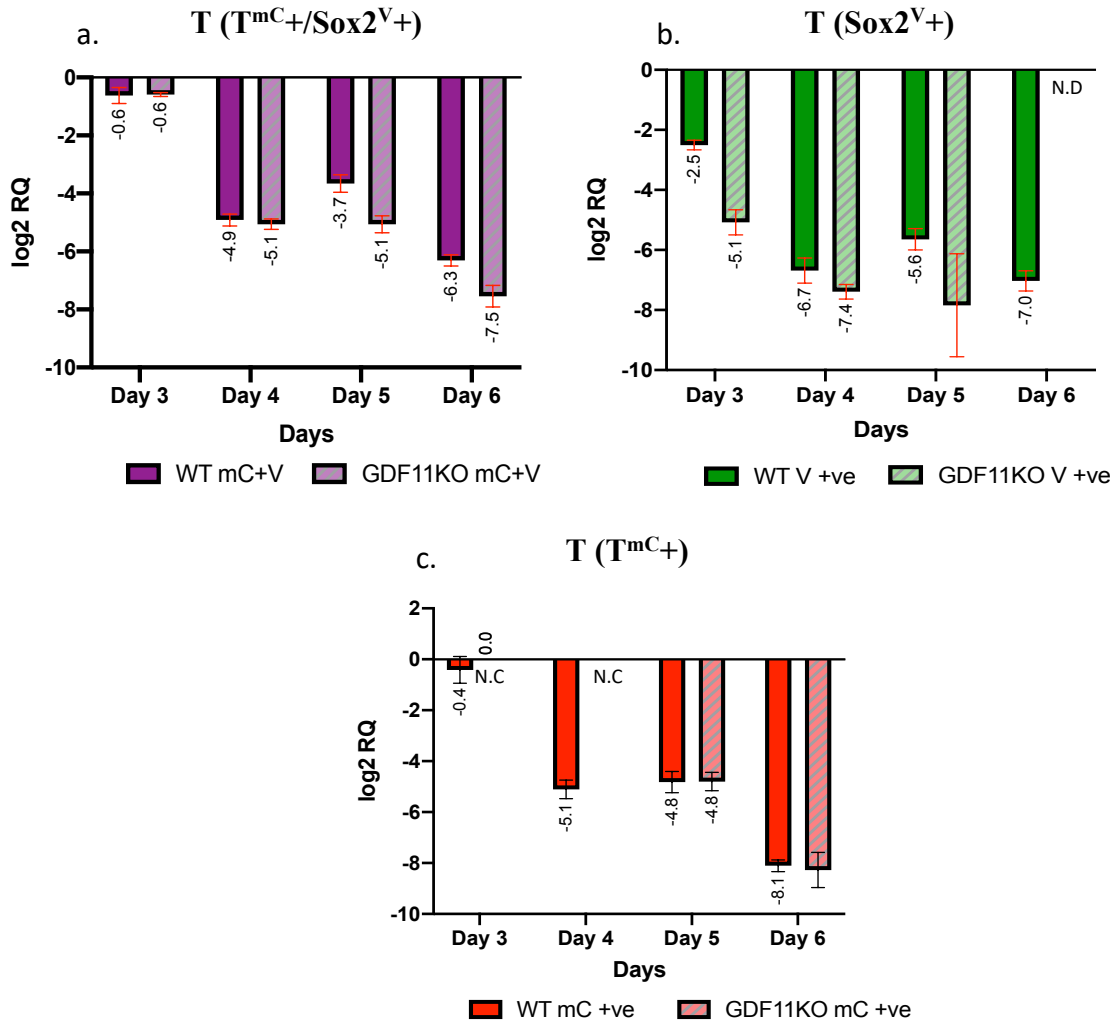

Figure 5.27 :
Regulation of *T* in WT and Gdf11 KO cells. Graphs represent log2 fold change ± error. **a.** Expression profile of *T* in mCherry+/Venus+ sorted cells. b. Expression profile of *T* in Venus+ve sorted cells. **c.** Expression profile of *T* in mCherry+ve sorted cells. N.C- no cells sorted , N.D- expression not detectable

In the population sorted for double positive cells, *Sox2*^{wt} expression is maintained from D3 to D4 following which there is a 2-fold upregulation at D5 and then this level is maintained at D6 (Fig 5.28-a). An upregulation of 2-fold is observed in *Sox2*^{m} expression from D3-D4 and the expression further increases by 2-fold at D5. D5 is the timepoint of highest *Sox2* expression and *Sox2* is downregulated by 3-fold over the next 24h (Fig 5.28-a).

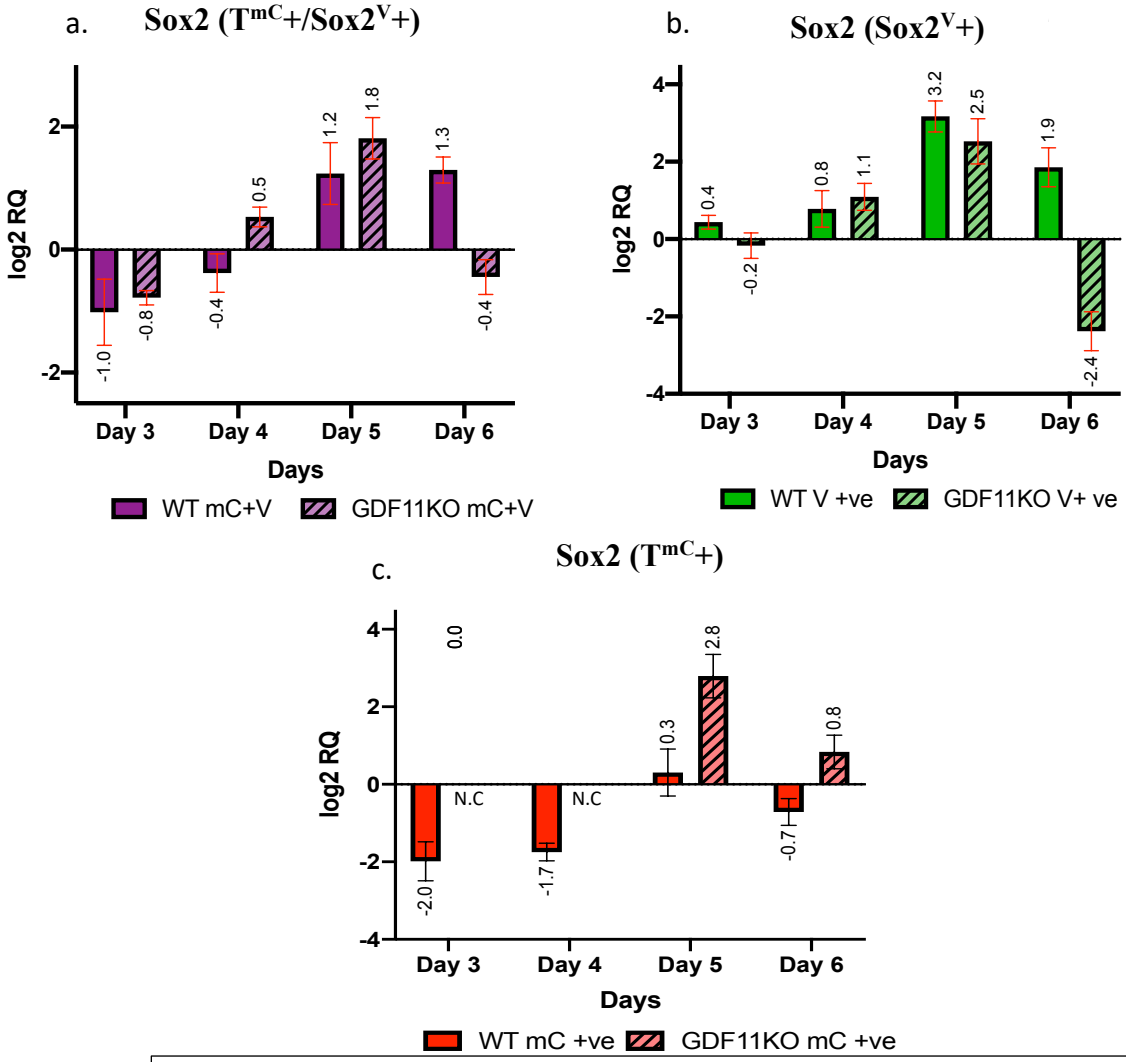

Figure 5.28 :
Regulation of *Sox2* in WT and Gdf11 KO cells. Graphs represent log2 fold change ± error. **a.** Expression profile of *Sox2* in mCherry+/Venus+ sorted cells. b. Expression profile of *Sox2* in Venus+ve sorted cells. **c.** Expression profile of *Sox2* in mCherry+ve sorted cells. N.C- no cells sorted , N.D- expression not detectable

Sox2 expression in cells sorted for single Venus+ cells, (Fig 5.28-b) is reproducible to expression levels in double positive population. The only difference in *Sox2* expression is observed during D5 to D6, where *Sox2*^{m} is downregulated whereas, *Sox2*^{wt} is maintained. Regulation of *Sox2* in WT cells sorted for mCherry is maintained at D3 and D4 (Fig 5.28-c),

becomes upregulated 3-fold at D5 and is then maintained at D6. At D5, *Sox2* expression in Gdf11 KO mCherry+ve cells is 8-fold higher than the *Sox2* bulk expression at D3. Expression is then downregulated by 4-fold at D6 (Fig 5.28-c). Expression of *Sox2* between double positive and Venus+ve population is reproducible and Gdf11 KO mCherry+ve cells showhigher *Sox2* expression than WT at D5.

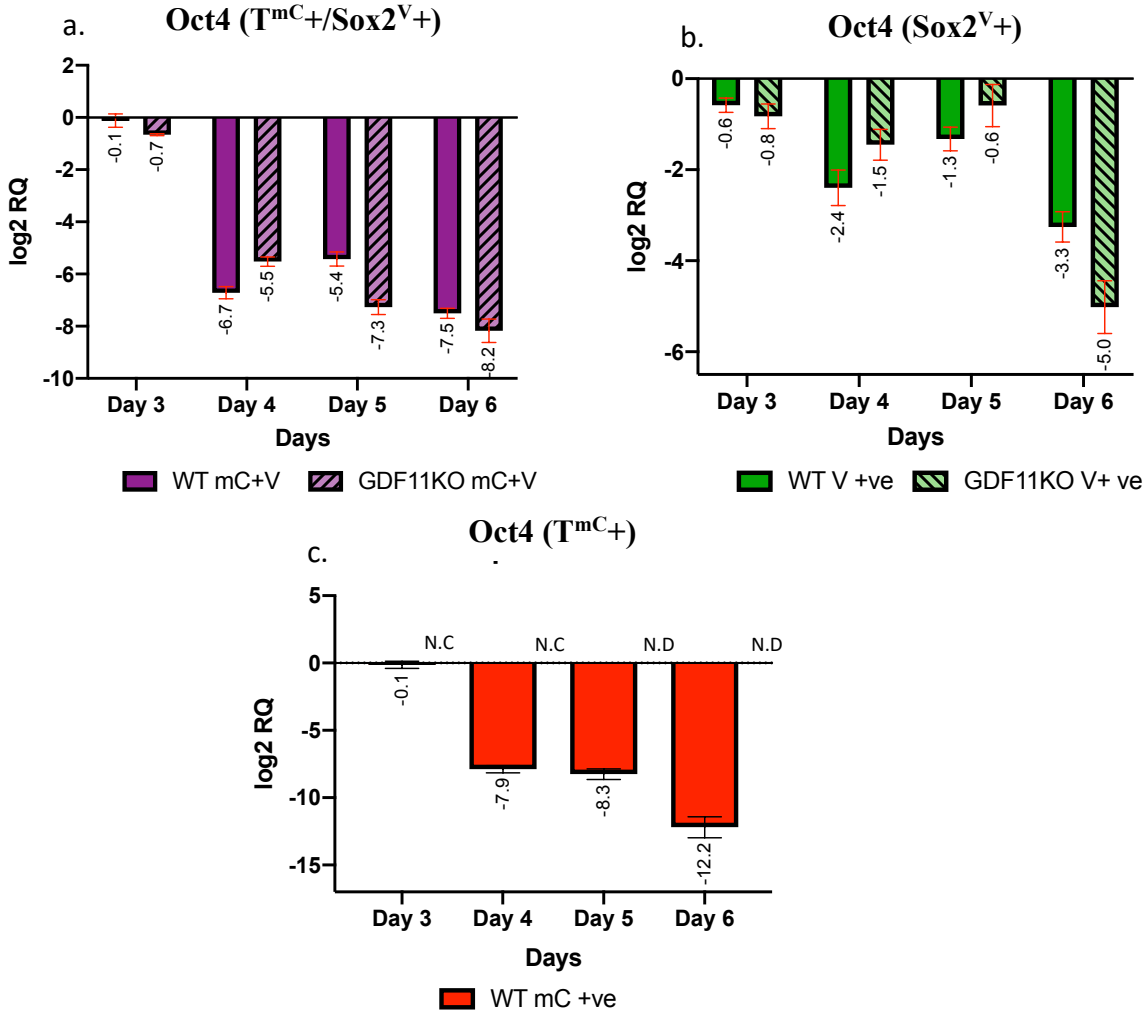

Figure 5.29 :
Regulation of *Oct4* in WT and Gdf11 KO cells. Graphs represent log2 fold change ± error. **a.** Expression profile of *Oct4* in mCherry+/Venus+ sorted cells. b. Expression profile of *Oct4* in Venus+ve sorted cells. **c.** Expression profile of *Oct4* in mCherry+ve sorted cells. N.C- no cells sorted, N.D- expression not detectable

Oct4 WT and mutant bulk expression at D3 are comparable. $Oct4^{wt}$ expression at D4 in mCherry+/Venus+ population is downregulated by 100-fold in comparison to D3. Expression level is then upregulated by 2.5-fold at D5 after which *Oct4* is further downregulated by 4-fold (Fig 4.29-a). On the other hand, *Oct4* in mutant cells is downregulated from D3-D6. Regulation of *Oct4* in WT population of Venus+ cells is downregulated by 3-fold at D4 after which

expression slightly increases and continues to drop by a fold change of 4-fold from D5-D6 (Fig 5.29-b). In mutant cells expression is maintained from D3 to D5 and is downregulated by 21-fold at D6 (Fig 5.29-b). *Oct4* expression is downregulated by 250-fold in WT mCherry sorted cells at D4 and the same level is maintained at D5(Fig 5.29-c). At D6 expression is further downregulated by 16-fold. *Oct4* expression in GDF11 KO cells is not detectable in mCherry sorted cells at D5 and D6 (Fig 5.29-c). In general, Oct4 expression is comparable between WT and Gdf11 KO at each timepoint and no differences were observed.

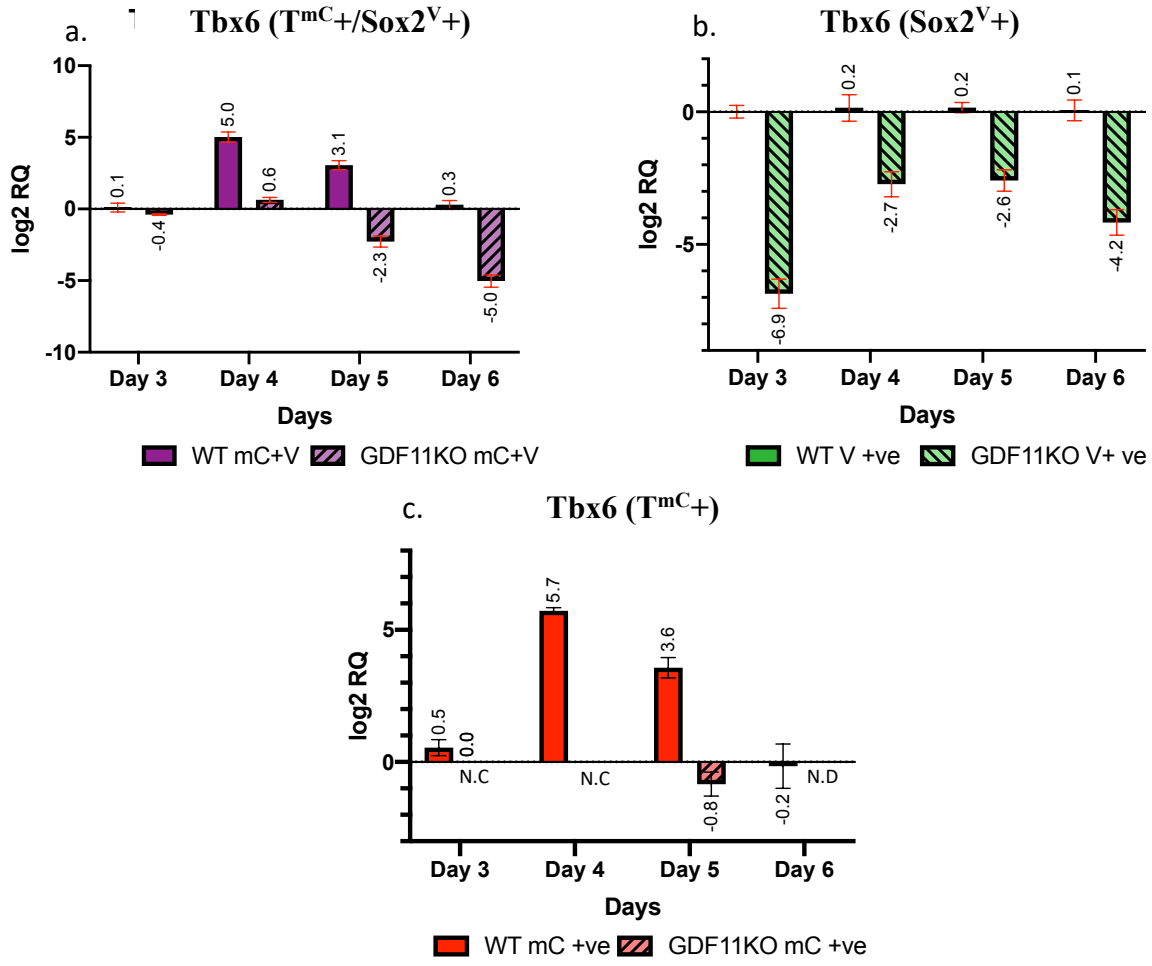

Figure 5.30 :
Regulation of *Tbx6* in WT and Gdf11 KO cells. Graphs represent log2 fold change ± error. **a.** Expression profile of *Tbx6* in mCherry+/Venus+ sorted cells. b. Expression profile of *Tbx6* in Venus+ve sorted cells. **c.** Expression profile of *Tbx6* in mCherry+ve sorted cells. N.C- no cells sorted, N.D- expression not detectable

Tbx6^{wt} expression is upregulated by 32-fold mCherry+/Venus+ from D3 to D4 and then downregulated by 4-fold at D5. *Tbx6*^{wt} continues to be downregulated at D6 by 8-fold. In the GDf11 KO cells expression is maintained from D3-D4, becomes downregulated by 4-fold at

D5 and an additional 6-fold in D6 (Fig 5.30-a). *Tbx6*^{wt} expression is maintained over all days in Venus+ve cells (Fig 4.30-b). *Tbx6*^{m} expression at D3 in Venus+ve cells is downregulated in comparison to expression at D3 in bulk cells. At D4 expression is upregulated 16-fold and this level is maintained in D5 after which a slight increase in expression is observed at D6 (Fig 5.30-b). Expression in WT mCherry sorted cells is upregulated by 32-fold from D3 to D4 and then downregulated by 4-fold at D5 and further by 12 fold at D6. Mutant cells at D5 express low levels of *Tbx6* comparable to the expression level in bulk cells at D3 (Fig 5.30-c). Comparing bulk expression of *Tbx6* between WT and Gdf11KO cells at D3, *Tbx6*^{m} expression is 32 fold higher than *Tbx6*^{wt} (expression data not shown).

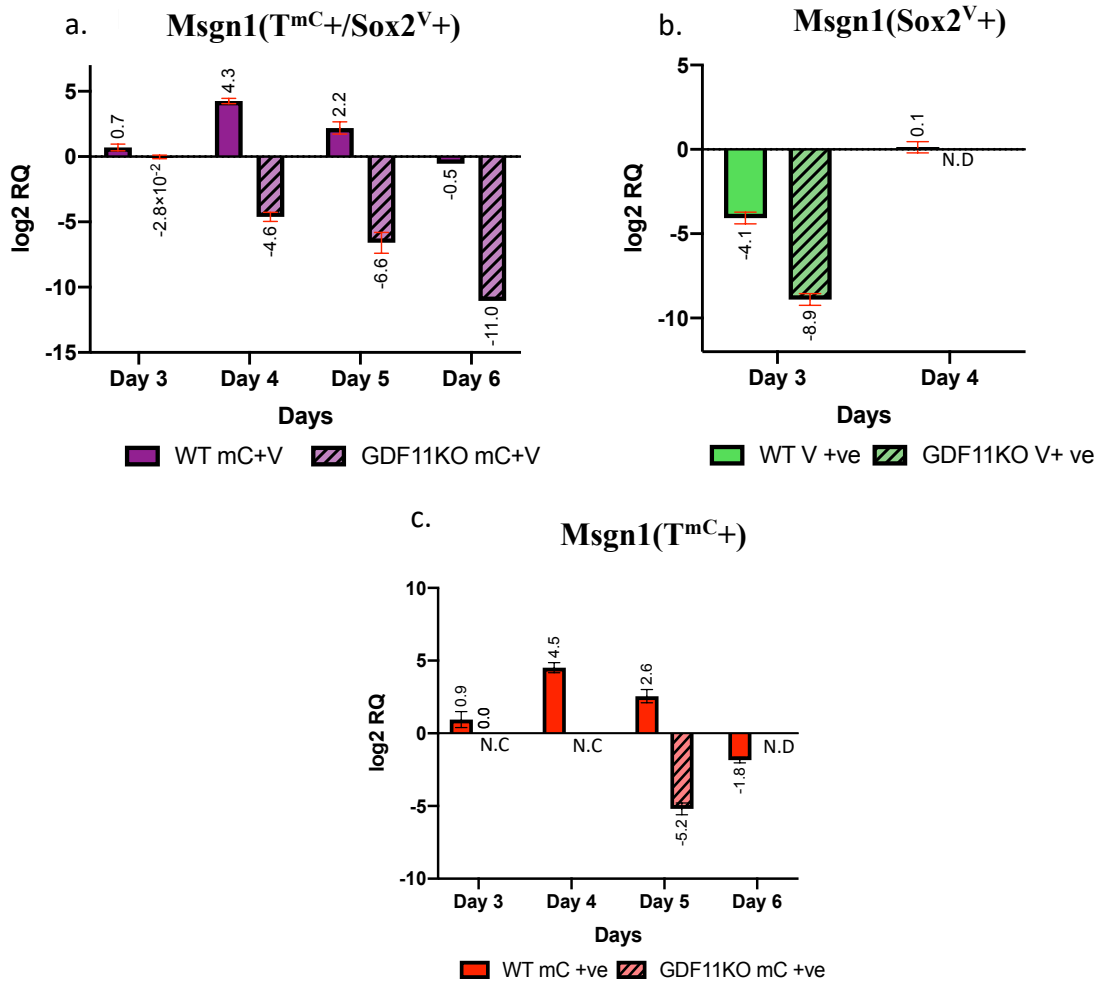

Figure 5.31 :
Regulation of *Msgn1* in WT and Gdf11 KO cells. Graphs represent log2 fold change ± error. **a.** Expression profile of *Msgn1* in mCherry+/Venus+ sorted cells. b. Expression profile of *Msgn1* in Venus+ve sorted cells. **c.** Expression profile of *Msgn1* in mCherry+ve sorted cells. N.C- no cells sorted, N.D- expression not detectable

Dynamics of *Msgn1* follows that of *Tbx6*. In WT double positive cells expression peaks at D4 by 16-fold after which it is downregulated by 4-fold at D5 and further downregulation of 5-

fold. In the mutant cells a downregulation of 18-fold is observed at D4 after which expression is downregulated at D5 and D6 as observed in the WT (Fig 5.31-a). Expression of *Msgn1* in WT mCherry sorted cells follow similar pattern as seen in double positive cells. Whereas, the expression level at D6 mCherry sorted mutant cell is not detectable (Fig 5.31-c).

Regulation of gene expression in sorted cells follow the bulk expression. Downregulation of *T* corresponds to a downregulation of *Tbx6* and *Msgn*. *Sox2*^{wt} is highest at D6 in double positive population. Inversely, *Tbx6*^{wt} is low at this timepoint. *Sox2*^{m} is highest at D5 and then downregulated at D6 and *Tbx6*^{m} is also downregulated from D5 to D6.

Additionally, expression of *Gdf11* was also measured by qPCR in WT and mutant bulk cells over the 4 timepoints. Expression of *Gdf11* in WT cells was upregulated by 4-fold at D4, remained the same at D5 and further increases by 2-fold at D6 (data not shown). The expression level was un detectable in Gdf11 KO cells. Gdf11 expression in WT is seen between D3 and D4. This made us further evaluate the possibility to rescue these effects in mutants by exogenous rGDF11 addition.

5.5 RESCUING KNOCKOUT EFFECTS IN GDF11 MUTANTS

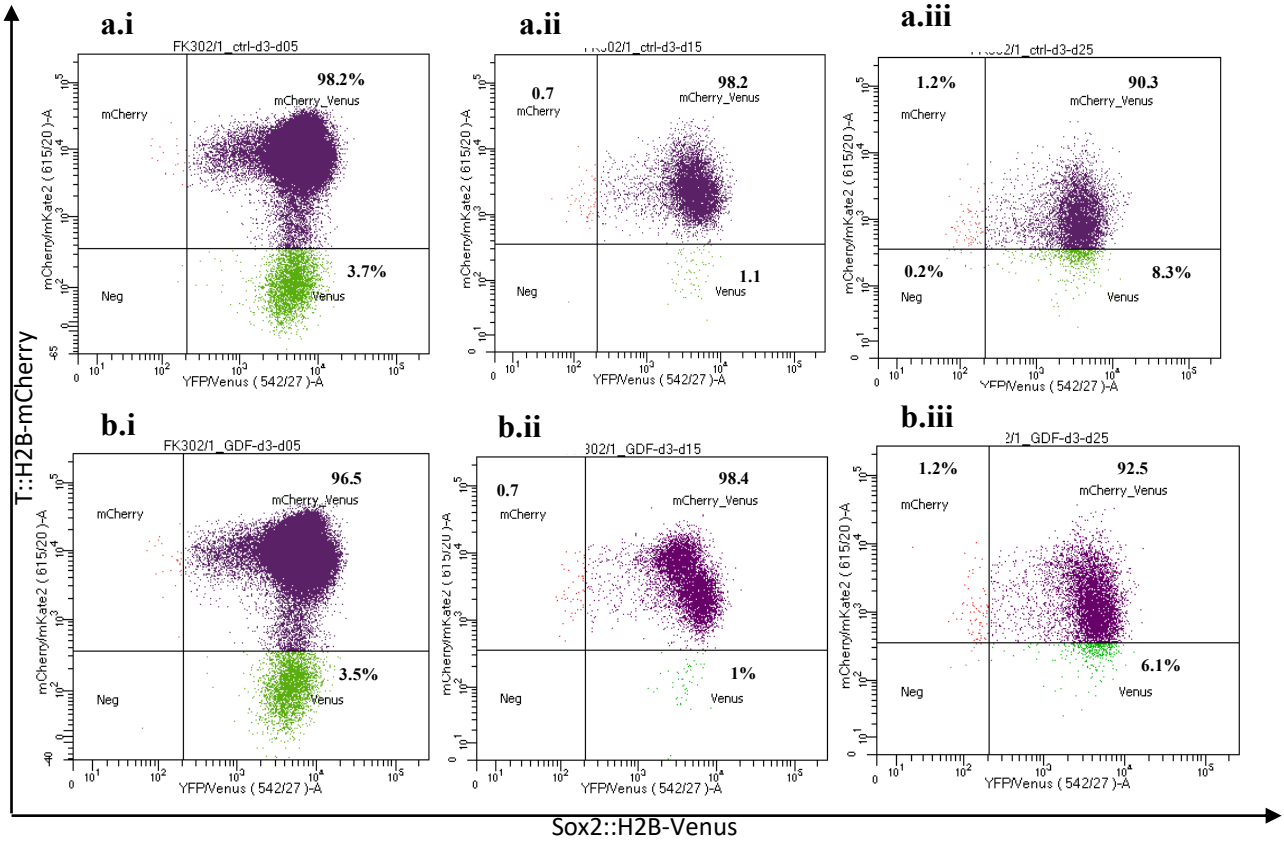

Figure 5.32:
FACS profile of **a.** Control and **b.** rGDF11 rescue at D3 over 3 timepoints.

Cells of the GDF11 KO were differentiated into NMPs (D1-D3) following which cells were induced with 20ng/ml of r.GDF11 in order to understand if the absence of GDF11 can be rescued. GDF11 KO cells without r.GDF11 were used as a control. Following D3, cells were differentiated using the PSM differentiation protocol either with or without GDF11 addition. Rescue with r.GDF11 was done at two different time points of differentiation, D3 and at D3.5 independently. Following the addition of GDF11, cells were analysed by both flow cytometry and qPCR at three time points.

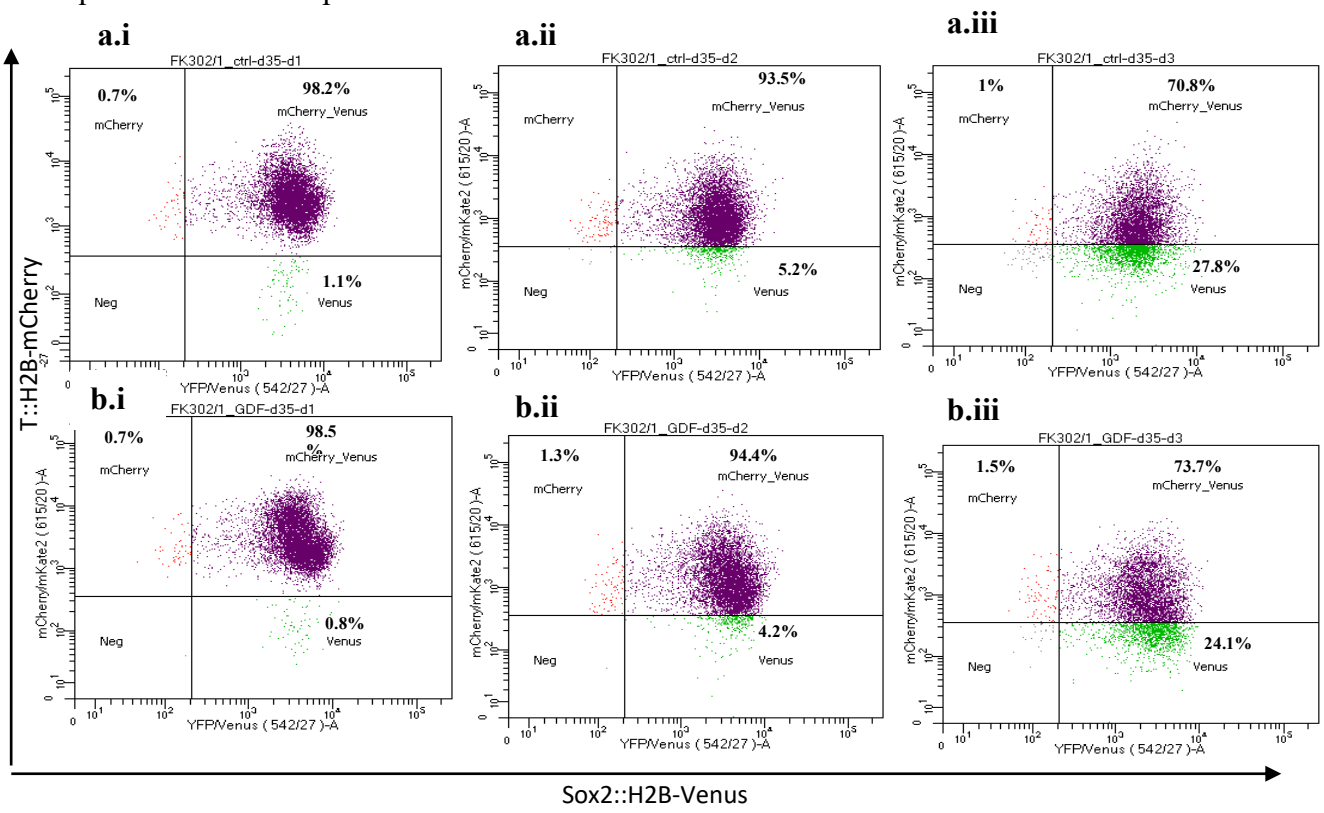

Figure 5.33:
FACS profile of **a.** Control and **b.** rGDF11 rescue at D3.5 over 3 timepoints.

Cells supplied with external GDF11 at D3 were first analysed after 12h of GDF11 exposure (D3-0.5). At this timepoint, the FACS profile of both the control (Fig 5.32-a.i) and the GDF recued cells (Fig 5.32-b.i) appear similar with majority of cells being double positive for both T^{mC}+/$SOX2^{V}$+ and 3.5% cells single positive for $SOX2^{V}$+. After an additional 24h of GDF11 exposure (D3-1.5), the percentages of cells that are double positive for both reporters and single positive cells are comparable between the control and treated cells. Under both condition there is a decrease of T^{mC} expression in double positive cells which differentiate to become mCherry single positive cells (Fig 5.32- a.ii, b.ii). In addition, double positive control cells of the

previous time point, have reduced mCherry expression. This is also observed in the treated cells. In addition to this population, the treated cells have an additional double positive population with less $Sox2^{V}$ expression and high mCherry expression (Fig 5.32-b.ii). After an additional 24h (D3-2.5h), some double positive cells have lost T^{mC} expression to become single $Sox2^{V}$+ve cells (Fig 5.32- a.iii, b.iii). The rest of the population have also reduced T^{mC} expression while most of the population retain $Sox2^{V}$expression, some cells become single T^{mC}+ve cells. A similar trend is also observed in the treated cells at this timepoint (Fig 5.32-b.iii).

For cells that were induced after the initial 3.5 days of differentiation, percentages of cells that are double and single positive for reporters are similar between the control and the treated cells. In addition, the percentages are also similar at the same timepoints independent of the timepoint of GDF11 recue. Graphs of D3.5 induced cells after 1 day (Fig 5.33-a.i, b.i) (D3.5-1) look similar to graph of D3 induced cells after 1.5 days (Fig 5.33-a.ii, b.ii) (D3-1.5). It also appears that after 6.5 days (Fig 5.33-a.iii, b.iii) of differentiation, number of double positive cells that move itnto $Sox2^{V}$ single +ve quadrant is more than the number of double positive cells that differentiate to become T^{mC} single +ve cells.

No major rescue effects of rGDF11 is observed from the flow cytometry data. Further, expression of T, Sox2, Tbx6, Msgn1 and Oct4 were measured by qPCR on D3 and D3.5 induced cells. No differences in expression between control and GDF11 induced cells was observed. (qPCR expression in Appendix).

6. DISCUSSION

Bipotent axial progenitors (NMPs) (Henrique, Abranches, Verrier, & Storey, 2015) and the LPMP (Wymeersch et al., 2016) present in the caudal end of the embryo contribute to most of the mesodermal sub lineages in the developing embryo axis. The NMPs give rise to mainly the PSM. On the other hand, LPMP give rise to both LPM and paraxial mesoderm depending on their location in the CLE. The decision of lineage choice is further influenced by signaling factors like Wnt, FGF and BMPs. Differentiation of PSM requires Wnt signaling and is inhibited by BMP signals whereas, differentiation of LPM is independent of Wnt signaling but requires BMP signals. Hence the ratio between Wnt and BMP signals is an import factor in mesoderm sublineage commitment. The mechanism in which BMP4 drives LPM differentiation during trunk development is not clearly understood. Additionally, the essential

role of BMP4 during early stages of embryonic development, gastrulation, has been a bottleneck in the establishment Bmp4 null embryo, since a complete loss of Bmp4 results in lethality of the embryo around the time of gastrulation.

In order to circumvent this, we attempted to generate a CRE dependent conditional Bmp4 KO cell line during two timepoints of development and study the effects of Bmp4 in mesodermal sublineage choice during these two timepoints. Chosen timepoints for conditional KO were mid-trunk (HoxC8::iCre) and late-trunk stage (HoxC10::iCre), where CRE expression is driven by Hox gene expression and therefore deletion of Bmp4 occurs at these specific timepoints of development. This method of conditional KO where CRE expression is driven by promoter activity has many advantages over the traditional tamoxifen induced CRE expression. Tamoxifen dependent CRE expression although useful for lineage tracing studies and for generating tissue specific KO, has some disadvantages when it comes to a development dependent conditional KO. The possible delay between administration of Tamoxifen and its time of action along with the uncertainty involved in determination of the exact stage of development in cells/embryo makes this system complicated. Hence, the use of a promoter driven CRE expression is much more timepoint specific and precise in generating the conditional KO.
In order to generate the conditional KO cell line, Bmp4 KO mESCs have to be electroporated with a BAC containing the floxed Bmp4 gene, to compensate for the lack of genomic Bmp4, which is required for gastrulation. Floxing Bmp4 gene was first attempted using homologous recombineering which resulted in insertion of 3' loxP sequence. The lack of the 5' loxP sequence could be due to the presence of polyA repeat sequences in the 5' end of the gene next to the 50bp homology sequence. Additionally, since the regions of the exon provides a larger homologous sequence, it is probable that recombination occurred somewhere on the exon instead of the 50bp homologues sequence. Taking into account the overall inefficiency of recombineering, which resulted in fewer clones, along with the above mentioned reasons could have resulted in the lack of a clone containing both the 5' and 3' loxP sequences.

Due to this, we used CRISPR-Cas9 system to knock in the missing 5'loxP sequence along with BAC (Bmp4) integration into the genome of Bmp4 KO ESC by co-electroporation of the BAC and CRISPR plasmid. Additionally, we also electroporated only Bmp4-loxP BAC into KO ESCs. Sequencing results of co-electroporated cells confirmed the missing 5' loxP site. Hence, we were unable to generate the Bmp4 conditional KO cells line. Furthermore, CRISPR can be

done in a sequential manner with electroporation of CRISPR plasmid into the Bmp4-loxP ESCs (above generated). On successful generation of the conditional KO cells lines by repetition and optimization of experiments, these ESC can be used to perform differentiation experiments to generate LPM and PSM as well as for *in-vivo* experiments in conditional KO embryos.

Differentiation of mESC to NMPs and further mesodermal progenitor has been performed by many labs but no differentiation protocol exists for the generation of LPM from mESC which faithfully recapitulates the process in the embryo. Adapting from experiments where LPM was generated from HPSC, we have established a differentiation protocol for LPM. Here, LPM was generated by exposing a population of NMP-like cells to BMP4 and FGF signals for 3 days. In the embryo, some LPM tissue is generated through NMPs and our experiment is a recapitulation of the events during development. Markers such as Foxf1, Hand1, Tbx6 was used to identify the identity of the differentiated cells. Foxf1 and Hand1 increased at D4 following which Foxf1 levels were maintained. This maintenance of Foxf1 was accompanied by an increase in Gata6 expression and decrease in Irx3 (Mahlapuu et al., 2001), implying that in this protocol we were able to successfully generate Splanchnic mesoderm.
Interestingly, FACS profile during early days of differentiation showed the increase in Foxf1^{V}+ cells upon addition of CHIRON (D3). This has been shown in hPSC, where addition of CHIRON caused the expression of mesoderm sub lineage markers – *Foxf1* and *Tbx6* (Lam et al., 2014). FACS profile of cells over additional 3 days of differentiation under FB20 condition have comparable percentage of Foxf1^{V}+ cells whereas, the percentages decrease under the B20 condition. This observation is supported by greater downregulation of Hand1 in B20 condition than FB20 condition. This led us to speculate whether cells differentiate into LPM slower in the FB20 condition and exist as a LPM progenitor under this differentiation condition. Conversely, the expression of Gata6 does not support this observation, since it is upregulated greater under FB20 conditions. Nevertheless, both these conditions generate LPM-like cells, but the FB20 condition was chosen for further experiments due its reproducibility to *in-vivo* conditions of the caudal embryo.
This differentiation protocol can additionally be used to generate large numbers of LPM-like cells to further understand markers for lineage commitment. Analysis of histone modifications by ChIP-Seq to look for candidate LPM markers and Proteomic analysis requires large amount of material which can be generated by this protocol.

GDF11(BMP11) which plays a role in modifying Hox genes during vertebral axis development. Its role in trunk to tail transition has been shown in mice by overexpression or mutants of the gene (Jurberg et al., 2013; Lee & Lee, 2013; Liu, 2006; McPherron et al., 1999).

Gdf11 mutant mice have additional vertebrae and an expansion of anterior Hox gene expression. Presence of additional vertebrae would indicate that additional somites have been generated from the axial progenitor cells. Our results of differentiating Gdf11 KO ESCs to NMPs and mesodermal progenitor cells show an accumulation of the NMP-like population in the mutant cells. This accumulation of NMPs (visualized by FACS) is also accompanied by their delayed differentiation into mesodermal cells. Accumulation of tailbud progenitors has also been shown in the embryo of GDF11 KO mice (Aires et al., 2019). Furthermore, NMP-like cells retain high levels of Sox2 in the flow cytometry profile. This is also observed in the real time data, where Sox2 expression was 8-fold higher than WT. FACS of tailbud NMPs from Gdf11 KO embryo (E10.5) revealed a higher number of Sox2+ cells compared to WT (Aires et al., 2019). A similar trend is observed in FACS of D6 Gdf11 mutants, where double positive cells become single positive $Sox2^{V}$. This result could suggest that NMPs might differentiate towards neural lineage when lacking GDF11.

Although the Gdf11 mutant cells have similar levels of Tbx6 and Msgn1 to that of WT, these levels are still insufficient to drive the PSM differentiation even in the presence of Wnt signals. It is possible that Gdf11 downregulates Sox2 in the progenitor population and thereby contribute to mesodermal tissue. We also observe the comparable dynamics of *Sox2* and *Tbx6* in Gdf11 mutants (Aires et al., 2019) whereas, *Tbx6* is known to suppress *Sox2* expression as observed in the WT (Takemoto et al., 2011) .

Since we also show through real time data that Gdf11 has no effect on differentiation of NMPs to LPM, we could speculate that the NMPs generated in this protocol are tailbud NMPs. In the embryo GDF11 is also required for the formation of hindlimbs. It is therefore possible that Gdf11 is required in the later stages of LPM and does not have an impact on the nascent LPM differentiation.

Downregulation of Oct4 in the progenitors causes the shift from contributing to trunk tissue to the generation of tail tissue. But, the expansion of tailbud NMPs in the Gdf11 mutant embryo has been shown to be Oct4 independent (Aires et al., 2019), which supports the real time data of Oct4, where it is regulated similarly between WT and mutant cells. Contradicting this, some studies also show that Oct4 is required for trunk development but not for tail development (Aires et al., 2016; DeVeale et al., 2013). Our data suggest that Gdf11 plays a role in maintenance of the progenitor population and the timely switch between contributing to tail and trunk tissue.

Although we were unable to elucidate the mechanism by which Gdf11 facilitates this trunk to tail transition, studying the Hox gene expression of the accumulated NMP-like cells could shed some light on the mechanism involved. Furthermore, addition of GDF11 to WT NMPs should cause their posteriorising and this can be confirmed by measuring late Hox gene expression.
Additional ChIP-Seq and RNA sequencing experiments could help us understand better how GDF11 influences gene expressions in the progenitor population which thereby influence shift from producing trunk to tail tissue. Additionally, *in-vivo* experiments can also be performed to understand the mechanism.
Attempts to rescue the absence of *Gdf11* in mutant cells was unsuccessful. No difference in FACS as well at real time data between control and GDF11 recued cells was observed. This could be because of the delayed response of cells to exogenous GDF11 or insufficient concentration of GDF11. Hence, optimization of rescue experiment by increasing the concentration and earlier addition of GDF11 (at D2) can be performed.

7. REFERENCES

Aires, R., de Lemos, L., Nóvoa, A., Jurberg, A. D., Mascrez, B., Duboule, D., & Mallo, M. (2019). Tail Bud Progenitor Activity Relies on a Network Comprising Gdf11, Lin28, and Hox13 Genes. *Developmental Cell*. https://doi.org/10.1016/j.devcel.2018.12.004

Aires, R., Dias, A., & Mallo, M. (2018). Deconstructing the molecular mechanisms shaping the vertebrate body plan. *Current Opinion in Cell Biology*. https://doi.org/10.1016/j.ceb.2018.05.009

Aires, R., Jurberg, A. D., Leal, F., Nóvoa, A., Cohn, M. J., & Mallo, M. (2016). Oct4 Is a Key Regulator of Vertebrate Trunk Length Diversity. *Developmental Cell*. https://doi.org/10.1016/j.devcel.2016.06.021

Anderson, M. J., Naiche, L. A., Wilson, C. P., Elder, C., Swing, D. A., & Lewandoski, M. (2013). TCreERT2, a transgenic mouse line for temporal control of Cre-mediated recombination in lineages emerging from the primitive streak or tail bud. *PloS One*, *8*(4), e62479. https://doi.org/10.1371/journal.pone.0062479

Andersson, O., Reissmann, E., & Ibáñez, C. F. (2006). Growth differentiation factor 11 signals through the transforming growth factor-beta receptor ALK5 to regionalize the anterior-posterior axis. *EMBO Reports*, *7*(8), 831–837. https://doi.org/10.1038/sj.embor.7400752

Arnold, S. J., & Robertson, E. J. (2009). Making a commitment: cell lineage allocation and axis patterning in the early mouse embryo. *Nature Reviews. Molecular Cell Biology*, *10*(2), 91–103. https://doi.org/10.1038/nrm2618

Becker, D., Eid, R., & Schughart, K. (1996). The limb/LPM enhancer of the murine Hoxb6 gene: reporter gene analysis in transgenic embryos and studies of DNA-protein interactions. *Pharmaceutica Acta Helvetiae*, *71*(1), 29–35. https://doi.org/10.1016/0031-6865(95)00049-6

Ben-Yair, R., & Kalcheim, C. (2005). Lineage analysis of the avian dermomyotome sheet reveals the existence of single cells with both dermal and muscle progenitor fates. *Development*. https://doi.org/10.1242/dev.01617

Beppu, H., Kawabata, M., Hamamoto, T., Chytil, A., Minowa, O., Noda, T., & Miyazono, K. (2000). BMP type II receptor is required for gastrulation and early development of mouse embryos. *Developmental Biology*, *221*(1), 249–258. https://doi.org/10.1006/dbio.2000.9670

Bragdon, B., Moseychuk, O., Saldanha, S., King, D., Julian, J., & Nohe, A. (2011). Bone morphogenetic proteins: a critical review. *Cellular Signalling*, *23*(4), 609–620. https://doi.org/10.1016/j.cellsig.2010.10.003

Brown, J. M., & Storey, K. G. (2000). A region of the vertebrate neural plate in which neighbouring cells can adopt neural or epidermal fates. *Current Biology : CB*, *10*(14), 869–872. https://doi.org/10.1016/s0960-9822(00)00601-1

Cambray, N., & Wilson, V. (2007). Two distinct sources for a population of maturing axial progenitors. *Development*, *134*(15), 2829 LP – 2840. https://doi.org/10.1242/dev.02877

Carapuço, M., Nóvoa, A., Bobola, N., & Mallo, M. (2005). Hox genes specify vertebral types in the presomitic mesoderm. *Genes and Development*. https://doi.org/10.1101/gad.338705

Catala, M. (2005). *Embryology of the Spine and Spinal Cord BT - Pediatric Neuroradiology: Brain* (P. Tortori-Donati & A. Rossi, Eds.). https://doi.org/10.1007/3-540-26398-5_38

Chalamalasetty, R. B., Garriock, R. J., Dunty, W. C., Kennedy, M. W., Jailwala, P., Si, H., & Yamaguchi, T. P. (2014). Mesogenin 1 is a master regulator of paraxial presomitic mesoderm differentiation. *Development*, *141*(22), 4285 LP – 4297. https://doi.org/10.1242/dev.110908

Chapman, D. L., Agulnik, I., Hancock, S., Silver, L. M., & Papaioannou, V. E. (1996). Tbx6, a mouse T-box gene implicated in paraxial mesoderm formation at gastrulation. *Developmental Biology*. https://doi.org/10.1006/dbio.1996.0326

Cheung, C., Bernardo, A. S., Trotter, M. W. B., Pedersen, R. A., & Sinha, S. (2012). Generation of human vascular smooth muscle subtypes provides insight into embryological origin–dependent disease susceptibility. *Nature Biotechnology*, *30*(2), 165–173. https://doi.org/10.1038/nbt.2107

Christ, B., Huang, R., & Scaal, M. (2004). Formation and differentiation of the avian sclerotome. *Anatomy and Embryology*. https://doi.org/10.1007/s00429-004-0408-z

Czyz, J., & Wobus, A. M. (2001). Embryonic stem cell differentiation: The role of extracellular factors. *Differentiation*. https://doi.org/10.1046/j.1432-0436.2001.680404.x

Davidson, A. J., & Zon, L. I. (2004). The "definitive" (and 'primitive') guide to zebrafish hematopoiesis. *Oncogene*, *23*(43), 7233–7246. https://doi.org/10.1038/sj.onc.1207943

Davis, R. L., & Kirschner, M. W. (2000). The fate of cells in the tailbud of Xenopus laevis. *Development*, *127*(2), 255 LP – 267. Retrieved from http://dev.biologists.org/content/127/2/255.abstract

DeVeale, B., Brokhman, I., Mohseni, P., Babak, T., Yoon, C., Lin, A., … van der Kooy, D. (2013). Oct4 Is Required ~E7.5 for Proliferation in the Primitive Streak. *PLOS Genetics*, *9*(11), e1003957. Retrieved from https://doi.org/10.1371/journal.pgen.1003957

Duboule, D. (1994). Temporal colinearity and the phylotypic progression: A basis for the stability of a vertebrate Bauplan and the evolution of morphologies through heterochrony. *Development*.

Eaton, G. J., & Green, M. M. (1963). Implantation and lethality of the yellow mouse. *Genetica*. https://doi.org/10.1007/BF01725754

Ferretti, E., & Hadjantonakis, A.-K. (2019). Mesoderm specification and diversification: from single cells to emergent tissues. *Current Opinion in Cell Biology*, *61*, 110–116. https://doi.org/https://doi.org/10.1016/j.ceb.2019.07.012

Fierro-González, J. C., White, M. D., Silva, J. C., & Plachta, N. (2013). Cadherin-dependent filopodia control preimplantation embryo compaction. *Nature Cell Biology*. https://doi.org/10.1038/ncb2875

Firulli, A. B., McFadden, D. G., Lin, Q., Srivastava, D., & Olson, E. N. (1998). Heart and extra-embryonic mesodermal defects in mouse embryos lacking the bHLH transcription factor Hand1. *Nature Genetics*, *18*(3), 266–270. https://doi.org/10.1038/ng0398-266

Funayama, N., Sato, Y., Matsumoto, K., Ogura, T., & Takahashi, Y. (1999). Coelom formation: Binary decision of the lateral plate mesoderm is controlled by the ectoderm. *Development*.

Fürthauer, M., Van Celst, J., Thisse, C., & Thisse, B. (2004). Fgf signalling controls the dorsoventral patterning of the zebrafish embryo. *Development*, *131*(12), 2853 LP – 2864. https://doi.org/10.1242/dev.01156

Garriock, R. J., Chalamalasetty, R. B., Kennedy, M. W., Canizales, L. C., Lewandoski, M., & Yamaguchi, T. P. (2015). Lineage tracing of neuromesodermal progenitors reveals novel Wnt-dependent roles in trunk progenitor cell maintenance and differentiation. *Development*, *142*(9), 1628 LP – 1638. https://doi.org/10.1242/dev.111922

George, S. H. L., Gertsenstein, M., Vintersten, K., Korets-Smith, E., Murphy, J., Stevens, M. E., … Nagy, A. (2007). Developmental and adult phenotyping directly from mutant embryonic stem cells. *Proceedings of the National Academy of Sciences of the United States of America*. https://doi.org/10.1073/pnas.0609277104

Gilbert, S. F., & Barresi, M. J. F. (2017). DEVELOPMENTAL BIOLOGY, 11TH EDITION 2016. *American Journal of Medical Genetics Part A*. https://doi.org/10.1002/ajmg.a.38166

Goto, H., Kimmey, S. C., Row, R. H., Matus, D. Q., & Martin, B. L. (2017). FGF and canonical Wnt signaling cooperate to induce paraxial mesoderm from tailbud neuromesodermal progenitors through regulation of a two-step epithelial to mesenchymal transition. *Development (Cambridge)*. https://doi.org/10.1242/dev.143578

Gouti, M., Delile, J., Stamataki, D., Wymeersch, F. J., Huang, Y., Kleinjung, J., … Briscoe, J. (2017). A Gene Regulatory Network Balances Neural and Mesoderm Specification during Vertebrate Trunk Development. *Developmental Cell*, *41*(3), 243-261.e7. https://doi.org/10.1016/j.devcel.2017.04.002

Gouti, M., Tsakiridis, A., Wymeersch, F. J., Huang, Y., Kleinjung, J., Wilson, V., & Briscoe, J. (2014). In vitro generation of neuromesodermal progenitors reveals distinct roles for wnt signalling in the specification of spinal cord and paraxial mesoderm identity. *PLoS Biology*, *12*(8), e1001937. https://doi.org/10.1371/journal.pbio.1001937

GRUNEBERG, H. (1958). Genetical studies on the skeleton of the mouse. XXIII. The development of brachyury and anury. *Journal of Embryology and Experimental Morphology*.

Hammonds Jr., R. G., Schwall, R., Dudley, A., Berkemeier, L., Lai, C., Lee, J., … Mason, A. J. (1991). Bone-Inducing Activity of Mature BMP-2b Produced from a Hybrid BMP-2a/2b Precursor. *Molecular Endocrinology*, *5*(1), 149–155. https://doi.org/10.1210/mend-5-1-149

Henrique, D., Abranches, E., Verrier, L., & Storey, K. G. (2015). Neuromesodermal progenitors and the making of the spinal cord. *Development*, *142*(17), 2864 LP – 2875. https://doi.org/10.1242/dev.119768

Hill, C. S. (2018). Spatial and temporal control of NODAL signaling. *Current Opinion in Cell Biology*, *51*, 50–57. https://doi.org/https://doi.org/10.1016/j.ceb.2017.10.005

Holley, S. A., & Ferguson, E. L. (1997). Fish are like flies are like frogs: conservation of dorsal-ventral patterning mechanisms. *BioEssays : News and Reviews in Molecular, Cellular and Developmental Biology*, *19*(4), 281–284. https://doi.org/10.1002/bies.950190404

Iyer, D., Gambardella, L., Bernard, W. G., Serrano, F., Mascetti, V. L., Pedersen, R. A., … Sinha, S. (2015). Robust derivation of epicardium and its differentiated smooth muscle cell progeny from human pluripotent stem cells. *Development (Cambridge, England)*, *142*(8), 1528–1541. https://doi.org/10.1242/dev.119271

James, R. G., & Schultheiss, T. M. (2003). Patterning of the avian intermediate mesoderm by lateral plate and axial tissues. *Developmental Biology*. https://doi.org/10.1006/dbio.2002.0863

Javali, A., Misra, A., Leonavicius, K., Acharyya, D., Vyas, B., & Sambasivan, R. (2017). Co-expression of Tbx6 and Sox2 identifies a novel transient neuromesoderm progenitor cell state. *Development*, *144*(24), 4522 LP – 4529. https://doi.org/10.1242/dev.153262

Jeong Kyo Yoon, & Wold, B. (2000). The bHLH regulator pMesogenin1 is required for maturation and segmentation of paraxial mesoderm. *Genes and Development*. https://doi.org/10.1101/gad.850000

Jurberg, A. D., Aires, R., Varela-Lasheras, I., Nóvoa, A., & Mallo, M. (2013). Switching axial progenitors from producing trunk to tail tissues in vertebrate embryos. *Developmental Cell*. https://doi.org/10.1016/j.devcel.2013.05.009

Kieny, M., Mauger, A., & Sengel, P. (1972). Early regionalization of the somitic mesoderm as studied by the development of the axial skeleton of the chick embryo. *Developmental Biology*. https://doi.org/10.1016/0012-1606(72)90133-9

Koch, F., Scholze, M., Wittler, L., Schifferl, D., Sudheer, S., Grote, P., … Herrmann, B. G. (2017). Antagonistic Activities of Sox2 and Brachyury Control the Fate Choice of Neuro-Mesodermal Progenitors. *Developmental Cell*. https://doi.org/10.1016/j.devcel.2017.07.021

Kojima, Y., Tam, O. H., & Tam, P. P. L. (2014). Timing of developmental events in the early mouse embryo. *Seminars in Cell and Developmental Biology*. https://doi.org/10.1016/j.semcdb.2014.06.010

Lam, A. Q., Freedman, B. S., Morizane, R., Lerou, P. H., Valerius, M. T., & Bonventre, J. V. (2014). Rapid and efficient differentiation of human pluripotent stem cells into intermediate mesoderm that forms tubules expressing kidney proximal tubular markers. *Journal of the American Society of Nephrology*. https://doi.org/10.1681/ASN.2013080831

Lawson, K. A., Meneses, J. J., & Pedersen, R. A. (1991). Clonal analysis of epiblast fate during germ layer formation in the mouse embryo. *Development*, *113*(3), 891 LP – 911. Retrieved from http://dev.biologists.org/content/113/3/891.abstract

Le Mouellic, H., Lallemand, Y., & Brûlet, P. (1992). Homeosis in the mouse induced by a null mutation in the Hox-3.1 gene. *Cell*. https://doi.org/10.1016/0092-8674(92)90406-3

Lee, Y. S., & Lee, S. J. (2013). Regulation of GDF-11 and myostatin activity by GASP-1 and GASP-2. *Proceedings of the National Academy of Sciences of the United States of America*. https://doi.org/10.1073/pnas.1309907110

Lei, H., Juan, A. H., Kim, M. S., & Ruddle, F. H. (2006). Identification of a Hoxc8-regulated transcriptional network in mouse embryo fibroblast cells. *Proceedings of the National Academy of Sciences of the United States of America*. https://doi.org/10.1073/pnas.0603552103

Li, R. A., & Storey, K. G. (2011). An emerging molecular mechanism for the neural vs mesodermal cell fate decision. *Cell Research*, *21*(5), 708–710. https://doi.org/10.1038/cr.2011.54

Linask, K. K. (1992). N-cadherin localization in early heart development and polar expression of Na+,K(+)-ATPase, and integrin during pericardial coelom formation and epithelialization of the differentiating myocardium. *Developmental Biology*, *151*(1), 213–224. https://doi.org/10.1016/0012-1606(92)90228-9

Liu, J.-P. (2006). The function of growth/differentiation factor 11 (Gdf11) in rostrocaudal patterning of the developing spinal cord. *Development*, *133*(15), 2865 LP – 2874. https://doi.org/10.1242/dev.02478

Loebel, D. A. F., Watson, C. M., De Young, R. A., & Tam, P. P. L. (2003). Lineage choice and differentiation in mouse embryos and embryonic stem cells. *Developmental Biology*. https://doi.org/10.1016/S0012-1606(03)00390-7

Mahlapuu, M., Ormestad, M., Enerbäck, S., & Carlsson, P. (2001). The forkhead transcription factor Foxf1 is required for differentiation of extra-embryonic and lateral plate mesoderm. *Development (Cambridge, England)*, *128*(2), 155–166.

Martin, B. L., & Kimelman, D. (2008). Regulation of Canonical Wnt Signaling by Brachyury Is Essential for Posterior Mesoderm Formation. *Developmental Cell*. https://doi.org/10.1016/j.devcel.2008.04.013

Martin, J. F., & Olson, E. N. (2000, April). Identification of a prx1 limb enhancer. *Genesis (New York, N.Y. : 2000)*, Vol. 26, pp. 225–229. United States.

Martinez Arias, A., & Steventon, B. (2018). On the nature and function of organizers. *Development (Cambridge, England)*, *145*(5). https://doi.org/10.1242/dev.159525

Matsubara, Y., Hirasawa, T., Egawa, S., Hattori, A., Suganuma, T., Kohara, Y., … Suzuki, T. (2017). Anatomical integration of the sacral-hindlimb unit coordinated by GDF11 underlies variation in hindlimb positioning in tetrapods. *Nature Ecology and Evolution*. https://doi.org/10.1038/s41559-017-0247-y

McPherron, A. C., Lawler, A. M., & Lee, S. J. (1999). Regulation of anterior/posterior patterning of the axial skeleton by growth/differentiation factor 11. *Nature Genetics*. https://doi.org/10.1038/10320

Mishina, Y., Suzuki, A., Ueno, N., & Behringer, R. R. (1995). Bmpr encodes a type I bone morphogenetic protein receptor that is essential for gastrulation during mouse embryogenesis. *Genes & Development*, *9*(24), 3027–3037. https://doi.org/10.1101/gad.9.24.3027

Motosugi, N., Bauer, T., Polanski, Z., Solter, D., & Hiiragi, T. (2005). Polarity of the mouse embryo is established at blastocyst and is not prepatterned. *Genes and Development*. https://doi.org/10.1101/gad.1304805

Mugele, D., Moulding, D. A., Savery, D., Molè, M. A., Greene, N. D. E., Martinez-Barbera, J. P., & Copp, A. J. (2018). Genetic approaches in mice demonstrate that neuro-mesodermal progenitors express T/Brachyury but not Sox2 *BioRxiv*, 503854. https://doi.org/10.1101/503854

Murry, C. E., & Keller, G. (2008). Differentiation of embryonic stem cells to clinically relevant populations: lessons from embryonic development. *Cell*, *132*(4), 661–680. https://doi.org/10.1016/j.cell.2008.02.008
Nakashima, M., Toyono, T., Akamine, A., & Joyner, A. (1999). Expression of growth/differentiation factor 11, a new member of the BMP/TGFβ superfamily during mouse embryogenesis. *Mechanisms of Development*. https://doi.org/10.1016/S0925-4773(98)00205-6
Nakayama, N., Lee, J., & Chiu, L. (2000). Vascular endothelial growth factor synergistically enhances bone morphogenetic protein-4-dependent lymphohematopoietic cell generation from embryonic stem cells in vitro. *Blood*. https://doi.org/10.1182/blood.v95.7.2275.007k30_2275_2283
Ng, E. S., Azzola, L., Sourris, K., Robb, L., Stanley, E. G., & Elefanty, A. G. (2005). The primitive streak gene Mixl1 is required for efficient haematopoiesis and BMP4-induced ventral mesoderm patterning in differentiating ES cells. *Development*. https://doi.org/10.1242/dev.01657
Nguyen, P. D., Hollway, G. E., Sonntag, C., Miles, L. B., Hall, T. E., Berger, S., … Currie, P. D. (2014). Haematopoietic stem cell induction by somite-derived endothelial cells controlled by meox1. *Nature*. https://doi.org/10.1038/nature13678
Nishimatsu, S., & Thomsen, G. H. (1998). Ventral mesoderm induction and patterning by bone morphogenetic protein heterodimers in Xenopus embryos. *Mechanisms of Development*, *74*(1), 75–88. https://doi.org/https://doi.org/10.1016/S0925-4773(98)00070-7
Nowicki, J. L., & Burke, A. C. (2000). Hox genes and morphological identity: Axial versus lateral patterning in the vertebrate mesoderm. *Development*.
Olivera-Martinez, I., Harada, H., Halley, P. A., & Storey, K. G. (2012). Loss of FGF-dependent mesoderm identity and rise of endogenous retinoid signalling determine cessation of body axis elongation. *PLoS Biology*, *10*(10), e1001415. https://doi.org/10.1371/journal.pbio.1001415
Olson, E. N. (2006). Gene regulatory networks in the evolution and development of the heart. *Science (New York, N.Y.)*, *313*(5795), 1922–1927. https://doi.org/10.1126/science.1132292
Papaioannou, V. E. (2014). The T-box gene family: emerging roles in development, stem cells and cancer. *Development (Cambridge, England)*, *141*(20), 3819–3833. https://doi.org/10.1242/dev.104471
Perantoni, A. O., Timofeeva, O., Naillat, F., Richman, C., Pajni-Underwood, S., Wilson, C., … Lewandoski, M. (2005). Inactivation of FGF8 in early mesoderm reveals an essential role in kidney development. *Development*, *132*(17), 3859 LP – 3871. https://doi.org/10.1242/dev.01945
Peterson, R. L., Jacobs, D. F., & Awgulewitsch, A. (1992). Hox-3.6: isolation and characterization of a new murine homeobox gene located in the 5′ region of the Hox-3 cluster. *Mechanisms of Development*. https://doi.org/10.1016/0925-4773(92)90077-W
Pourquié, O., Fan, C. M., Coltey, M., Hirsinger, E., Watanabe, Y., Bréant, C., … Le Douarin, N. M. (1996). Lateral and axial signals involved in avian somite patterning: A role for BMP4. *Cell*. https://doi.org/10.1016/S0092-8674(00)81291-X
Rallis, C., Del Buono, J., & Logan, M. P. O. (2005). Tbx3 can alter limb position along the rostrocaudal axis of the developing embryo. *Development*, *132*(8), 1961 LP – 1970. https://doi.org/10.1242/dev.01787
Rojas, A., De Val, S., Heidt, A. B., Xu, S.-M., Bristow, J., & Black, B. L. (2005). Gata4 expression in lateral mesoderm is downstream of BMP4 and is activated directly by Forkhead and GATA transcription factors through a distal enhancer element. *Development*, *132*(15), 3405 LP – 3417. https://doi.org/10.1242/dev.01913
Rosenquist, G. C. (1970). Location and movements of cardiogenic cells in the chick embryo: the heart-forming portion of the primitive streak. *Developmental Biology*, *22*(3), 461–475. https://doi.org/10.1016/0012-1606(70)90163-6
Rossant, J., & Tam, P. P. L. (2009). Blastocyst lineage formation, early embryonic asymmetries and axis patterning in the mouse. *Development*, *136*(5), 701 LP – 713. https://doi.org/10.1242/dev.017178
Row, R. H., & Kimelman, D. (2009). Bmp inhibition is necessary for post-gastrulation patterning and morphogenesis of the zebrafish tailbud. *Developmental Biology*, *329*(1), 55–63. https://doi.org/10.1016/j.ydbio.2009.02.016
Row, R. H., Pegg, A., Kinney, B. A., Farr, G. H., Maves, L., Lowell, S., … Martin, B. L. (2018). BMP and FGF signaling interact to pattern mesoderm by controlling basic helix-loop-helix transcription factor activity. *ELife*. https://doi.org/10.7554/eLife.31018
Saga, Y., & Takeda, H. (2001). The making of the somite: Molecular events in vertebrate segmentation. *Nature Reviews Genetics*. https://doi.org/10.1038/35098552
Schier, A. F., & Talbot, W. S. (2005). Molecular Genetics of Axis Formation in Zebrafish. *Annual Review of Genetics*, *39*(1), 561–613. https://doi.org/10.1146/annurev.genet.37.110801.143752
Sharma, R., Shafer, M. E. R., Bareke, E., Tremblay, M., Majewski, J., & Bouchard, M. (2017). Bmp signaling maintains a mesoderm progenitor cell state in the mouse tailbud. *Development*, *144*(16), 2982 LP – 2993. https://doi.org/10.1242/dev.149955
Shashikant, C. S., & Ruddle, F. H. (1996). Combinations of closely situated cis-acting elements determine tissue-specific patterns and anterior extent of early Hoxc8 expression. *Proceedings of the National Academy of Sciences of the United States of America*. https://doi.org/10.1073/pnas.93.22.12364

Sheng, G., dos Reis, M., & Stern, C. D. (2003). Churchill, a zinc finger transcriptional activator, regulates the transition between gastrulation and neurulation. *Cell*, *115*(5), 603–613. https://doi.org/10.1016/s0092-8674(03)00927-9

Showell, C., Binder, O., & Conlon, F. L. (2004). T-box genes in early embryogenesis. *Developmental Dynamics : An Official Publication of the American Association of Anatomists*, *229*(1), 201–218. https://doi.org/10.1002/dvdy.10480

Sim, Y. J., Kim, M. S., Nayfeh, A., Yun, Y. J., Kim, S. J., Park, K. T., … Kim, K. S. (2017). 2i Maintains a Naive Ground State in ESCs through Two Distinct Epigenetic Mechanisms. *Stem Cell Reports*. https://doi.org/10.1016/j.stemcr.2017.04.001

Suh, J., Eom, J. H., Kim, N. K., Woo, K. M., Baek, J. H., Ryoo, H. M., … Lee, Y. S. (2019). Growth differentiation factor 11 locally controls anterior–posterior patterning of the axial skeleton. *Journal of Cellular Physiology*. https://doi.org/10.1002/jcp.28904

Suzuki, A., Raya, Á., Kawakami, Y., Morita, M., Matsui, T., Nakashima, K., … Belmonte, J. C. I. (2006). Nanog binds to Smad1 and blocks bone morphogenetic protein-induced differentiation of embryonic stem cells. *Proceedings of the National Academy of Sciences of the United States of America*. https://doi.org/10.1073/pnas.0506945103

Takada, S., Stark, K. L., Shea, M. J., Vassileva, G., McMahon, J. A., & McMahon, A. P. (1994). Wnt-3a regulates somite and tailbud formation in the mouse embryo. *Genes and Development*. https://doi.org/10.1101/gad.8.2.174

Takemoto, T., Uchikawa, M., Yoshida, M., Bell, D. M., Lovell-Badge, R., Papaioannou, V. E., & Kondoh, H. (2011). Tbx6-dependent Sox2 regulation determines neural or mesodermal fate in axial stem cells. *Nature*, *470*(7334), 394–398. https://doi.org/10.1038/nature09729

Tam, P. P., & Beddington, R. S. (1987). The formation of mesodermal tissues in the mouse embryo during gastrulation and early organogenesis. *Development*, *99*(1), 109 LP – 126. Retrieved from http://dev.biologists.org/content/99/1/109.abstract

Tam, P. P., & Behringer, R. R. (1997). Mouse gastrulation: the formation of a mammalian body plan. *Mechanisms of Development*, *68*(1–2), 3–25. https://doi.org/10.1016/s0925-4773(97)00123-8

Tam, P. P. L., & Tan, S. S. (1992). The somitogenetic potential of cells in the primitive streak and the tail bud of the organogenesis-stage mouse embryo. *Development*.

Thomson, M., Liu, S. J., Zou, L.-N., Smith, Z., Meissner, A., & Ramanathan, S. (2011). Pluripotency factors in embryonic stem cells regulate differentiation into germ layers. *Cell*, *145*(6), 875–889. https://doi.org/10.1016/j.cell.2011.05.017

Tickle, C., Summerbell, D., & Wolpert, L. (1975). Positional signalling and specification of digits in chick limb morphogenesis. *Nature*. https://doi.org/10.1038/254199a0

Tonegawa, A., & Takahashi, Y. (1998). Somitogenesis controlled by Noggin. *Developmental Biology*. https://doi.org/10.1006/dbio.1998.8895

Tsakiridis, A., Huang, Y., Blin, G., Skylaki, S., Wymeersch, F., Osorno, R., … Wilson, V. (2014). Distinct Wnt-driven primitive streak-like populations reflect in vivo lineage precursors. *Development*, *141*(6), 1209 LP – 1221. https://doi.org/10.1242/dev.101014

Turner, D. A., Hayward, P. C., Baillie-Johnson, P., Rué, P., Broome, R., Faunes, F., & Martinez Arias, A. (2014). Wnt/β-catenin and FGF signalling direct the specification and maintenance of a neuromesodermal axial progenitor in ensembles of mouse embryonic stem cells. *Development (Cambridge, England)*, *141*(22), 4243–4253. https://doi.org/10.1242/dev.112979

Watanabe, Y., & Buckingham, M. (2010). The formation of the embryonic mouse heart. *Annals of the New York Academy of Sciences*, *1188*(1), 15–24. https://doi.org/doi:10.1111/j.1749-6632.2009.05078.x

Wellik, D. M. (2007). Hox patterning of the vertebrate axial skeleton. *Developmental Dynamics*. https://doi.org/10.1002/dvdy.21286

Wilkinson, D. G., Bhatt, S., & Herrmann, B. G. (1990). Expression pattern of the mouse T gene and its role in mesoderm formation. *Nature*. https://doi.org/10.1038/343657a0

Wilson, V., Olivera-Martinez, I., & Storey, K. G. (2009). Stem cells, signals and vertebrate body axis extension. *Development*, *136*(10), 1591 LP – 1604. https://doi.org/10.1242/dev.021246

Winnier, G., Blessing, M., Labosky, P. A., & Hogan, B. L. M. (1995). Bone morphogenetic protein-4 is required for mesoderm formation and patterning in the mouse. *Genes and Development*. https://doi.org/10.1101/gad.9.17.2105

Wittler, L., Shin, E. H., Grote, P., Kispert, A., Beckers, A., Gossler, A., … Herrmann, B. G. (2007). Expression of Msgn1 in the presomitic mesoderm is controlled by synergism of WNT signalling and Tbx6. *EMBO Reports*. https://doi.org/10.1038/sj.embor.7401030

Wymeersch, F. J., Huang, Y., Blin, G., Cambray, N., Wilkie, R., Wong, F. C. K., & Wilson, V. (2016). Position-dependent plasticity of distinct progenitor types in the primitive streak. *ELife*, *5*, e10042. https://doi.org/10.7554/eLife.10042

Xu, P.-F., Houssin, N., Ferri-Lagneau, K. F., Thisse, B., & Thisse, C. (2014). Construction of a Vertebrate Embryo from Two Opposing Morphogen Gradients. *Science*, *344*(6179), 87 LP – 89. https://doi.org/10.1126/science.1248252

Yoshida, M., Uchikawa, M., Rizzoti, K., Lovell-Badge, R., Takemoto, T., & Kondoh, H. (2014). Regulation of mesodermal precursor production by low-level expression of B1 Sox genes in the caudal lateral epiblast. *Mechanisms of Development*, *132*, 59–68. https://doi.org/10.1016/j.mod.2014.01.003

Zhang, L., Lander, A. D., & Nie, Q. (2012). A reaction-diffusion mechanism influences cell lineage progression as a basis for formation, regeneration, and stability of intestinal crypts. *BMC Systems Biology*. https://doi.org/10.1186/1752-0509-6-93

Zhang, P., Li, J., Tan, Z., Wang, C., Liu, T., Chen, L., … Deng, H. (2008). Short-term BMP-4 treatment initiates mesoderm induction in human embryonic stem cells. *Blood*, *111*(4), 1933–1941. https://doi.org/10.1182/blood-2007-02-074120

Zhao, S., Nichols, J., Smith, A. G., & Li, M. (2004). SoxB transcription factors specify neuroectodermal lineage choice in ES cells. *Molecular and Cellular Neurosciences*, *27*(3), 332–342. https://doi.org/10.1016/j.mcn.2004.08.002

Statement of independent work

Herewith I confirm that I wrote this Master's Thesis in its entirety and that no additional assistance was provided, other than from the sources listed.

Date, Signature

1st October, 2020 Aparna Sekar

ACKNOWLEDGEMENTS

I would like to first thank Prof. Dr Herrman for the opportunity to work in the department of developmental genetics, MPIMG. I am very thankful for all the constant guidance and supervision that I received from Dr Frederic Koch during the duration my thesis project. A very special note of gratitude to our lab technician Manuela Scholze for patiently training me in cell culture techniques as well as general techniques in the lab.

I also take this opportunity to thank Dr Sigmar Stricker for graciously agreeing to my second evaluator.

I would additionally, like to thank the program coordinators Eddy and Sarah for being available at times of need and guiding me through concerns during the program.

APPENDIX

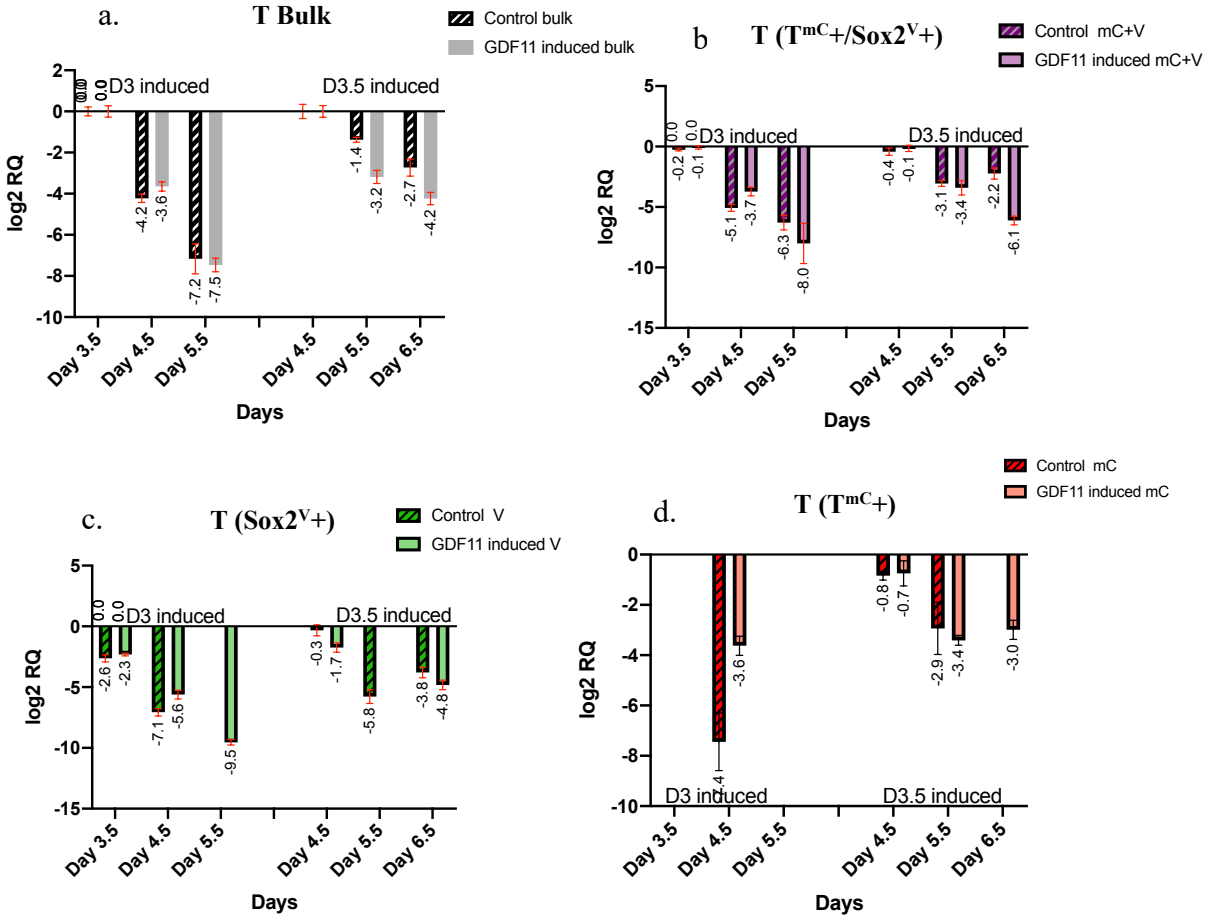

Figure I:
Expression of *T* in control and rGdf11 induced cells. Graphs represent log2 fold change +/- error. **a**. Expression in Bulk **b**. Expression profile in T^{mC}+/$Sox2^{V}$+ sorted cells. **c.** Expression profile in $Sox2^{V}$+ve sorted cells. **d.** Expression profile in T^{mC}+ve sorted cells.

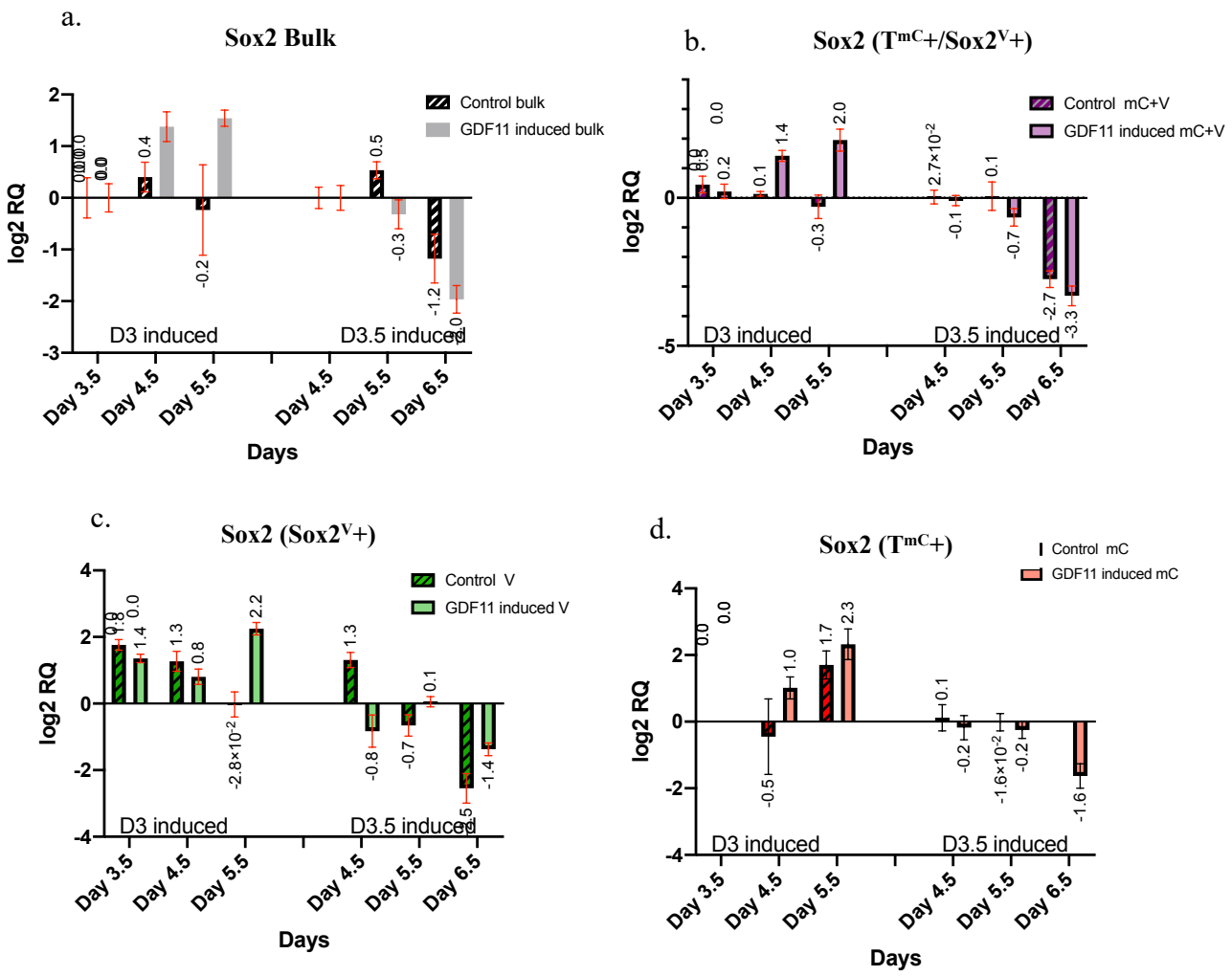

Figure II:
Expression of *Sox2* in control and rGdf11 induced cells. Graphs represent log2 fold change +/- error. **a**. Expression in Bulk **b**. Expression profile in T^{mC}+/$Sox2^{V}$+ sorted cells. **c.** Expression profile in $Sox2^{V}$+ve sorted cells. **d.** Expression profile in T^{mC}+ve sorted cells.

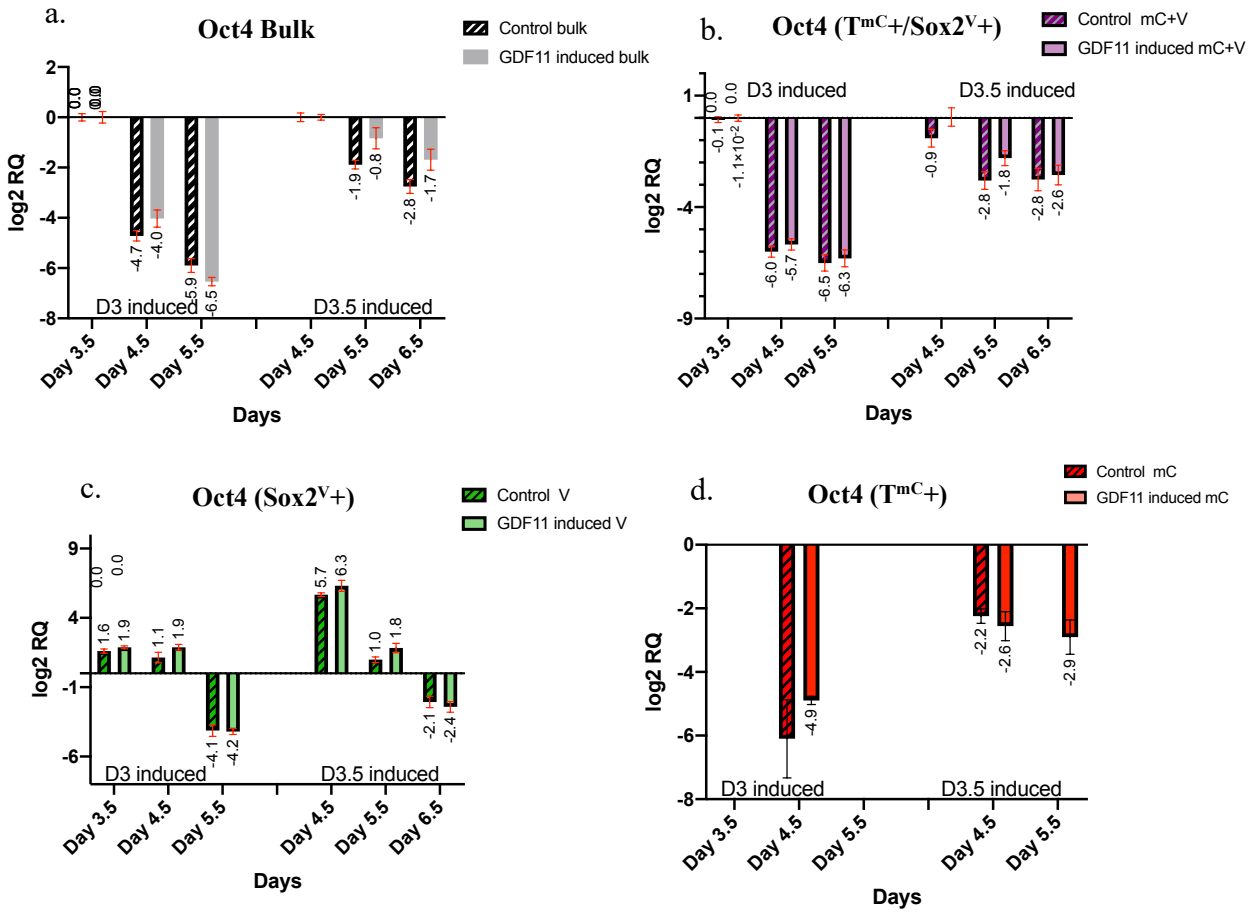

Figure III:
Expression of *Oct4* in control and rGdf11 induced cells. Graphs represent log2 fold change +/- error. **a**. Expression in Bulk **b**. Expression profile in T^{mC}+/$Sox2^{V}$+ sorted cells. **c.** Expression profile in $Sox2^{V}$+ve sorted cells. **d.** Expression profile in T^{mC}+ve sorted cells.

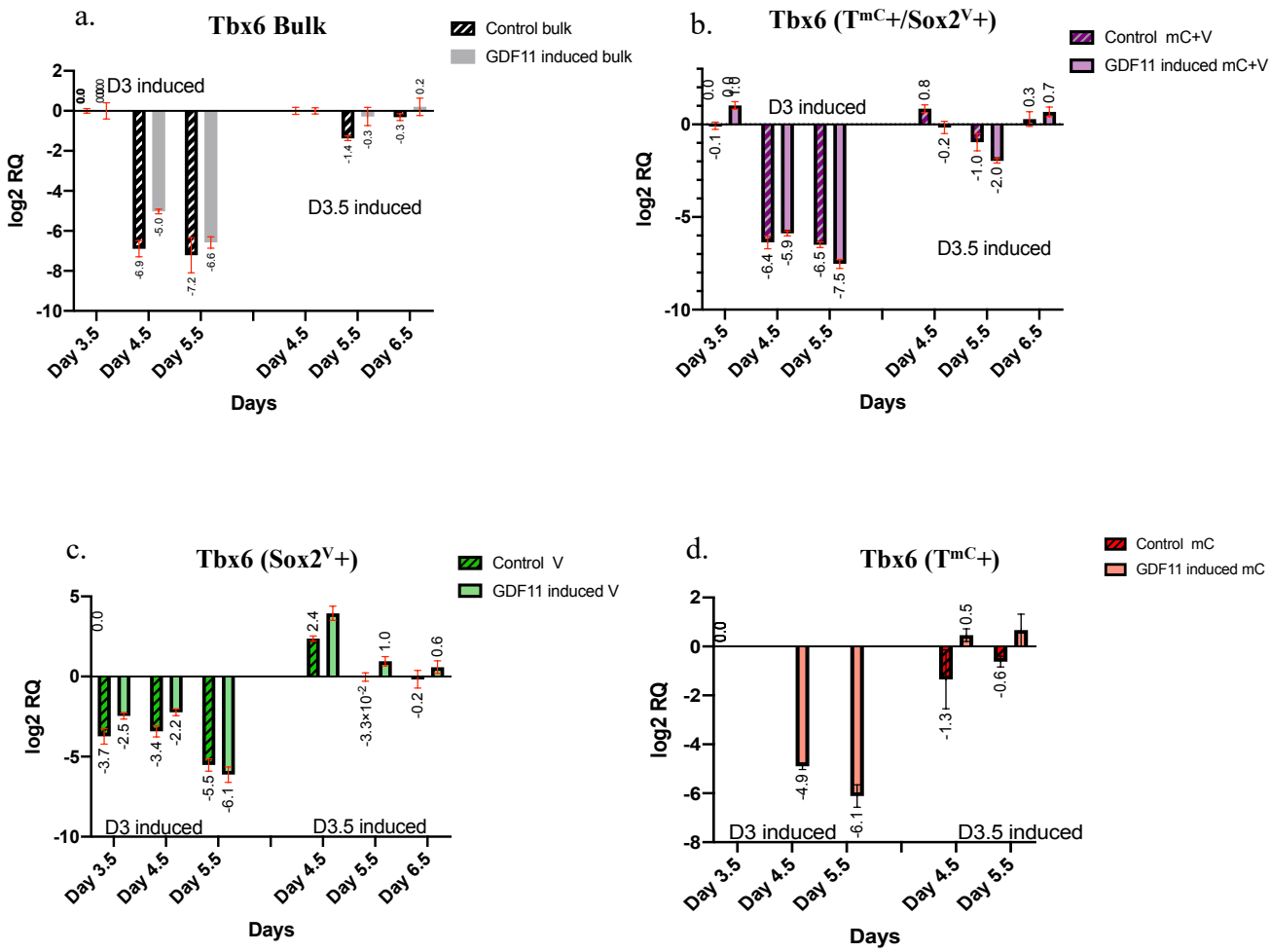

Figure IV:
Expression of *Tbx6* in control and rGdf11 induced cells. Graphs represent log2 fold change +/- error. **a**. Expression in Bulk **b**. Expression profile in T^{mC}+/$Sox2^{V}$+ sorted cells. **c.** Expression profile in $Sox2^{V}$+ve sorted cells. **d.** Expression profile in T^{mC}+ve sorted cells.

ABBREVIATIONS

2-ME	2-mercaptoethanol	GFP	green fluorescence protein
AMP	ampicillin	HPSC	human pluripotent stem cell
BAC	bacterial artificial chromosome	IPA	Isopropanol
BMP	bone morphogenic protein	KAN	kanamycin
BSA	Bovine serum albumin	LIF	leukocyte inhibitory factor
cDNA	complimentary deoxyribonucleic acid	LPM	lateral plate mesoderm
CHL	chloramphenicol	LPMP	lateral/paraxial mesoderm progenitors
CLE	caudal lateral epiblast	NEO	neomycin
CNH	caudal neural hinge	NMP	neuromesodermal progenitors
CRISPR	Clustered regularly interspaced short palindromic repeats	NSB	node streak border
DMEM	Dulbecco´s Modified Eagle´s Medium	O/N	overnight
DMSO	Dimethyl sulfoxide	PCR	polymerase chain reaction
DNA	deoxyribonucleic acid	PS	primitive streak
dNTP	Deoxyribonucleotide triphosphate	PSM	presomatic mesoderm
ES	embryonic stem	PURO	puromycin
ESC	embryonic stem cell	qPCR	quantitative PCR
EtOH	ethanol	RA	retinoic acid
FACS	fluorescence assisted cell sorting	RT PCR	real time PCR
FCS	fetal calf serum	SIIC	Synthemax II-SC substrate
FGF	fibroblast growth factor	T/E	trypsin-EDTA
GDF	growth differentiation factor	TET	tetracyclin
TGF	transforming growth factor	UTR	untranslated region